NeXtRAD Antenna Design

X-Band Dual Polarised Conical Horn Antenna

Prepared by:
Po-Kai Cheng
BSc(Eng) University of Cape Town

Under the supervision of
Professor Michael Inggs
and
Professor Barry Downing
Department of Electrical Engineering
University of Cape Town

A dissertation submitted to the Department of Electrical Engineering,
University of Cape Town, in fulfilment of the requirements
for the degree of

Master of Science
in
Electrical Engineering

February 15, 2016

Declaration

1. I know that plagiarism is wrong. Plagiarism is to use another's work and pretend that it is one's own.
2. I have used the IEEE convention for citation and referencing. Each contribution to, and quotation in, this dissertation from the work(s) of other people has been attributed, and has been cited and referenced.
3. This dissertation report is my own work.
4. I have not allowed, and will not allow, anyone to copy my work with the intention of passing it off as their own work or part thereof.

Signature of Author:.....

P. Cheng

Date: February 15, 2016

Abstract

The purpose of the dissertation is to investigate a design and implementation of a dual polarised X-band antenna. The desired specifications include a centre frequency of 8.5 GHz and a 10° azimuth-half power beamwidth in both vertical and horizontal polarisations. Other requirements include peak power handling of 400 W over a 50 MHz instantaneous bandwidth and the facility to be mounted on a standard tripod. The dissertation begins by introducing NeXtRAD, a radar project developed jointly by UCL and UCT, outlines the objective of the study and lists all the requirements to be achieved.

After considering several types of antenna, horn antenna has been the most practical when trying to meet project requirements. Two of the horn antennas examined here have been the square and conical horn antennas using square and circular waveguides respectively. Each of these waveguides support dual polarisation as they provide a symmetrical structure in two orthogonal planes of polarisation. The square waveguide is flared into a square horn whereas the circular waveguide is flared into a conical horn to increase the gain and reduce the half-power beamwidth to the required angle.

The antennas have been designed and simulated using FEKO and the simulation results have been used to analyse the performance of the antennas. The conical horn antenna showed better performance in simulation than the square horn and has been further investigated. A revised version of the conical horn antenna has been simulated to avoid other higher-order modes but the it has not been fabricated due to manufacturing limitations. FEKO has a built in iterative optimiser that takes in a range of the waveguide diameter steps to find the best response.

The conical horn antenna has been fabricated and tested to measure the two most important parameters; the S-parameters and radiation patterns. In the absence of an anechoic chamber, the UCT Sports Centre and Menzies Building rooftop have been used as antenna test sites to measure the radiation patterns.

After collecting test measurements, the recorded measurements have been compared to simulated results. The prototyped antenna achieved an azimuth half-power beamwidth of 10.4° and 9.1° when vertically and horizontally polarised respectively. The simulation achieved azimuth HPBW of 10.7° and 9.3° when V- and H-polarised respectively. The best comparison is to compare outside measurements with anechoic chamber measurements. However,

without anechoic chamber measurements, the only comparison that can be done is with simulation results. In comparison to the azimuth HPBW of the prototype when V- and H-polarised respectively, there is approximately 0.2° to 0.3° difference, thus an accuracy of up to one decimal place.

The overall results showed that the requirements are met. The prototype measurements and the FEKO simulations corresponds well together with a distortion in the main lobe due to the next higher-order mode. This distortion disappeared in the revised FEKO design where the waveguide dimension has been designed to only allow the fundamental mode to propagate as shown in Section 4.2.5.

Acknowledgements

Firstly, I would like to express my gratitude to my supervisor, Prof. Barry Downing, for proposing this topic to me and allowing me to be exposed to the radar field. I would also like to thank him for his continuous advice, expert guidance, motivation, and immense knowledge. He was also my lecturer for the course Transmission Line Theory, and Microwave Components and Antennas, which contributed to the understanding of the theory for this dissertation.

I would like to express my appreciation to Prof. Michael Inggs for also providing advice, comments, and contribution to my dissertation. Furthermore, I would also like to thank Prof. Riana Geschke for helping me measure the S-parameters for my antenna and guiding me through the operation of the new network analyser.

Thanks to all the members in the Radar Remote Sensing Group (RRSG) who were involved in my project. A special thanks to Stephen Paine, who has been involved in designing the L-Band antennas for the NeXtRAD project, providing assistance with FEKO simulations, and the setting up of the antennas for testing. Another individual I would like thank is Abhisek Bhatta, who provided moral support, as well as feedback throughout my design process. Thank you to Stephen, Abhisek, Ashiv Dhondea, Dominique Gouveia, Johan Burger, Darryn Jordan, and Stephanie Jonkers for the company and laughter during free times.

I am grateful for my mother who has supported me throughout my entire life and continues to support me, who has motivated me and provided company in times of need. I am also grateful for my father who unfortunately past away at age 56, but I am forever in his debt for providing me with food on my plate and a roof over my head. Lastly, I would like to thank my girlfriend, Ming Gao, for the laughter and joy. I am fortunate to have her support me through all the difficulties. Thank you for being the best companion for the past five years and still counting.

Contents

List of Figures

List of Tables

List of Symbols

A_e	Effective aperture
A_{em}	Maximum effective aperture
c	speed of light in a vacuum (3×10^8 m/s)
d	Distance between the antenna and the target or another antenna
D	Physical dimension width of an antenna's aperture
Dir	Directivity
η	Radiation efficiency
F/D	Focal length to aperture dimension ratio
$f_\circ$	Centre frequency or operating frequency
f_c	Cutoff frequency
G_p	Power gain
$\lambda_\circ$	Freespace wavelength
λ_c	Cutoff wavelength
λ_g	Waveguide wavelength
S_{11}	Forward reflection coefficient (input match)
S_{22}	Reverse reflection coefficient (output match)
S_{21}	Forward transmission coefficient (gain or loss)
S_{12}	Reverse transmission coefficient (isolation)
θ_{az}	Azimuth half-power beamwidth
$\theta_{az(H\text{-}pol)}$	Azimuth half-power beamwidth of a horizontally polarised antenna
$\theta_{az(V\text{-}pol)}$	Azimuth half-power beamwidth of a vertically polarised antenna
θ_{el}	Elevation half-power beamwidth
$\theta_{el(H\text{-}pol)}$	Elevation half-power beamwidth of a horizontally polarised antenna
$\theta_{el(V\text{-}pol)}$	Elevation half-power beamwidth of a vertically polarised antenna
ϑ	Misalignment angle between transmitting and receiving polarisations

List of Abbreviations

E-field	Electric field
E-plane	Electric plane
EM	Electromagnetic
FEKO	Feldberechnung fÃijr KÃűrper mit beliebiger OberflÃďche
FNBW	First Null Beamwidth
HPBW	3 dB Half-Power Beamwidth
H-field	Magnetic field
H-plane	Magnetic plane
NetRAD	Netted RADAR in S-Band
NeXtRAD	Netted RADAR in X- and L-Band
RADAR	Radio Detection And Ranging
RF	Radio Frequency
SLL	Sidelobe Level
TEM	Transverse Electric and Magnetic
TE	Transverse Electric
TM	Transverse Magnetic
UCL	University College London
UCT	University of Cape Town

Nomenclature

3 dB half-power beamwidth — Angular width of the main lobe at 3 dB below peak power.

Azimuth plane — Horizontal plane or the plane in which the azimuth is measured.

Elevation plane — Vertical plane or the plane in which the elevation is measured.

Co-polarisation — Where the transmitter and receiver have the same polarisation.

Cross-polarisation — Opposite polarisation between the transmitter and receiver.

Dual polarisation — Transmitter/receiver can transmit/receive vertical, horizontal, co-, and cross-polarisations (HH and HV, VV and VH, HH and VV).

Far field — The field in which the radiation pattern of the antenna is well formed.

H-polarisation — Horizontal polarisation, where the magnetic field is perpendicular, and electric field is parallel to ground.

Polarisation — Propagation of electromagnetic wave where the electric and magnetic field's orientation is with respect to the ground plane.

S-parameters — Scattering parameters measured in an N-port network.

Sidelobe level — Measures the difference between the main lobe's peak and the first side-lobe's peak.

V-polarisation — Vertical polarisation, where the electric field is perpendicular, and magnetic field is parallel to ground.

Chapter 1

Introduction

1.1 Background to the Project

Several countries are investigating a means to detect and track low cross-sectional targets using multistatic radar. The University of Cape Town (UCT) and University College London (UCL) have been working together since 2005 on a program called NetRAD to measure sea clutter and detect target position in S-band from multiple perspectives. NetRAD only operates in one frequency band and single polarised commercial antennas have been used. Now a new and improved system, NeXtRAD, is being developed to investigate various aspects of multistatic radar [1].

The NeXtRAD system operates in two frequency ranges, X-band and L-band. X-band has a short range with high resolution, whereas the L-band has longer range of measurement. The system is required to perform full polarimetric measurements, both co-polar and cross-polar components. The system configuration is shown in Figure 1-1 where the antennas are placed at three different locations along the coast. These antennas are dual polarised in both the vertical and horizontal planes. The centre node transmits the radar pulse and all the three nodes receive the target reflected signal at different planes of polarisation. In total, there will be eight antennas mounted on tripods, four for X-band and four for L-band. Thus, the antennas need to be portable and manageable in size.

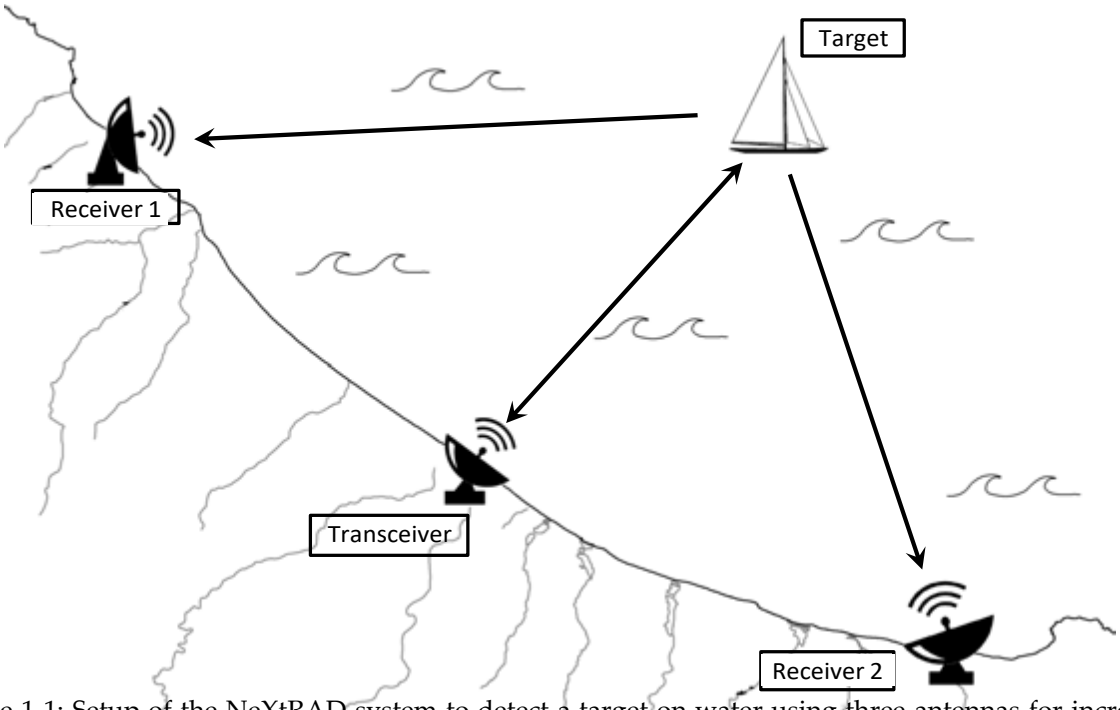

Figure 1-1: Setup of the NeXtRAD system to detect a target on water using three antennas for increased accuracy, one active transceiver and two receivers.

A 10° half-power beamwidth (HPBW) for NeXtRAD is necessary to compare its results directly with NetRAD. Maintaining the same HPBW will ensure the same cross range and pointing requirements for both systems, thus an equal patch of the sea surface can be illuminated. A networked camera shall be mounted at each antenna site to stream images of the illuminated scene and store the data for further analysis. Video feeds shall also be used to enhance the understanding between target or clutter visual behaviour and the radar signal received [1].

1.2 Project Requirements

The NeXtRAD project has to preserve the same illumination as NetRAD with the azimuth HPBW of 10° in both X-band and L-band, be portable and withstand environmental conditions such as wind. Table 1-1 shows all the requirements for the X-band and L-band antennas.

Table 1-1: NeXtRAD project specifications

Parameter	X-band	L-band
Frequency range	8.5 GHz - 10.5 GHz	1.2 GHz - 1.4 GHz
Instantaneous bandwidth	50 MHz	50 MHz
Total bandwidth	130 MHz	130 MHz
Peak power	400 W	1.5 kW
Average power	40 W	150 W
Dual Polarisation	Yes	Yes

With these required specifications the antenna could be large, especially for L-band which has a lower centre frequency. Due to the large size of the antennas, problems can arise to mount on tripods at the coastal region in the presence of strong winds. The total bandwidth of 130 MHz is not required for the work in this dissertation, but the system must be able to operate over the instantaneous bandwidth of 50 MHz.

1.3 Research Objectives

The main objectives of this dissertation are to:

- Investigate different types of antennas that most suitably meet the specifications, such as size, portability, and ability to handle the environment. This dissertation focuses on the design, simulation, and implementation of the X-band antenna to achieve the requirements shown in the X-band column of Table 1-1.
- Design a waveguide that supports dual polarisation. The waveguide needs two orthogonal ports for vertical and horizontal polarisations, where each port needs to provide acceptable reflection coefficients and isolation from the orthogonal port, generally below -10 dB for both measurements. A reflection coefficient of -10 dB indicates 10% of the transmitted power is being reflected back to the transmitter, whereas -20 dB indicates that 1% of the transmitted power gets reflected back to the transmitter. Although a reflection coefficient of -20 dB would improve the response of the system, system engineers are commonly prepared to accept a reflection coefficient -10 dB.
- Design the waveguide feed and antenna using the relevant calculations and equations. Simulate the antenna using appropriate software to analyse the radiation pattern and scattering parameters (S-parameters) of the dual polarised ports.

- Fabricate the antenna that produces the best results from the simulation. The cost of the manufactured antenna should be kept to a minimum since it is the first functional prototype for NeXtRAD at UCT.
- Test and characterise the antenna and its radiation pattern in both planes of polarisation.
- Verify the accuracy of the simulation software by comparing the results with the fabricated antenna. Measurements from the prototype are experimental results that will or will not perform under test (That is assuming all the experimental tests have been done accurately). Simulations are based on algorithms. When comparing simulation and experimental tests the measured prototype has more validity and can be served as the standard for validation.

These objectives are subject to budget limitations, and the availability of testing and fabrication facilities.

1.4 Polarisation Theory

Polarisation of an electromagnetic (EM) wave refers to the directions of the electric (E-) and magnetic (H-) fields. Figure 1-2 illustrates the E- and H-fields in vertical (V-) polarisation where the direction of propagation is in the positive z-axis.

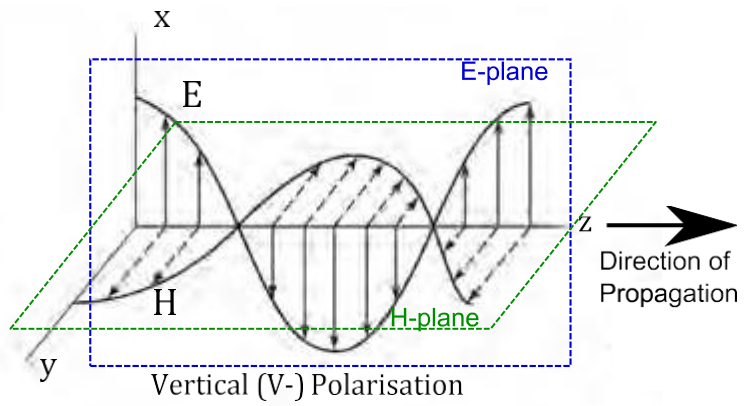

Figure 1-2: E- and H-fields shown in both vertical (left) and horizontal (right) polarisations [2].

Polarisation is dependent on the orientation of the E-field with respect to earth. Considering

that the yz-plane is the ground plane, a vertically polarised (V-polarised) antenna has its E-field oscillating vertically in the electric plane (E-plane) perpendicular to ground, and the H-field in the magnetic plane (H-plane) parallel to ground. This is also true for a horizontally polarised (H-polarised) antenna, except the E-plane and H-plane are rotated 90° about the z-axis.

1.4.1 Orientation

An important aspect of antenna polarisation is that a receiving antenna responds efficiently to receiving EM waves with the same polarisation. For example, ideally, a V-polarised antenna will receive only the V-polarised EM waves and not the H-polarised waves. However, in reality, alignment is crucial. A V-polarised antenna will still be able to receive weak H-polarised waves because the orthogonal polarisations will not be perfectly aligned [3]. This is known as antenna mismatch, polarisation mismatch, or polarisation loss factor. The power loss due to polarisation mismatch can be determined using the following equation [4]:

$$\text{Polarisation mismatch loss} = 20\log(\cos\vartheta) \quad [\text{dB}] \tag{1-1}$$

where ϑ is the misalignment angle between the antenna and the receiving signal. Thus, as ϑ tends towards 90° the loss increases. A skew polarisation can be used where the antenna is orientated at 45° and will receive both V- and H-polarised waves equally. However, due to the 45° orientation, from (1-1), the antenna will have a 3 dB loss when receiving either V- and/or H-polarised waves [3].

1.4.2 Polarimetry

When an antenna transmits at a particular polarisation, the scattered signals from reflections and refractions can change the polarisation, and the receiving antenna will have mismatch losses. To counter this, an antenna can be designed to switch between V- and H-polarisation. Generally, polarimetry will utilise two feeds orthogonal to each other such that the antenna can either transmit and receive both polarisations simultaneously or switch between the polarisations. This is known as dual polarisation, alternating polarisation, or polarimetry. The following terms are used for transmitting and receiving polarisation and Table 1-2 shows

the four different polarisations [5][6]:

- **VV polarisation** — Transmit vertical, receive vertical
- **HH polarisation** — Transmit horizontal, receive horizontal
- **VH polarisation** — Transmit vertical, receive horizontal
- **HV polarisation** — Transmit horizontal, receive vertical

Table 1-2: Four different polarisations with its polarised transmitting and receiving antennas [5].

Single Polarisation	HH or VV
Dual Polarisation	HH and HV, VV and VH, HH and VV
Alternating Polarisation	HH and HV, alternating with VV and VH
Polarimetric	HH, VV, HV, and VH

VV and HH are known as co-polarised because of the same polarisation for transmission and reception. VH and HV are cross-polarised because polarisation is orthogonal to each other for transmission and reception. Due to its dual feeds, there is mutual coupling where EM waves interact between the ports. Another possibility is there is fringing fields at the tip of the transmitting probe and can interfere the other port. Cross polarisation interference will result from the E-field vectors not being perfectly horizontal or vertical within the antenna and waveguide feed. This causes polarisation mismatch as well as a decrease in isolation between the ports. The reflection coefficient of each port and isolation between the ports can be tested to analyse the efficiency and impedance matching, this is known as S-parameters measurement and is discussed in Section 3.4.1.

1.5 Literature Survey

There are several antenna designs that can support dual polarisation. Some of these designs from the literature survey include the slotted waveguide array, microstrip patch array, and horn antenna fed by a microstip patch, and will be discussed in this section.

1.5.1 Slotted Waveguide Arrays

Slotted waveguide arrays (SWGA) are widely used in satellite communications and have high power capability and low manufacturing cost. The slotted waveguide arrays presented in [7] operates in X-band and are dual polarised. The V-polarisation is achieved by implementing broad wall slots, and the H-polarisation by using non-inclined edge wall slots as shown in Figure 1-3.

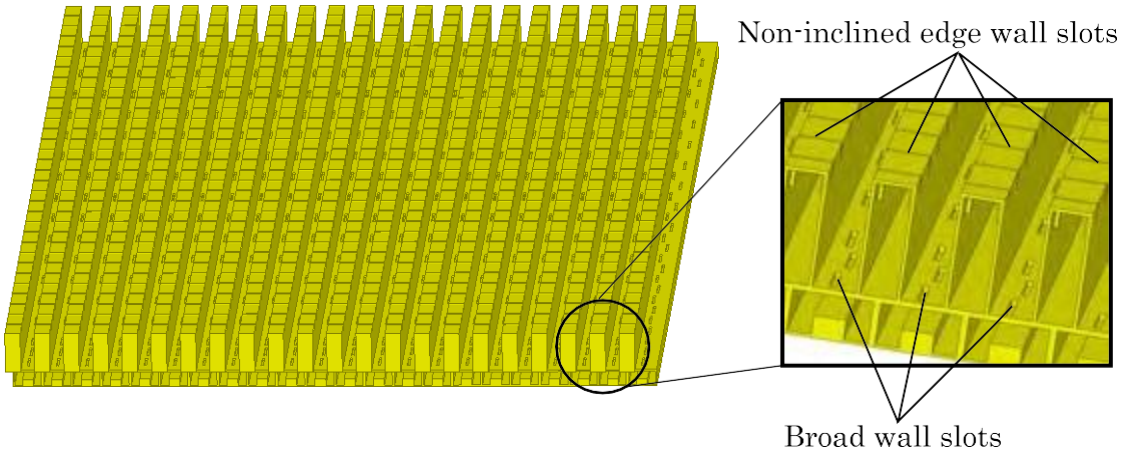

Figure 1-3: Dual polarised slotted waveguide array with the vertical and horizontal slots [7].

The SWGA has the manufacturing complexity of cutting the slots to the required length and thickness to provide matching impedances for each slots. The positioning and spacing of the slots also contributes to impedance matching. The SWGA achieved -35 dB sidelobe level (SLL), 600 MHz bandwidth with 90% efficiency and 35° elevation HPBW.

For the SWGA, a 10° HPBW and low sidelobes are achievable. High power capability is also possible, which satisfies the NeXtRAD requirements. However, the idea of SWGA has been eliminated due to the mechanical complexity.

1.5.2 Microstrip Patch Array

A dual polarised microstrip patch antenna array with a waveguide feed design operating in X-band is presented in [8]. The patch antenna provides compact size, allows different

excitation techniques, dual and triple frequency operation, polarisation and radiation pattern flexibility. However, it does not have high gain or high power handling capability. The design of a dual polarised 2x2 patch array has been simulated and built. The complexity is in the transmission line that consists of a square waveguide, two quarter-wave transformers, and a standard WR-90 rectangular waveguide. Figure 1-4 displays a cross-section of this design.

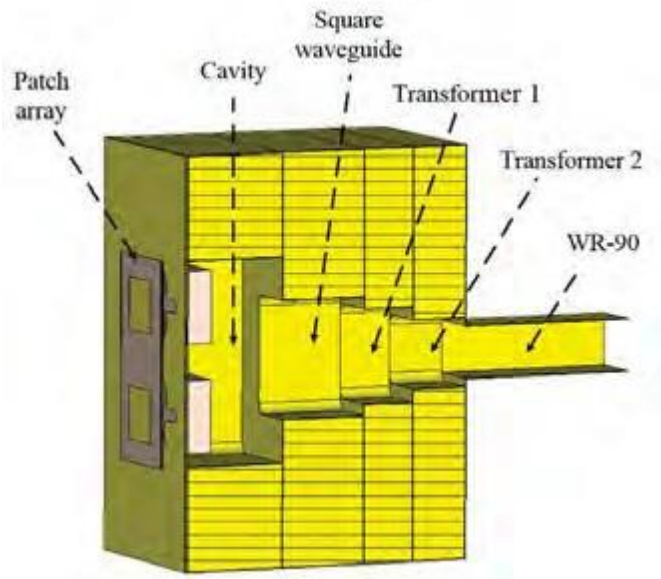

Figure 1-4: Dual polarised microstrip patch array consisting of a square waveguide, and two-step transformer to a rectangular waveguide [8].

Square patches are used to support dual polarisation and an array of patches improves the gain and reduces the HPBW. Two quarter-wave transformers match the WR-90 rectangular waveguide to the square waveguide and cover a wider bandwidth. The results show that the antenna achieved a HPBW of 38° in both planes and covers a bandwidth of 3.75 GHz from 7.7 GHz to 11.45 GHz. The same antenna can be rotated 90° to operate in the other polarisation [8].

This design can achieve a 10° HPBW by increasing the number of patches. However, it only operates in a single plane of polarisation. Another array of patches is required to support dual polarisation which increases the overall size of the antenna. Furthermore, patch antennas cannot withstand high power of more than 70 W. Thus, this design is not suitable for the NeXtRAD requirements.

1.5.3 Horn Antenna Fed by Microstrip Patch

A dual polarised horn antenna fed by a microstrip patch has been proposed in [9]. The antenna operates at a centre frequency of 14.9 GHz in the Ku-band, with a bandwidth of 600 MHz. The horn antenna consists of two microstrip lines, a gap-fed dual polarised patch, a square waveguide and a pyramidal horn shown in Figure 1-5.

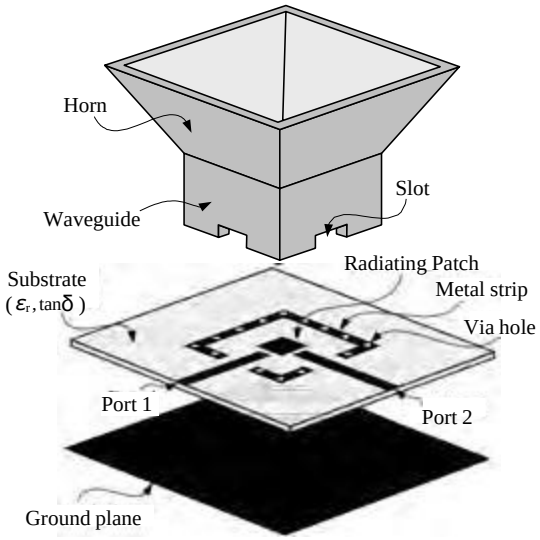

Figure 1-5: A dual polarised horn antenna fed by a microstrip patch [9].

The square waveguide receives fundamental TE_{10} and TE_{01} modes launched by the patch. The manufactured horn shows a reflection coefficient of less than -10 dB, port isolation greater than 30 dB over 14.6 GHz to 15.2 GHz, gain of 12.34 dBi at 14.9 GHz, and -10 dB beamwidths of 87° in the E-plane and 88° in the H-plane. The proposed design shows acceptable impedance matching, high port isolation, and can be easily integrated with printed circuits.

Although this design met most of the requirements, the microstrip patch is not capable of handling the required power level and therefore, this design has also been eliminated.

1.5.4 Summary

In the current literature survey, the antenna designs were not suitable for the NeXtRAD requirements. However, [7] and [9] stated that the square waveguide with the square horn

antenna supports dual polarisation and has high power handling capability. This design, along with the circular waveguide and conical horn antenna, will be investigated further.

1.6 Dissertation Overview

Chapter 1 provides an overview of the NeXtRAD project and describes the basic configuration of the multistatic radar intended for detecting low cross-sectional targets. This dissertation will investigate the design of a dual polarised X-band antenna that meets the NeXtRAD antenna specifications. The fundamentals of polarisation theory have been studied, and a literature survey has been conducted to explore the alternative antenna designs that could possibly achieve the requirements.

Chapter 2 discusses the approach of designing the dual polarised waveguide with a horn antenna to provide the required HPBW. Square and circular shaped waveguides and antennas are considered which support dual polarisation due to their symmetrical structure. This chapter also presents all the relevant mathematical expressions used to determine the dimensions of the dual polarised waveguide and the horn antenna. Both square and conical antennas are simulated in FEKO and the comparison shows that the circular waveguide and conical horn antenna provide the better results.

Chapter 3 discusses the implementation and fabrication of the waveguide and horn antenna. A full description of the equipment used, test locations, the testing procedure and S-parameters measurements are given. Modified simulations have been performed to match the dimensions of the simulated antenna with the fabricated antenna due to fabrication constraints. A revised version of the antenna has been designed in FEKO to provide a further comparison.

Chapter 4 presents all the results obtained from the simulations and testing the antenna, which includes S-parameters measurements and radiation pattern plots measuring HPBWs and SLLs. These results can be analysed to observe whether the antenna meets the NeXtRAD specifications. Comparisons are made between the antenna prototype and simulation results to determine the accuracy of the simulation model.

Chapter 5 draws conclusions from the results obtained. Detailed conclusions are made on

the fabrication flaws, dual polarisation, the antenna design, the chosen test locations and the simulation software used. This chapter concludes if the NeXtRAD requirements are met and a list of recommendations has been given for improvements and future work.

Appendix A provides all the relevant theory that discusses the characteristics of antennas. Appendix B aims to provide further understanding of microwave transmission lines, propagation modes, and waveguide theory. These theories serve as a basis of understanding antenna design as well as further progressing the design to support dual polarisation.

Chapter 2

Design Procedure

This chapter provides the antenna requirements for the NeXtRAD project. Detailed mathematical analyses have been presented for the design of waveguides and antennas along with the insertion of the probe to radiate efficiently. FEKO is an Electromagnetic simulation software that is based on numerical methods (Method of Moments (MoM), Multi-level Fast Multipole Method (MLFMM), Finite Element Method (FEM)) that can solve a diverse set of EM problems. FEKO is capable of simulating antennas, thus makes it a suitable software for the task. The antennas have been simulated in FEKO suite 7.0 and the chapter is concluded with a discussion of the entire design procedure. The design procedure requires the understanding of the theory and some of the relevant equations available in Appendix A and B.

2.1 Antenna Requirements

Table 2-1 shows the requirements for the X-band antenna design. The aim of the X-band antenna is to achieve an azimuth HPBW of 10° in both V- and H-polarisation with an operating frequency of 8.5 GHz.[1] The waveguide design is crucial as it determines the field distribution and the launching method, such as single or dual polarisation. The operating

[1]During the early stages of the design process, the available network analysers could only operate at a maximum frequency of 8.5 GHz. The new network analyser that could operate up to 67 GHz was only available at the end of the design procedure.

Table 2-1: X-band antenna specifications

Parameter	**X-band**
Operating Frequency	8.5 GHz
Instantaneous Bandwidth	50 MHz
Peak Power	400 W
Average Power	40 W
Dual Polarisation	Yes

frequency, $f_\circ$, is 8.5 GHz and using (A-1), the freespace wavelength is:

$$\begin{aligned}\lambda_\circ &= \frac{c}{f_\circ} \\ &= \frac{3 \times 10^8 \text{ m/s}}{8.5 \times 10^9 \text{ Hz}} \\ &= 35.29 \text{ mm}\end{aligned}$$

Different types of antennas that are capable of achieving the specifications have been considered.

2.2 Antennas Considered

Antenna design is heavily dependent on the frequency and wavelength. The size of an antenna is inversely proportional to the operating frequency and increasing the aperture size increases the gain and reduces the HPBW. In X-band, the size of an antenna with a 10° HPBW is not a major issue. A list of antennas have been considered in Chapter 1 including a discussion of their advantages, disadvantages and applicability for the NeXtRAD project. All the antennas are directional antennas and support dual polarisation. The following antennas have been considered in [2], [10], and [11]:

Horn Antenna

- Advantage — Ease of design, ease of manufacture, durable, cost effective, broad bandwidth, high gain, low loss, and high power handling capability.
- Disadvantage — Relatively large overall size especially in length.

The horn antenna satisfies most of the antenna requirements for the NeXtRAD project. The

only trade-off is that the length of the horn contributes to the overall size. However, in X-band, the size of the horn antenna is still tolerable.

Parabolic Dish Antenna

- Advantage — Small in size, high gain, low loss, low sidelobes, and high power handling capability.
- Disadvantage — Difficult to manufacture, costly, and difficulty of alignment between the dish and the feed.

The dish antenna provides a small size while still achieving high gain and low sidelobes. A commercial satellite caravan dish antenna has been considered in Appendix F. However, the antenna feed operates at 12.5 GHz. This antenna has been simulated with a 8.5 GHz waveguide feed in FEKO, and the result shows a 5.7° azimuth HPBW when vertically polarised and therefore too narrow to meet the 10° azimuth HPBW. A custom designed dish would be required which involves a complex fabrication process.

Pillbox Antenna

- Advantage — High gain, low loss, high power handling capability, broad bandwidth, ease of manufacture, and cost effective.
- Disadvantage — Large structure, not wind resistant, and difficult to mount.

The pillbox antenna has similar characteristics to the dish antenna. However, due to its parallel plates and parabolic reflector, the overall structure is large and difficult to handle. The structure also makes it difficult to mount on a standard tripod. The pillbox antenna meets the specifications but the large size and structure of the pillbox antenna is not feasible.

Microstrip Patch Antenna

- Advantage — Compact size, ease of manufacture, and cost effective.
- Disadvantage — Low power handling capability, narrow bandwidth, and low gain.

As discussed in Section 1.5.2, the advantage of a patch antenna is the cost efficiency and the compact size. However, the power handling requirement of 400 W makes the patch antenna not suitable.

Slotted Waveguide

- Advantage — High gain, low loss, high power handling capability, ease of manufacture, durable, and cost effective.
- Disadvantage — Highly complex design, difficulty of feeding an entire waveguide array simultaneously.

A slotted waveguide array increases the aperture size to achieve the required HPBW. The waveguide array needs to be fed in phase simultaneously with a power splitter. With the lack of equipment to perform the required task, the idea of a slotted waveguide has been discarded as discussed in Section 1.5.1.

Consideration
Considering all the advantages and disadvantages of each type of antenna, the horn antenna has been selected as the best and most feasible choice. Other factors that have been considered include the complexity of fabrication, and the availability of the equipment and facilities. Furthermore, the two horn antennas suitable for dual polarisation are the square horn and conical horn antennas. The rest of this chapter shows all the important calculations needed to design the waveguides and the horn antennas. The simulations in FEKO further finalise the most suitable design to meet the NeXtRAD antenna specifications.

2.3 Waveguide Design

This section will outline the waveguide design. Due to dual polarisation where both planes need to be symmetrical, a rectangular waveguide is not feasible. Only square waveguides and circular waveguides will be able to support dual polarisation [7][12]. A coaxial to waveguide transition is required to deliver the transmitted or received signal through the waveguide and coaxial line. This section shows how the size of the waveguide must be designed such that only the fundamental mode can propagate, it also shows how the probe length and position are chosen for appropriate impedance matching.

2.3.1 Waveguide Modes

Waveguide modes are represented as TE_{mn} and TM_{mn} where the mode of propagation is identified by the two subscripts 'mn'. The subscript 'm' represents the number of half wavelengths across the width of the waveguide and 'n' represents the number of half wavelengths across the height of the waveguide [12][13]. For example, a TE_{10} mode means that the E-field is transverse to the direction of propagation, with half a wavelength across the width and no half wavelength across the height of the waveguide.

The field inside a waveguide is a combination of several modes, such that each mode has a critical or cutoff frequency. A waveguide has a fundamental mode of operation and is generally designed to only allow the fundamental mode to propagate so that other higher-order modes are attenuated. The dimensions are calculated such that only the fundamental mode can propagate between the fundamental mode's cutoff frequency and the next higher-order mode's cutoff frequency. This is the main reason that waveguides have a limited bandwidth. Any frequencies operating below the cutoff frequency will not propagate through the waveguide and if the operating frequency is above the cutoff frequency, there is a possibility that other higher-order modes will propagate [12][14].

The fundamental mode for a rectangular waveguide is the TE_{10} mode, and TE_{11} mode for a circular waveguide. More details on hollow waveguides are discussed in Appendix B.4.3 (rectangular waveguide) and Appendix B.4.4 (circular waveguide), including their respective fundamental modes, waveguide wavelength calculations and cutoff frequency calculations.

2.3.2 Polarisation Field Distribution

Dual polarisation allows an antenna to transmit and receive in HH and HV, VV and VH, HH and VV polarisations. For the waveguide to support dual polarisation, the width of the waveguide must be equal in both planes, where the two probes are inserted orthogonal to each other. Thus, one probe is responsible for transmitting and/or receiving V-polarisation and the other probe for H-polarisation.

Figure 2-1 shows the chart of the field distribution inside the square and circular waveguides and the difference on the E-field orientation between V- and H-polarisation.

	V-Polarisation	H-Polarisation
Square Waveguide	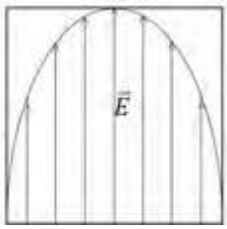	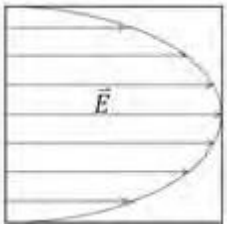
Fundamental Mode	TE_{10}	TE_{01}
Circular Waveguide	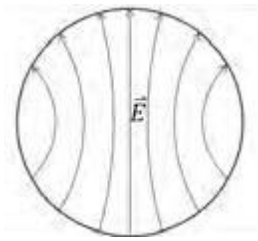	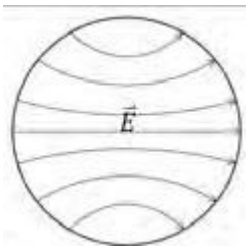
Fundamental Mode	TE_{11}	TE_{11}

Figure 2-1: E-field distribution between V- and H-polarisation for square and circular waveguides.

From Figure 2-1 it can be observed that the E-field is parallel to the plane of polarisation. There is always half a wavelength across the waveguide aperture in the fundamental modes. The E-field strength of the square waveguide is at its peak in the centre and decreases while approaching the edges of the waveguide. The E-field of a circular waveguide behaves similarly, except that it is more uniform across the aperture.

With the symmetrical structure of the waveguides, the HPBWs in both planes are not equal. Figure 2-2 shows the orientation of the E-field in TE_{11} mode. The azimuth and elevation HPBW measurements differ between V- and H-polarisation where the blue arrow represents the HPBW in the E-plane, and the red arrow represents the HPBW in the H-plane.

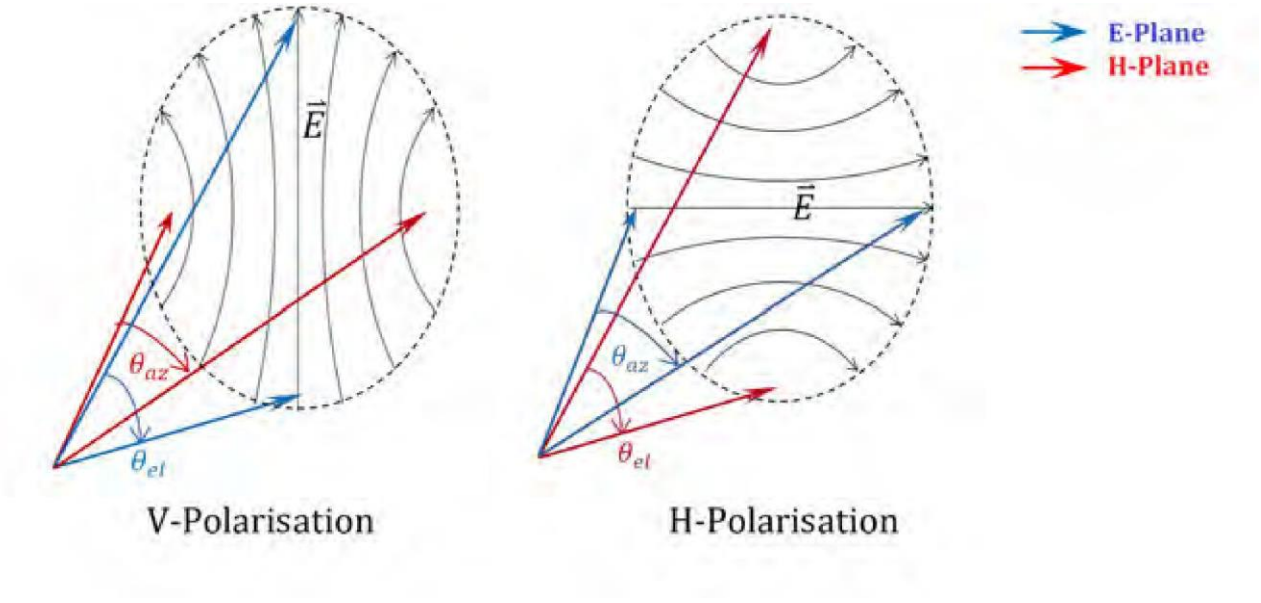

Figure 2-2: HPBW placements for circular E-field distribution in V- and H-polarisations.

Referring to the V-polarised circular waveguide in Figure 2-2, the azimuth HPBW, $\theta_{az(V\text{-}pol)}$, measures segments of the E-field in the horizontal plane. The elevation HPBW, $\theta_{el(V\text{-}pol)}$, measures the entire E-field vertically. The H-polarised circular waveguide switches the roles.

2.3.3 Coaxial to Waveguide Transition

A coaxial line and a hollow waveguide are combined to feed an antenna. The waveguide needs a coaxial launcher (i.e., SMA or N-type) for the coaxial line to deliver the signal into the waveguide [15]. Figure 2-3 displays a coaxial launcher attached to the waveguide with a probe.

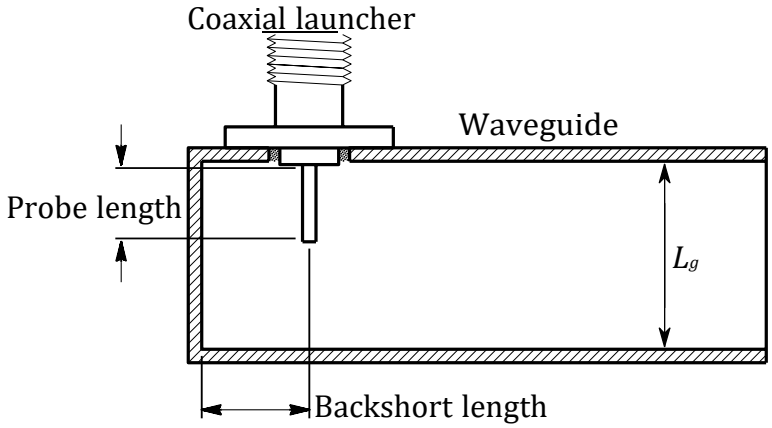

Figure 2-3: A coaxial launcher and probe inserted into a hollow waveguide [16].

Generally, EM waves travel from the coaxial line into freespace in the following way [16]:

- The coaxial line carries the waves in TEM mode to the coaxial launcher with a probe attached to it.
- The probe acts as an extension of the inner conductor of the coaxial line. Without the outer conductor, the waves radiate away from the probe and are reflected inside the waveguide. With the boundary condition[2], the TEM mode from the coaxial line transitions to TE mode within the waveguide.
- The closed wall of the waveguide acts as an open circuit, if the probe is placed appropriately (quarter of a waveguide wavelength λ_g in (2-2)).
- Finally, waves travel through the antenna and radiate through freespace.

There are two main factors that have an impact on impedance matching: the positioning of the probe away from the backshort and the length of the probe. The estimations and reasons for the length of the backshort and probe are [15][16]:

- Probe length:

$$L_{\text{probe}} \approx \frac{\lambda_\circ}{4} \tag{2-1}$$

[2]Discussed in Appendix B.4.1

The probe acts as an impedance quarter-wave transformer for the transition from low impedance of the coaxial line (generally 50 Ω) to high impedance of the waveguide (generally freespace ≈ 377 Ω).

- Backshort length:

$$L_{\text{backshort}} \approx \frac{\lambda_g}{4} \tag{2-2}$$

A shorted $\lambda_g/4$ acts as an open circuit at the waveguide wall and the resultant is a null every $\lambda_g/2$ from the short.

The approximation is justified because an ideal probe is assumed to have no inductance or capacitance. Since the probe acts as a wire, it introduces inductance and capacitance to the waveguide wall [15]. However, the dimensions can start from the approximations and can be adjusted to get the best impedance matching.[3]

2.3.4 Square Waveguide and Probe Calculations

Table 2-2 shows the standard off-the-shelf rectangular waveguides in their respective frequency bands and cutoff frequencies, and Figure 2-4 shows the corresponding dimensions [14].

Table 2-2: Standard rectangular waveguide dimensions

Freq. Band	a (mm)	b (mm)	f (GHz)	f_c (GHz)
L	165.1	82.55	1-2	0.908
S	72.14	34.04	2-4	2.08
C	47.55	22.15	4-8	3.155
X	22.86	10.16	8-12.4	6.56
Ku (J)	15.8	7.9	12-18	9.49

[3]Paul Wade in [15] did many experiments on varying the lengths of the backshort and the probe, concluding that the exact $\lambda_g/4$ for the probe and $\lambda_g/4$ for backshort length are acceptable but not optimum. However, experiments have shown that the optimum lengths are not very far away from the approximation of the quarter wavelengths.

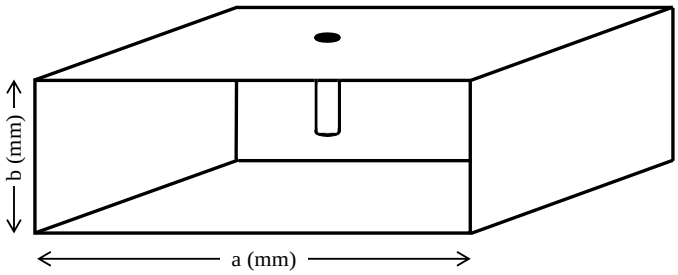

Figure 2-4: Rectangular waveguide dimensions

X-band is the required operating frequency for this dissertation. Consequently, Table 2-2 shows the length of the square waveguide a is chosen to be 22.86 mm. The width of a = 22.86 mm from Table 2-2 considers the cutoff frequency and will propagate its fundamental TE_{10} mode when V-polarised. For the square waveguide to support dual polarisation, the height must also be equal to the width such that $a = b =$ 22.86 mm. Equation (B-2) finds the cutoff wavelength to confirm that the given dimension in the table is valid.

$$\begin{aligned}\lambda_c &= 2a \\ &= 2 \times 22.86 \text{ mm} \\ &= 45.72 \text{ mm}\end{aligned}$$

Leading to the cutoff frequency:

$$\begin{aligned}f_c &= \frac{c}{\lambda_c} \\ &= \frac{3 \times 10^8 \text{ m/s}}{0.4572 \text{ m}} \\ &= 6.56 \text{ GHz}\end{aligned}$$

which is equal to the cutoff frequency shown in Table 2-2 for X-band. Thus, an operating frequency of 8.5 GHz is above the cutoff frequency. It will therefore propagate through this square waveguide.

From (B-3), the waveguide wavelength is:

$$\lambda_g = \frac{\lambda_\circ}{\sqrt{1 - \left(\frac{\lambda_\circ}{\lambda_c}\right)^2}}$$
$$= \frac{35.29\ \text{mm}}{\sqrt{1 - \left(\frac{35.29\ \text{mm}}{45.72\ \text{mm}}\right)^2}}$$
$$= 55.51\ \text{mm}$$

The length of the probe and backshort can be calculated using (2-1) and (2-2) respectively. The length of the probe is:

$$L_{\text{probe}} = \frac{\lambda_\circ}{4}$$
$$= \frac{35.29\ \text{mm}}{4}$$
$$= 8.82\ \text{mm}$$

and the length of the backshort is:

$$L_{\text{backshort}} = \frac{\lambda_g}{4}$$
$$= \frac{55.51\ \text{mm}}{4}$$
$$= 13.88\ \text{mm}$$

With these calculated values, the square waveguide can be designed with the relative dimensions.

2.3.5 Circular Waveguide and Probe Calculations

Circular waveguides have no standard sizes designed for different frequency bands, unlike with rectangular waveguides. However, the circular waveguide can be designed using the required equations found in Appendix B.4.4.

Aluminium water pipes of thickness 2 mm and inner diameter of 28 mm have been chosen as they were the only practical dimensions available. Since the outer diameter of the water

pipes are kept constant, pipes with a smaller inner diameter would become thicker and impractical for the fabrication process, especially when drilling holes for the coaxial launcher. The fundamental TE_{11} mode is required for the circular waveguide to propagate efficiently. The next higher-order TM_{01} mode and the second higher-order TE_{21} mode have also been considered to find their cutoff frequencies to prevent the modes from propagating. Using (B-6), (B-7), and (B-8), the cutoff wavelengths for the given diameter (l_g = 28 mm) for TE_{11} mode is:

$$\begin{aligned}\lambda_{c(\mathrm{TE11})} &= 1.706 \times l_g \\ &= 47.77 \text{ mm}\end{aligned}$$

TM_{01} mode is:

$$\begin{aligned}\lambda_{c(\mathrm{TM01})} &= 1.306 \times l_g \\ &= 36.57 \text{ mm}\end{aligned}$$

and TE_{21} mode is:

$$\begin{aligned}\lambda_{c(\mathrm{TE21})} &= 1.029 \times l_g \\ &= 28.80 \text{ mm}\end{aligned}$$

Therefore, the cutoff frequency for the fundamental TE_{11} mode is:

$$\begin{aligned}f_{c(\mathrm{TE11})} &= \frac{c}{\lambda_{c(\mathrm{TE11})}} \\ &= \frac{3 \times 10^8 \text{ m/s}}{0.04777 \text{ m}} \\ &= 6.28 \text{ GHz}\end{aligned}$$

The cutoff frequency for the next higher-order TM_{01} mode is:

$$f_{c(\mathrm{TM01})} = 8.20 \text{ GHz}$$

and the cutoff frequency for the second higher-order TE_{21} mode is:

$$f_{c(\mathrm{TE21})} = 10.12 \text{ GHz}$$

An operating frequency of 8.5 GHz is above the cutoff frequency of 6.28 GHz and 8.20 GHz,

which leads to the possibility of introducing the next higher-order TM_{01} mode but not the TE_{21} mode. However, the way that the launcher is positioned in the waveguide excites mostly TE modes. Thus, the next higher-order TM_{01} mode is not a major problem at this preliminary stage. The launching methods for TE and TM modes within a waveguide is shown in Appendix C.

From (B-10), the waveguide wavelength is:

$$\begin{aligned}\lambda_g &= \frac{\lambda_\circ}{\sqrt{1-\left(\frac{\lambda_\circ}{\lambda_c}\right)^2}} \\ &= \frac{35.29\text{ mm}}{\sqrt{1-\left(\frac{35.29\text{ mm}}{47.77\text{ mm}}\right)^2}} \\ &= 52.36\text{ mm}\end{aligned}$$

The method for calculating the length of the probe and backshort is identical to the square waveguide. Thus:

$$\begin{aligned}L_{\text{probe}} &= \frac{\lambda_\circ}{4} \\ &= \frac{35.29\text{ mm}}{4} \\ &= 8.82\text{ mm}\end{aligned}$$

and

$$\begin{aligned}L_{\text{backshort}} &= \frac{\lambda_g}{4} \\ &= \frac{52.36\text{ mm}}{4} \\ &= 13.09\text{ mm}\end{aligned}$$

With these calculated values, the circular waveguide can be designed.

2.3.6 Dual Polarising a Waveguide

To dual polarise a waveguide, two probes can be inserted orthogonal to each other. Theoretically, the probes will not interact with each other due to different polarisation. Nevertheless,

in reality, while one probe is transmitting, there is a possibility that the radiated power can be received by the other orthogonal probe due to misalignment as discussed in Section 1.4.1. Since the two probe tips are not far apart, there is an added possibility that the fringing fields at the tip of the transmitting probe can interfere with the other probe.

The S-parameters measurement is tested on a network analyser to analyse the reflection coefficients of each port and the transmission coefficient between the ports. Acceptable isolation is achievable between the two probes by positioning them orthogonal to each other. To avoid the fringing field interference, the two probes can be spaced half a waveguide wavelength apart. This method has not been tested due to the time constraints and limited resources, therefore testing has only been limited to placing the probes orthogonal to each other.

2.3.7 Discussion

Table 2-3 shows the dimensions of the square and circular waveguides from the calculations.

Table 2-3: Dimensions of the square and circular waveguides.

	Square Waveguide	**Circular Waveguide**
Dimension	22.86 mm × 22.86 mm	28 mm in diameter
f_c	6.56 GHz	6.28 GHz
λ_c	45.72 mm	47.77 mm
λ_g	55.51 mm	52.36 mm
L_{probe}	8.82 mm	8.82 mm
$L_{backshort}$	13.88 mm	13.09 mm

As discussed previously for the circular waveguide, operating at a frequency of 8.5 GHz might introduce the next higher-order TM_{01} mode with the dimension of 28 mm but does not excite other higher-order TE modes. Due to the limitation of resources, this was the smallest dimension available at the time. Additionally, comparing the freespace wavelength and cutoff wavelength for TM_{01}, the difference of 1.28 mm has been considered tolerable. Thus, the dimension of $l_g = 28$ mm has still been chosen.

A comparison of the square and circular waveguides shows no major size differences. The circular waveguide has a lower cutoff frequency of $f_c = 6.28$ GHz and a shorter waveguide

wavelength of $\lambda_g = 52.36$ mm. As long as the operating frequency is not near the cutoff frequency, the fundamental waveguide mode will propagate.

2.4 Horn Antenna

Horn antennas are directional antennas that radiate or receive EM waves more effectively in the direction of the aperture. An open ended waveguide has the ability to radiate on its own. Equation A-18 shows that the gain of the waveguide is low due to its small aperture. Flaring the waveguide into a larger aperture increases the gain and reduces the HPBW. The flaring can increase either in the H-plane or E-plane. In this dissertation, both the E-plane and H-plane have been flared to reduce the HPBW in each plane, creating a pyramidal horn [10]. Figure 2-5 shows the radiation pattern of a pyramidal horn antenna, the E- and H-fields of the radiation pattern and the aperture distribution.

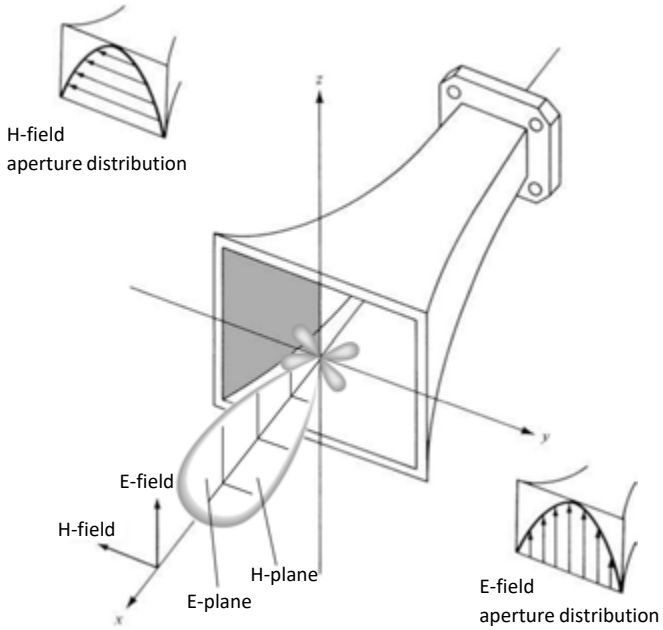

Figure 2-5: Radiation patterns showing the E- and H-plane, and the E- and H-field aperture distributions of a pyramidal horn antenna [10].

Conical horn antennas are usually fed by a circular waveguide that supports the fundamental TE_{11} mode. The design calculations in Section 2.4.1 for the conical horn antenna are similar to the square horn antenna. Both the conical horn and the square horn antenna are

symmetrical in both planes. However, the conical horn antenna has rotational symmetry in the E- and H-Plane because of its circular shape. Unlike a square shape, it does not have any sharp edges, therefore the E-field distribution is smoother throughout the whole aperture as shown in Figure 2-1.

2.4.1 Square Horn Equations

Figure 2-6 displays the side view of the horn antenna and its dimensions for designing the antenna.

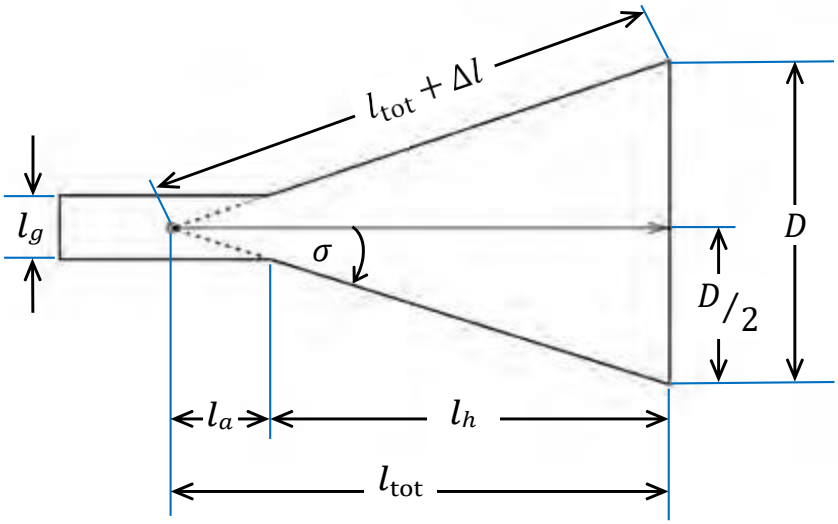

Figure 2-6: Side view of a horn antenna showing its dimensions.

The following list shows the representation of the variables in Figure 2-6:

$l_{tot} + \Delta l$	—	Slant length of the horn
l_a	—	Length from the apex to the opening of the horn
l_h	—	Length of the horn from the opening of the horn to the centre aperture
l_{tot}	—	Total length from the apex to the centre aperture
D	—	Length of the aperture in its respective plane
l_g	—	Length of the waveguide or opening of the horn in its respective plane
σ	—	Angle from the centre to the slant of the horn

For a square horn antenna, l_{tot} formulated to be [14]:

$$l_{\text{tot}} = \frac{D^2}{2\lambda_\circ} \tag{2-3}$$

By analysing (2-3), it can be seen that the length of the horn antenna is directly proportional to half of the aperture squared ($l \propto D^2/2$). It is noted that l_{tot} is not the actual length of the horn antenna. Basic trigonometry can be used to calculate the actual length of the horn l_h:

$$l_h = l_{\text{tot}} \left(1 - \frac{l_g}{D}\right) \tag{2-4}$$

2.4.2 Square Horn Calculations

To calculate the length of the horn, the aperture and wavelength is needed. For the required azimuth HPBW of 10°, the aperture can be calculated using (A-5):

$$\begin{aligned} D &= \frac{60\lambda_\circ}{\theta} \\ &= \frac{60 \times 35.29 \text{ mm}}{10^\circ} \\ &= 211.74 \text{ mm} \end{aligned}$$

In order to achieve dual polarisation in both V- and H-planes with 10° HPBW, the square horn antenna is designed with an aperture side of 211.74 mm. Similarly, the opening of the antenna is also a square with l_g = 22.86 mm, chosen from the industry standard dimension '*a*' in X-band.

Therefore, using (2-3), the total length is:

$$\begin{aligned} l_{\text{tot}} &= \frac{D^2}{2\lambda_\circ} \\ &= \frac{(211.74 \text{ mm})^2}{2 \times 35.29 \text{ mm}} \\ &= 635.22 \text{ mm} \end{aligned}$$

From (2-4), the length of the horn is:

$$\begin{aligned} l_h &= l_{\text{tot}}\left(1 - \frac{l_g}{D}\right) \\ &= 635.22 \text{ mm}\left(1 - \frac{22.86 \text{ mm}}{211.74 \text{ mm}}\right) \\ &= 566.64 \text{ mm} \end{aligned}$$

Using (A-18), the gain equation of the square horn antenna is:

$$\begin{aligned} G &= \frac{4\pi}{\lambda_\circ^2} A_e \\ &= \frac{4\pi}{\lambda_\circ^2} \times A_{\text{em}} \times e_r \end{aligned}$$

where $A_{\text{em}} = D \times D$ is the physical aperture of the horn antenna and the radiation efficiency, e_r, ranges between 0.4 to 0.8 for a practical antenna and generally assumed to be 0.5 for a horn antenna [17]. Thus, the gain is:

$$\begin{aligned} G &= \frac{4\pi}{35.29 \text{ mm}^2} \times 211.74 \text{ mm} \times 211.74 \text{ mm} \times 0.5 \\ &= 226.19 \\ &\approx 23.54 \text{ dBi} \end{aligned}$$

2.4.3 Conical Horn Calculations

Again referring to Figure 2-6, the conical horn can be designed. Firstly, the diameter D of a circular uniform aperture approximation is [2]:

$$D = \frac{58.4\lambda_\circ}{\theta} \tag{2-5}$$

Even though the aperture diameter in (2-5) can be found, it is evident from simulation that this equation does not give the approximate 10° azimuth HPBW in both polarisations. The design is shown in Appendix E. Thus, the better approximation for the circular aperture diameter is [17]:

$$D = \frac{70\lambda_\circ}{\theta} \tag{2-6}$$

Substituting the known variables, the diameter for the aperture is:

$$D = \frac{70 \times 35.29 \text{ mm}}{10^{\circ}}$$
$$= 247.06 \text{ mm}$$

For an optimum conical horn, the aperture of the horn is dependent on the length of the antenna. The total length of the cone from the apex to the centre aperture of the horn is given as [17]:

$$l_{\text{tot}} = \frac{D^2}{3\lambda_{\circ}} \tag{2-7}$$

Substituting the found diameter D and $\lambda_{\circ}$ into (2-7):

$$l_{\text{tot}} = \frac{(247.06 \text{ mm})^2}{3 \times 35.29 \text{ mm}}$$
$$= 576.47 \text{ mm}$$

To find the length of the horn l_h, the same calculations can be done in (2-4). The diameter of the circular waveguide is 28 mm, so the opening of the antenna l_g will also be 28 mm. Thus, the length of the horn is:

$$l_h = 576.47 \text{ mm} \left(1 - \frac{28 \text{ mm}}{247.06 \text{ mm}}\right)$$
$$= 511.14 \text{ mm}$$

With $e_r = 0.5$ and $A_{\text{em}} = \pi(D/2)^2$, the gain of the conical horn antenna is:

$$G = \frac{4\pi}{\lambda_{\circ}^2} \times \pi(D/2)^2 \times e_r$$
$$= \left(\frac{\pi D}{\lambda_{\circ}}\right)^2 e_r$$
$$= \left(\pi \frac{247.06 \text{ mm}}{35.29 \text{ mm}}\right)^2 \times 0.5$$
$$= 241.86$$
$$\approx 23.84 \text{ dBi}$$

2.4.4 Discussion

Table 2-4 summarises the dimensions of the square and conical horn from the calculations.

Table 2-4: Dimensions of the square and conical horn antennas.

	Square Horn	**Conical Horn**
Length (l_h)	566.64 mm	511.14 mm
Aperture width (D)	211.74 mm	247.06 mm in diameter
Opening (l_g)	22.86 mm	28 mm in diameter

The conical horn is shorter in length but larger in aperture since a different equation is used to calculate the aperture. The square waveguide and circular waveguide are attached to the square horn and conical horn respectively. Both the antennas are simulated in FEKO and the simulations is shown in Section 2.5.

2.5 FEKO Measurements

Using the dimensions in Table 2-3 and Table 2-4, both waveguides and horn antennas are simulated in FEKO version 7.0 to analyse the performance. In FEKO, the numerical method of MLFMM has been chosen which enables the analysis of antennas in electrically large environments that allows near-field and far-field radiation pattern measurements. The antennas have been constructed by designing the waveguide and the horn antenna with the calculated dimensions, merged, meshed, and finally inserting a waveguide port function on the waveguide. The waveguide port function is the easiest way to excite the antenna that allows only the fundamental mode to propagate. There are two ways to feed the waveguide: using the 'waveguide port' function in FEKO or manually designing the probes and coaxial launchers to excite the TEM mode which feeds the waveguide. Due to the limited documentation on FEKO's ability to simulate manually designed feeds, the waveguide port function has been chosen. The far field radiation patterns in the polar plots and Cartesian plots are measured along with the azimuth and elevation HPBWs and SLLs in both polarisations. The antenna with the best results that satisfies the project requirements is chosen to be fabricated.

2.5.1 FEKO Square Horn

The square horn design is similar to the square horn in Appendix D that has been designed in a previous investigation in 2014 [18], but this antenna was substantially long and therefore impractical. The new and optimised design shows that the length has been reduced significantly. Figure 2-7 and Figure 2-8 show the results for the square horn antenna simulated in FEKO. The simulations have been constructed such that the xz-plane represents the elevation, and the yz-plane represents the azimuth or ground plane.

Figure 2-7 displays the 3D radiation pattern for the square horn in V- and H-polarisation.

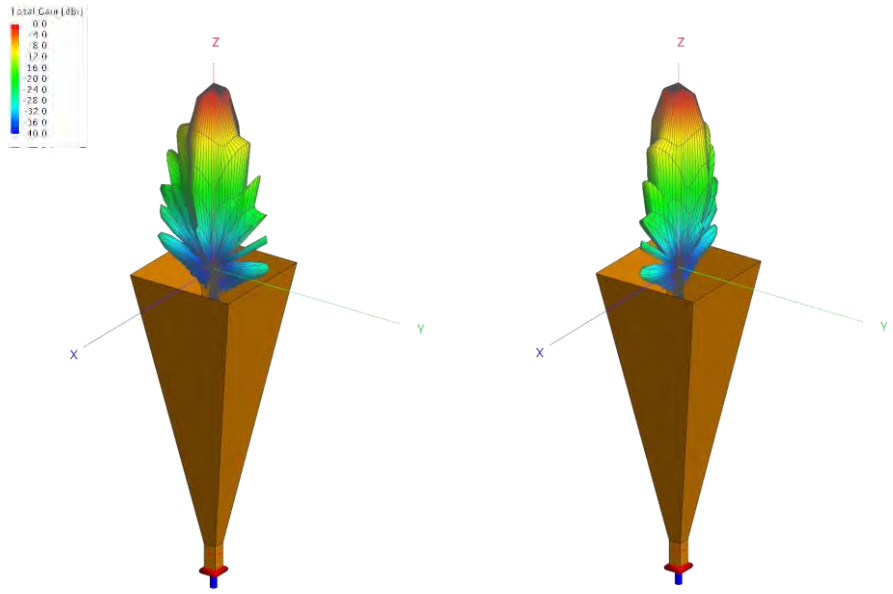

V-Polarisation H-Polarisation

Figure 2-7: Square horn antenna 3D radiation pattern in V- and H-polarisation simulated in FEKO.

From Figure 2-7, it can be observed that the radiation pattern is symmetrical and has large sidelobes. For V-polarisation, sidelobes are large in the azimuth plane. However, in the case of the H-polarisation, by observation, the radiation pattern is rotated by 90°, the sidelobes are large in the elevation plane.

Figure 2-8 shows the polar plots and Cartesian plots of the elevation plane (labelled as el-plane) and azimuth plane (labelled as az-plane) when the antenna is V- and H-polarised.

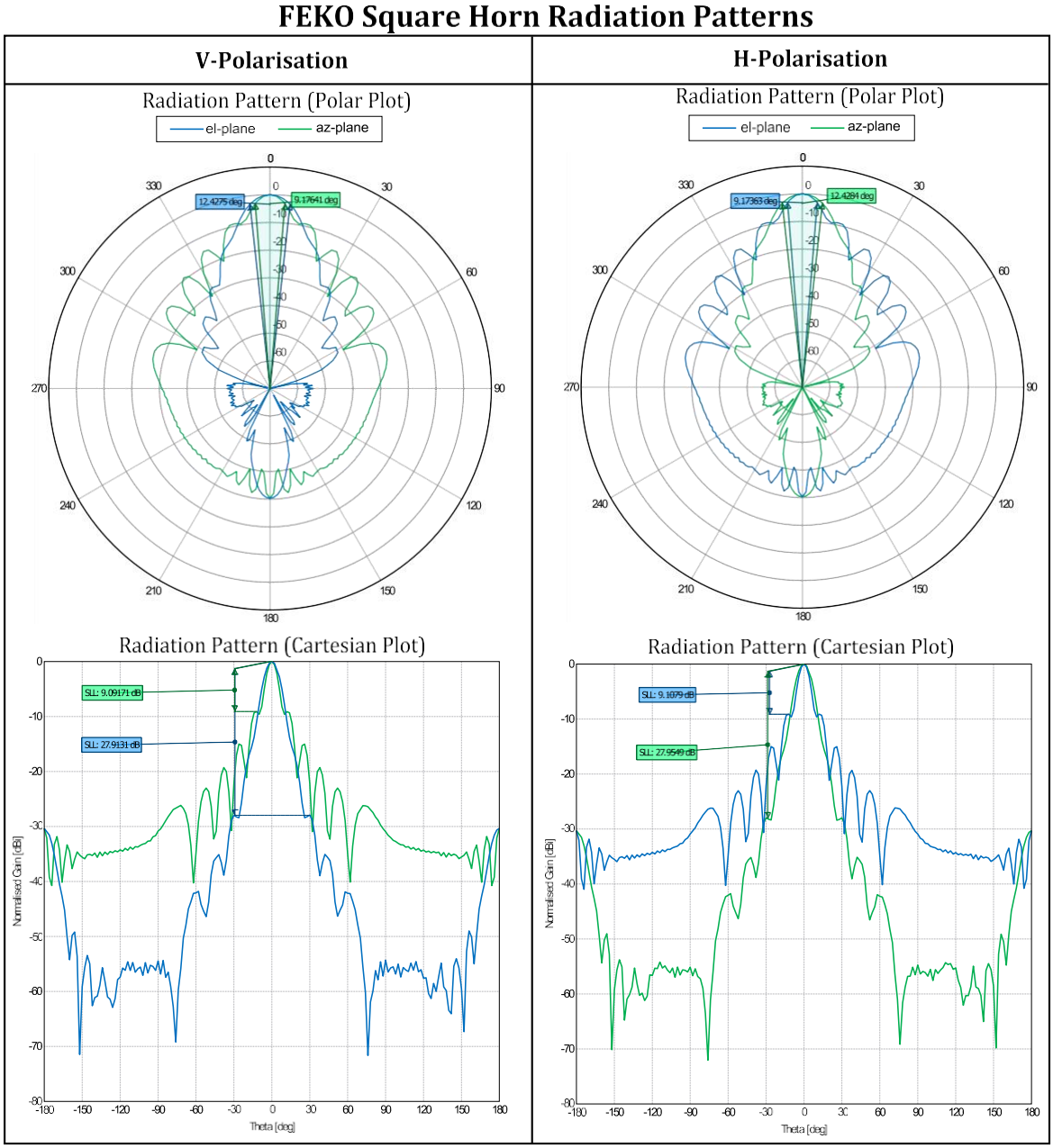

Figure 2-8: FEKO square horn radiation patterns in polar and Cartesian plots for V- and H-polarisations in the elevation and azimuth plane.

From the NeXtRAD requirements, only the azimuth plane in both polarisations are required. Analysing the results in Figure 2-8, when V-polarised and H-polarised respectively, the polar plots show the azimuth HPBWs of 9.2˚ and 12.4˚, and the Cartesian plots show the SLLs in the azimuth plane of 9.09 dB and 27.95 dB. The gain of the square horn antenna predicted to be 23.85 dBi in FEKO .

2.5.2 FEKO Conical Horn

Similar to the square horn, the conical horn was also simulated in FEKO where the yz-plane represents the ground plane. Figure 2-9 displays the 3D radiation pattern for the conical horn in V- and H-polarisation.

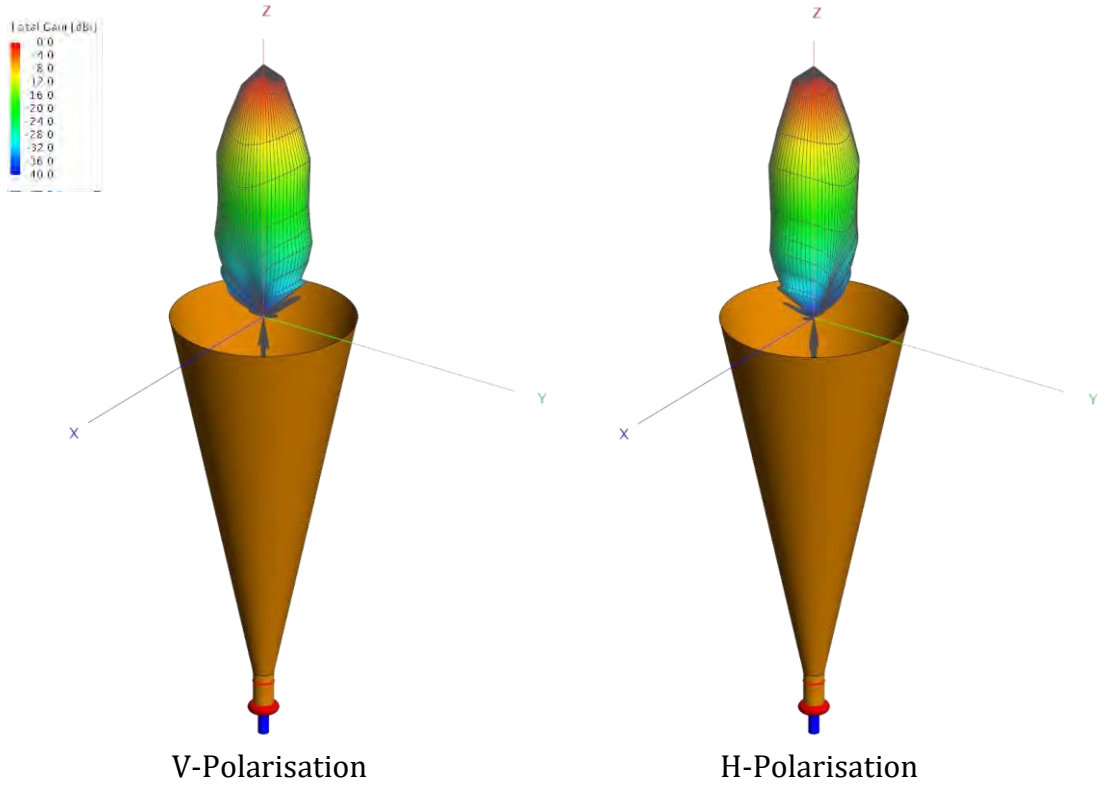

Figure 2-9: Conical horn antenna 3D radiation pattern in V- and H-polarisation simulated in FEKO.

From observing Figure 2-9, the radiation pattern is symmetrical as well, but the sidelobes are substantially lower than the square horn antenna in Figure 2-7. For a clearer analysis, Figure 2-10 shows the measurements in the polar plots and Cartesian plots of the elevation and azimuth plane when the antenna is V- and H-polarised.

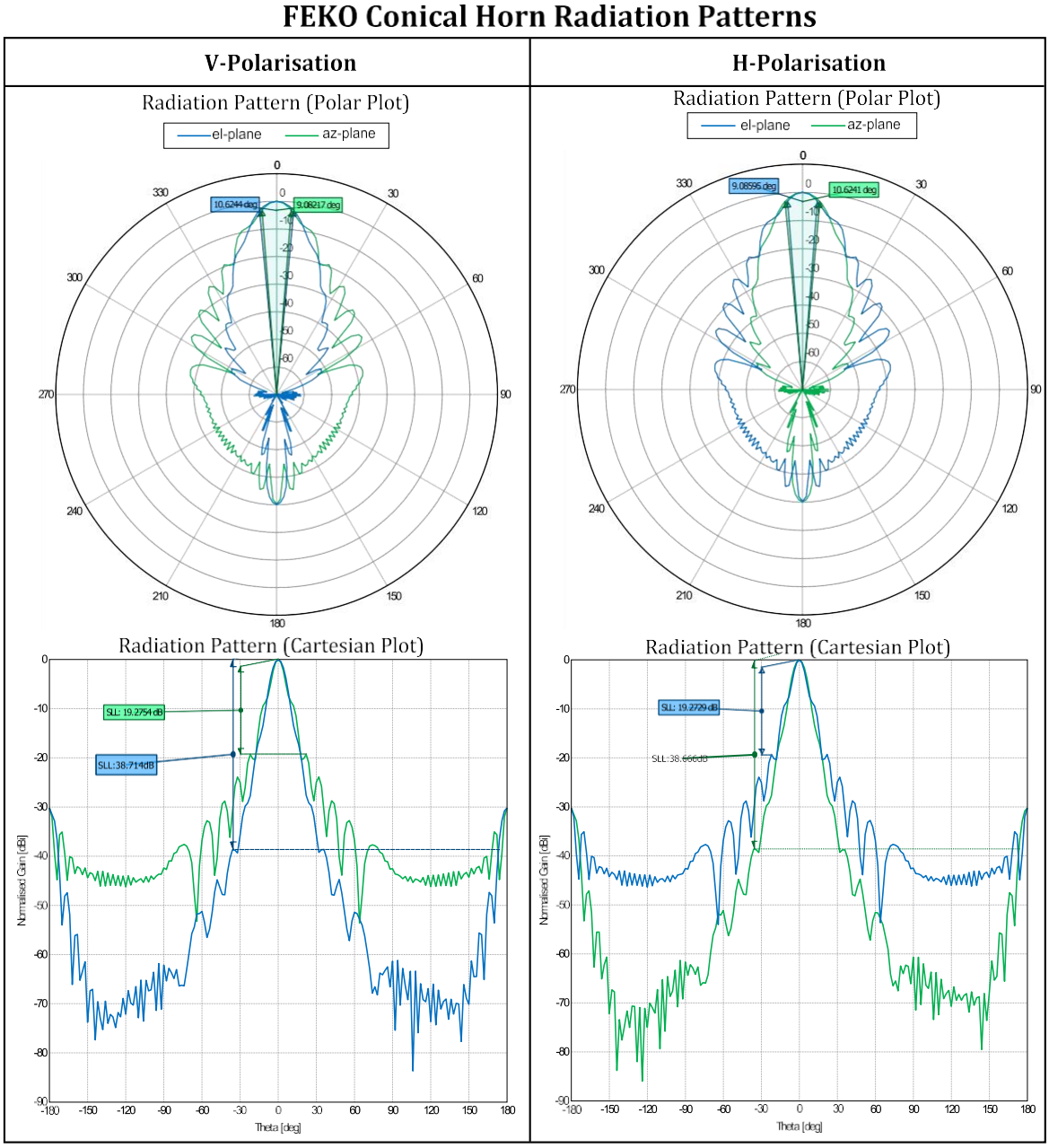

Figure 2-10: FEKO conical horn radiation patterns in polar and Cartesian plots for V- and H-polarisations in the elevation and azimuth plane.

Analysing the results in Figure 2-10, when V- and H-polarised respectively, the polar plots show the azimuth HPBWs of 9.1° and 10.6°, and the Cartesian plots show the SLLs in the azimuth plane of 19.28 dB and 38.67 dB. Unlike the polar plots for the square horn antenna, the shoulders that appear at both -15° and 15° are not first sidelobes. The shoulders did not reach to a null and are not considered as the first sidelobe peak. The gain of the conical horn antenna has been predicted to be 24.19 dBi in FEKO.

2.5.3 Modified and Revised Conical Horn Design on FEKO

Due to the dimensions of the prototype differing from the calculated dimensions, the FEKO simulation of the antenna has been altered to match the prototype which will be discussed in Chapter 3. Figure 2-11 shows the newly modified horn antenna with the dual polarised waveguide in FEKO.

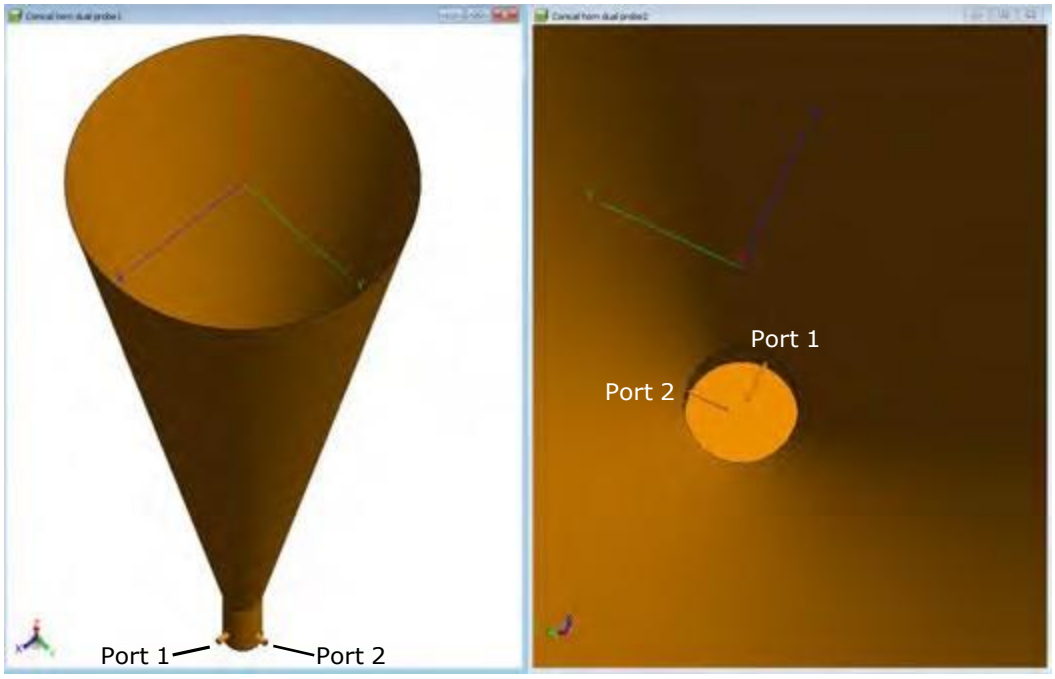

Figure 2-11: Conical horn antenna designed to match the dimension of fabricated antenna in FEKO including the dual polarised ports.

For this modified FEKO version, two launchers that represent Port 1 and Port 2 have been set to excite the launchers in TEM mode. This provides a more realistic simulation compared to that of Section 2.5. The yz-plane still represents the ground plane. Similar measurements have been conducted for HPBWs and SLLs in both planes and both polarisations. With this feeding method, the S-parameters have been measured from the simulation.

The revised conical horn has been designed by choosing the diameter of the waveguide to only allow the fundamental mode to propagate. FEKO has a built in iterative optimiser that takes in a range of the waveguide diameter steps to find the best response. The optimiser found that a waveguide diameter of 24 mm provides the best response. The feeding method has been implemented in the same manner as the modified FEKO version. The same methods and equations in Sections 2.3.5 and 2.4.3 have been followed in designing the circular waveguide

and conical horn with the waveguide diameter l_g = 24 mm. The detailed calculation is shown in Appendix H. The probe length has been kept at $\lambda_\circ/4$ without tuning.

2.5.4 Discussion

FEKO simulations have been successful and showed that both antennas can achieve close to the required azimuth HPBW in both polarisations. However, even with the symmetrical dimensions in both planes of the antennas, it is not possible to achieve exactly 10° azimuth HPBW due to the different distributions in either polarisations as discussed in Section 2.3.2. Table 2-5 shows the square and conical horn results simulated in FEKO.

Table 2-5: FEKO results comparison between square and conical horn antenna.

		V-Polarisation		H-Polarisation		Gain	
	Plane	**HPBW**	**SLL**	**HPBW**	**SLL**	**Calc.**	**FEKO**
Square	**Elevation**	12.4°	−27.91 dB	9.2°	−9.11 dB	23.54 dBi	23.85 dBi
	Azimuth	9.2°	−9.09 dB	12.4°	−27.95 dB		
Conical	**Elevation**	10.6°	−38.71 dB	9.1°	−19.27 dB	23.84 dBi	24.19 dBi
	Azimuth	9.1°	−19.28 dB	10.6°	−38.67 dB		

The square horn has an approximate 3° difference between the azimuth HPBWs in both polarisations ($\theta_{az(V\text{-}pol)}$ = 9.2°, $\theta_{az(H\text{-}pol)}$ = 12.4°) and has a high SLL in the V-polarised azimuth plane of −9.09 dB. As mentioned in Section 2.5.2 for the conical horn antenna, the shoulders that appear at both −15° and 15° are not first sidelobes. However, the shoulder for the square horn that appear at both −15° and 15° are the first sidelobes due to dipping to a null and change in gradient and thus results in a poor SLL. On the other hand, the conical horn has an approximate 1° difference between the azimuth HPBWs in both polarisations ($\theta_{az(V\text{-}pol)}$ = 9.1°, $\theta_{az(H\text{-}pol)}$ = 10.6°) and excellent SLL in the azimuth plane of −19.28 dB and −38.67 dB in V- and H-polarisations respectively.

Comparing the 3D radiation pattern of the two antennas, it can be observed that the square horn has large sidelobes in one plane, which explains the high SLL in the V-polarised azimuth plane. However, the conical horn has an improved main lobe with small sidelobes in both planes. Only the conical horn antenna has a HPBW error margin within ±1° of 10° for both polarisations. Both antennas have above 23 dBi gain, moreover the conical horn has a higher gain because of its larger aperture size. The difference in value between the calculated gain and FEKO gain is due to the estimated radiated efficiency for the calculated gain.

The conical horn has lower SLLs and the HPBW in both polarisations are close to the required 10°. The conical horn has a shorter length and larger aperture compared to the square horn as well as better overall results. Therefore, the conical horn antenna has been chosen to be developed further.

The manually designed dual probes and coaxial launchers have been implemented in the modified and revised design in FEKO. As discussed earlier, it was not known whether this feeding method would yield proper results in FEKO. Nevertheless, since the prototype has been fabricated, comparisons have been made to determine whether this feeding method will be successful in Chapter 3.

Chapter 3

Fabrication and Testing

This chapter provides a detailed description of the waveguide and the flared conical horn fabrication process. Furthermore, this chapter describes all the equipment used, explains all the testing procedures, and the locations chosen for testing radiation pattern measurements. A modified version of the antenna was simulated in FEKO to match the fabricated antenna and a FEKO revised version was also simulated that ignores the limitation of resources. Neither the modified nor the revised version of the antennas used the 'waveguide port' function. The feeding method of manually designed probes and launchers in FEKO is included in this chapter.

3.1 Fabrication

After completion of all the calculations and FEKO simulations on the conical horn antenna and the waveguide, the antenna was ready to be fabricated as the first experimental prototype. The horn antenna has been made from 2 mm thick aluminium plates. Aluminium plates are fairly lightweight, easy to bend, roll, and drill.

3.1.1 Waveguide Fabrication

Standard 2 mm thick aluminium water pipes with a diameter of 28 mm have been chosen because of the small hollow tube size. The flanges have been fabricated by the Mechanical Workshop at UCT. The pipes have been cut into 50 mm in length, welded with a flange, and one side of the pipe sealed. Figure 3-1 shows the completed waveguide.

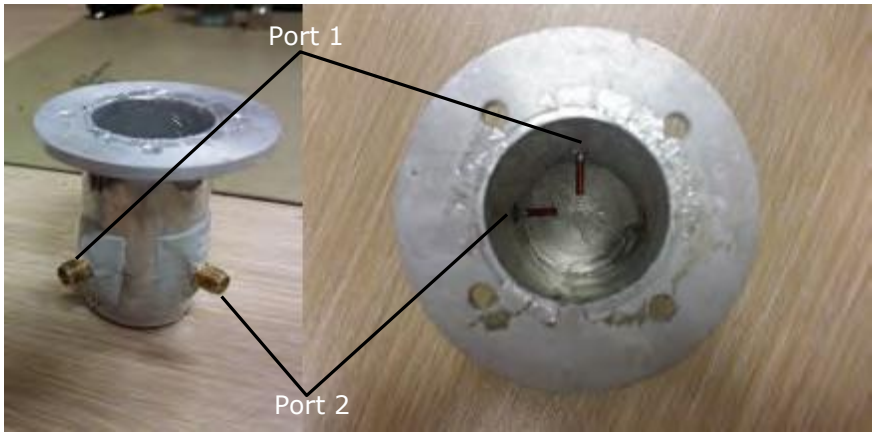

Figure 3-1: Dual polarised waveguide fabricated from aluminium water pipe.

In Figure 3-1, two SMA launchers with quarter-wave probes are attached to the waveguide orthogonal to each other for dual polarisation. SMA launchers have been used due to their compact size and their ability to operate at high frequencies, including X-band. Steel putty has been used to attach the two SMA launchers to avoid nuts and bolts interfering with the performance. The steel putty has been applied on the flanges of the SMA connectors. The resistivity does not make a difference because it has been used for structural integrity on the outer surface and should therefore not cause any interference. Port 1 has been tested as V-polarisation and Port 2 as H-polarisation.

To match the probe to the waveguide, the probe has been soldered with a length longer than $\lambda_0/4$ and connected to the network analyser to find the best reflection coefficient. The length of the probe was then gradually shortened until the reflection coefficient was at an acceptable level of less than -10 dB. The length of the probe for optimum performance was 11 mm long and the backshort length was 14 mm. Both lengths are slightly longer than the calculated probe and backshort lengths, but the differences were negligible.

3.1.2 Conical Horn Fabrication

The conical horn has been drawn in AutoCAD. Flanges have been designed to be welded onto the horn and waveguide so they can be assembled together. The calculations, AutoCAD drawings of the flat horn, bracket, and flanges are shown in Appendix G.

The horn drawing has been sent to 'CFW Fans (Pty) Ltd', a metalwork company, for fabrication. The slanted structure of the conical horn makes it difficult to mount the horn on any tripod or stand. Thus a bracket has been designed to be welded onto the horn for an easier tripod mount. Figure 3-2 shows the completed conical horn with its flange attached, the bracket, and the waveguide screwed onto the opening of the horn.

Figure 3-2: The manufactured conical horn with the dual polarised waveguide.

Due to physical constraints in the rolling process, the horn has not been fabricated perfectly. The plate has been 'bent' into sections as shown in the right photo of Figure 3-2. The fabricated inner diameter of the aperture, D, is 248 mm and the length of the horn, l_h, is 510 mm. However, the dimension of the opening, l_g, is 28 mm in diameter so the waveguide, which is also 28 mm in diameter, aligned with the conical horn.

3.2 Equipment

The following essential equipment has been used for testing the various antenna parameters and can be seen in Figure 3-3:

(a) Reference X-band horn antenna (Transmitting antenna or transmitter)

(b) Prototyped conical horn antenna with dual feed waveguide (Receiving antenna or receiver)

(c) SMA cables (Coaxial cables)

(d) Rotatable tripod mount

(e) Rohde & Schwarz SMF 100A Signal Generator [19]
(Operating freq. up to 170 GHz, output power of +25 dBm)

(f) ThinkRF WSA5000-220 Spectrum Analyser [20]
(Operating freq. up to 20 GHz, instantaneous bandwidth 100 MHz, noise figure of < 15 dB)

(g) Agilent Technologies PNA-X Network Analyser N5247A [21]
(Operating freq. up to 67 GHz, noise floor of -118 dBm, output power of 13 dBm)

(h) Termination SMA 50 Ω DC-18 GHz MCL Anne-50+

Figure 3-3: Equipment required for the testing procedure.

The equipment have been set up in the appropriate location for testing, which will further be elaborated upon in Section 3.3 and Section 3.4.

3.3 Testing Locations

When an antenna is transmitting, EM waves can be reflected off objects and the environment, such as walls, the ground, poles, etc. These EM waves can still be received by the receiving antenna, which is known as multipath. For antenna testing, multipath can be an issue because the receiving antenna can receive EM waves in different directions and consequently, it would be difficult to determine if the received wave is a multipath or the sidelobes of the antenna.

Anechoic chambers are designed to reduce the effects of multipath interference. This allows for more accurate and repeatable testing of antennas. Without access to an anechoic chamber at local facilities, testing of the antenna can only be performed in areas where there are minimal obstructions to avoid multipath. This can be challenging because to find a reflection-free environment is impossible. The best solution has been to test the areas where there are minimal obstructions. The two locations (both at UCT upper campus) that have been chosen were the Sports Centre and the rooftop of Menzies Building. The configuration of the two antennas are shown in Figure 3-4.

UCT Sports Centre

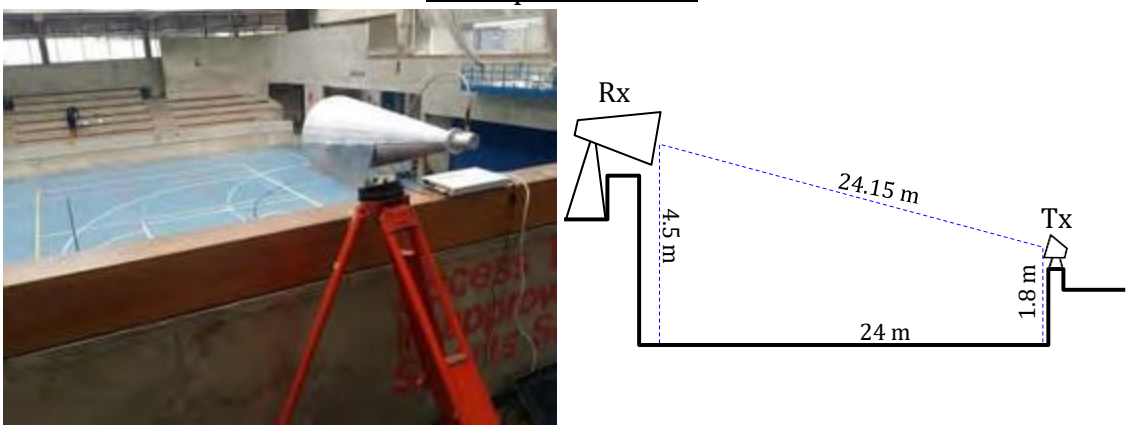

Menzies Building Rooftop

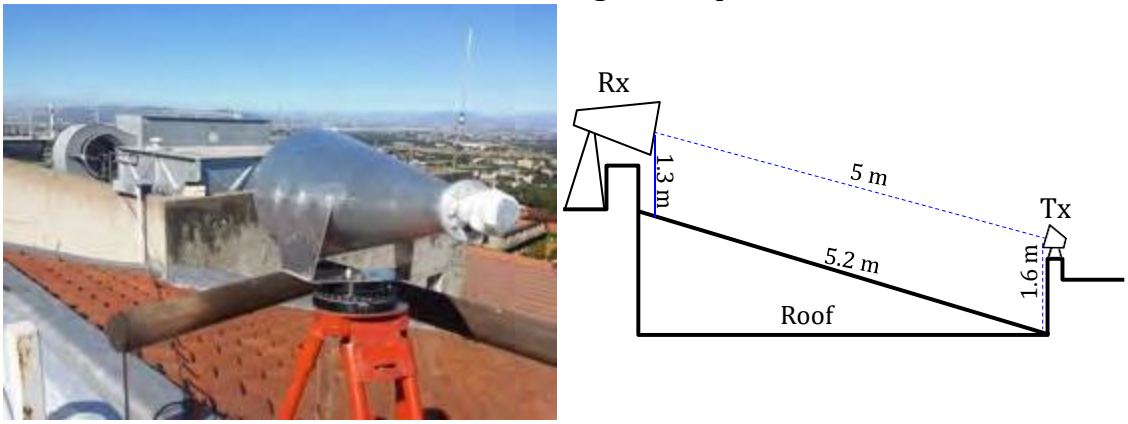

Figure 3-4: Photos and side view of the testing configurations at UCT Sports Centre and Menzies Building rooftop.

Both antennas need to be placed at least in the far field region. Using (A-4) the far field region is:

$$d > \frac{2D^2}{\lambda_\circ}$$

$$d > \frac{2 \times (248\ \text{mm})^2}{35.29\ \text{mm}}$$

$$d > 3485.63\ \text{mm} \approx 3.49\ \text{m}$$

Therefore, the two antennas need to be placed at least 3.49 m apart to measure the radiation pattern in the far field region. The line of sight (LOS) between the antennas were 24.15 m and 5 m apart in the Sports Centre and Menzies rooftop respectively. The Sports Centre has a large open area, and it also eliminates weather interference such as wind. The rooftop of

Menzies Building does not have several obstructions which eliminates most of the multipath interference, and the configuration also reduces ground reflections.

3.4 Testing Procedure

Two main tests have been done: S-parameters measurement and radiation pattern measurements. The S-parameters measurement has been used to analyse the reflection coefficient of each port and the isolation between the two ports. The radiation patterns obtained in the the azimuth and elevation plane can be used to analyse the HPBW and SLL in their respective planes. Specifications and references to the equipment are in Section 3.2.

3.4.1 S-Parameters Measurement

S-parameters or scattering parameters are complex, linear quantities used to describe the input-output relationship between two ports in an electrical system [22]. They are useful for systems operating at high frequencies and measured using modern network analysers. The S-parameters are represented as S_{mn} where 'm' indicates the input port number and 'n' indicates the output port number. The S-parameters for a two-port system are as follows [23]:

- S_{11} - Forward reflection coefficient (input match)
- S_{22} - Reverse reflection coefficient (output match)
- S_{21} - Forward transmission coefficient (gain or loss)
- S_{12} - Reverse transmission coefficient (isolation)

Figure 3-5 describes how each S-parameter is measured in a two-port device under test (DUT).

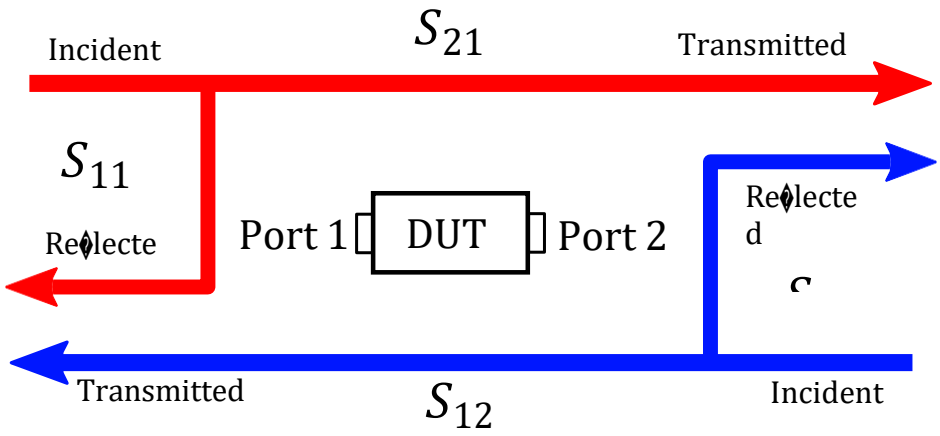

Figure 3-5: S-parameters measurement of a two port network [23].

The unit for S-parameters are in decibels and can be represented as a percentage:

$$S_{mn} = 10^{\frac{S_{mn(dB)}}{10}} \times 100 \quad [\%] \tag{3-1}$$

If the value is less than 0 dB, this implies that there are power losses. A value greater than 0 dB implies the gain is amplified. For antennas, the most common measurement is S_{11} which measures the amount of power that is reflected back to the input port. For example, if $S_{11} = -10$ dB, when port 1 transmits at 100 W, 90 W is radiated, and 10 W is reflected back into port 1 which is referred to as power loss. Better impedance matching between the coaxial to waveguide transition will lead to lower power loss.

The network analyser, shown in Figure 3-3(g), can perform calibrations to remove background noises and losses in the cables at 8.5 GHz. After the calibrations, the network analyser has been connected directly to the antenna. The measurements for the S-parameters have been saved into an Excel spreadsheet, the data analysed, and measurements including the responses at centre frequency and instantaneous bandwidth have been determined.

3.4.2 Radiation Pattern Measurements

Two antennas are placed apart in the far field region to measure the radiation pattern of the antenna in the elevation and azimuth plane. The following procedure has been used to test the antenna's radiation pattern:

1. A stationary horn antenna has been used as the transmitter. The linearly polarised horn antenna has been connected to the signal generator via SMA cables. The signal generator has been set to transmit a power of 30 dBm.

2. The prototyped conical horn antenna is the receiver which has been mounted on a rotatable tripod. The prototype has been connected to the ThinkRF via SMA cables and has the same polarisation as the transmitter. The ThinkRF has been connected to the laptop via CAT-6 Ethernet cable with RJ45 connectors and is responsible for receiving the data. The data has been observed on the laptop in real time and recorded for later analysis.

3. The rotatable tripod can only rotate in the azimuth plane. Only Port 1 has been connected to the ThinkRF to test for its radiation pattern in the azimuth and elevation planes while Port 2 has been terminated with a 50 Ω terminator.

4. Both antennas have been placed in the far field region with a height separation from ground level to minimise ground reflection. At UCT Sports Centre, the transmitter and receiver has a 1.8 m and 4.5 m height separation from ground respectively. On the Menzies Building Rooftop, the transmitter and receiver has a 1.6 m and 1.3 m height separation from ground respectively.

5. Since both antennas are not in the same height level and the LOS plane is slanted, the tripod is elevated downwards and the transmitting antenna is elevated upwards so both antennas are in the same plane as LOS as shown in the side-view diagrams of Figure 3-4.

6. While the transmitter has been transmitting at 30 dBm, the conical horn has been rotated through 360° in increments of 1°. The received power has been recorded for all angles in the given range in both polarisations by the ThinkRF.

7. When both antennas are V-polarised, the azimuth plane of the radiation pattern has been recorded following Step 6. Both antennas have been rotated 90° so that they are both H-polarised. The elevation plane of the radiation pattern has been recorded.

8. The recorded data has been saved into an Excel spreadsheet and has been plotted into MATLAB to analyse the results.

9. The whole process has been repeated with one small difference, Port 2 has been set as active and Port 1 has been terminated. This allows elevation and azimuth radiation pattern measurements for Port 2.

After completion of testing, the elevation and azimuth radiation patterns have been measured for both planes of polarisation.

3.5 Discussion

The dimensions of the circular waveguide and conical horn for the prototype, modified FEKO and revised FEKO design have been summarised in Table 3-1. The modified and revised design have been discussed earlier in Section 2.5.3 and the dimensions of the revised design are found in Appendix H.

Table 3-1: Dimensions of the circular waveguide and conical horn for the prototype, modified FEKO and revised FEKO designs.

	Dimension	Prototype and Modified FEKO Design	Revised FEKO Design
Circular Waveguide	l_g	28 mm in diameter	24 mm in diameter
	L_{probe}	11 mm	8.82 mm
	$L_{backshort}$	14 mm	17.40 mm
	$L_{waveguide}$	50 mm	69.62 mm
Conical Horn	l_h	510 mm	520.47 mm
	D	248 mm in diameter	247.06 mm in diameter

The dimensions of the prototype are similar to the calculated dimensions. The modified FEKO design has been re-simulated to match the prototype dimensions. Dual polarised ports that allowed a more realistic V- and H-polarised simulation have been inserted in the modified and revised FEKO designs. The revised version has been designed without the limitation of readily available hollow metallic tubes for the waveguide.

The waveguide and conical horn antenna have been fabricated using aluminium plates and water pipes, costing below ZAR 2 000 per antenna. Fabricating the conical shape is difficult because of the small dimension of the opening, l_g. Even though the dimensions of the prototype differ from the calculations due to physical constraints, there has not been a major size difference.

Finding a location that offers minimal multipath has been a challenge. Weather conditions should be optimal when using an outdoor location. It has been a challenge for the tripod mount to be rotated manually. Only the azimuth HPBW in V- and H-polarisations have

been part of the NeXtRAD requirements. Additionally, the elevation plane has been tested to characterise the complete specification of the conical horn if required for future work.

Chapter 4

Results

This chapter contains all the results obtained from the prototype and the simulated results from FEKO. The results need to be compared to determine the accuracy of the FEKO models, and simultaneously analyse whether the prototype achieved the NeXtRAD antenna specifications. The comparison involves the prototype, modified FEKO design, and revised FEKO design of the antenna.

4.1 S-Parameters Result

The S-parameter measurements of the prototype, modified and revised designs have been acquired. Different colours are used to distinguish between the graphs in the following plots. Blue represents S_{11}, red S_{12}, and green S_{22}. The S_{12} and S_{21} parameters for all the designs are nearly identical, thus S_{21} has been omitted.

4.1.1 Fabricated Design S-parameters

Figure 4-1 illustrates the S-parameters measured using a network analyser over the 6.5 GHz to 10.5 GHz range. The key at the top right corner of the graph lists the responses at 8.5 GHz.

Figure 4-1: S-parameters of the dual polarised antenna measured by the network analyser.

The data in Figure 4-1 is difficult to analyse due to the wide frequency range. Figure 4-2 has been plotted using Excel to investigate the data between 8 GHz and 9 GHz.

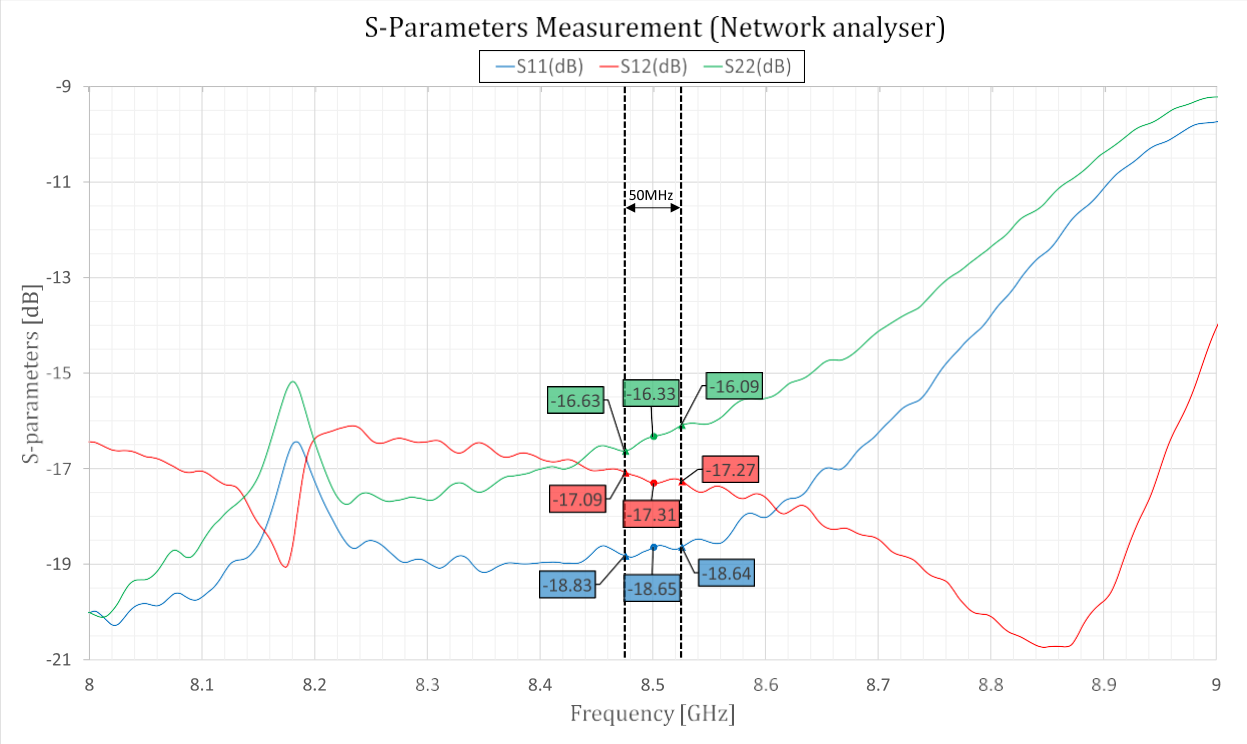

Figure 4-2: Prototyped antenna S-parameters graph between 8 GHz and 9 GHz.

At 8.5 GHz, the reflection coefficient for Port 1 (S_{11}) and Port 2 (S_{22}) are -18.65 dB and -16.33 dB respectively. From (3-1), this implies 1.36%[1] and 2.33%[2] of the incident power is being reflected back to port 1 and port 2 respectively. The response of S_{12} is -17.31 dB, implying that on transmission, only 1.86% of the transmitted power will be received by the other port.

4.1.2 Modified FEKO Design S-Parameters

Figure 4-3 shows the plot of the S-parameters measurement from the modified FEKO design.

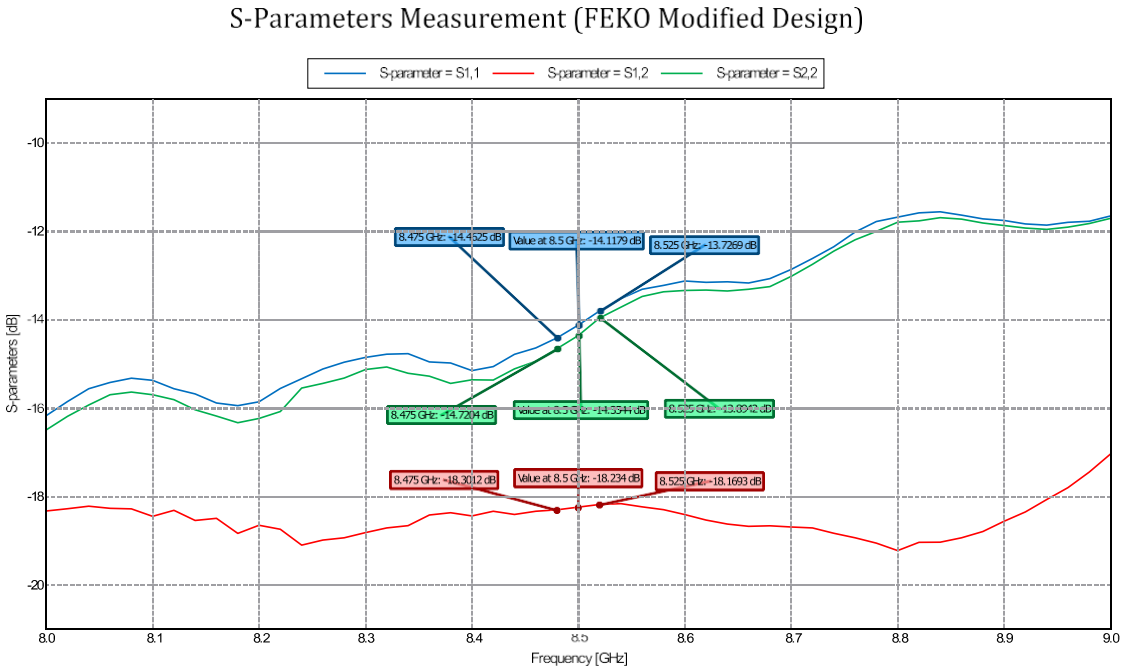

Figure 4-3: Modified FEKO design S-parameters graph between 8 GHz and 9 GHz.

The S-parameters of the modified FEKO design are below -14 dB at 8.5 GHz. This implies that more than 90% of the power is being radiated and less than 2% is being transmitted between the two ports. An instantaneous bandwidth of 50 MHz (8.5 GHz $\pm$ 25 MHz) has been measured on all plots.

[1] $S_{11} = 10^{S_{11}\ [\mathrm{dB}]/10} \times 100 = 1.36\%$
[2] $S_{22} = 10^{S_{22}\ [\mathrm{dB}]/10} \times 100 = 2.33\%$

4.1.3 Revised FEKO Design S-parameters

Figure 4-3 shows the plot of the S-parameters measurement from the revised FEKO design.

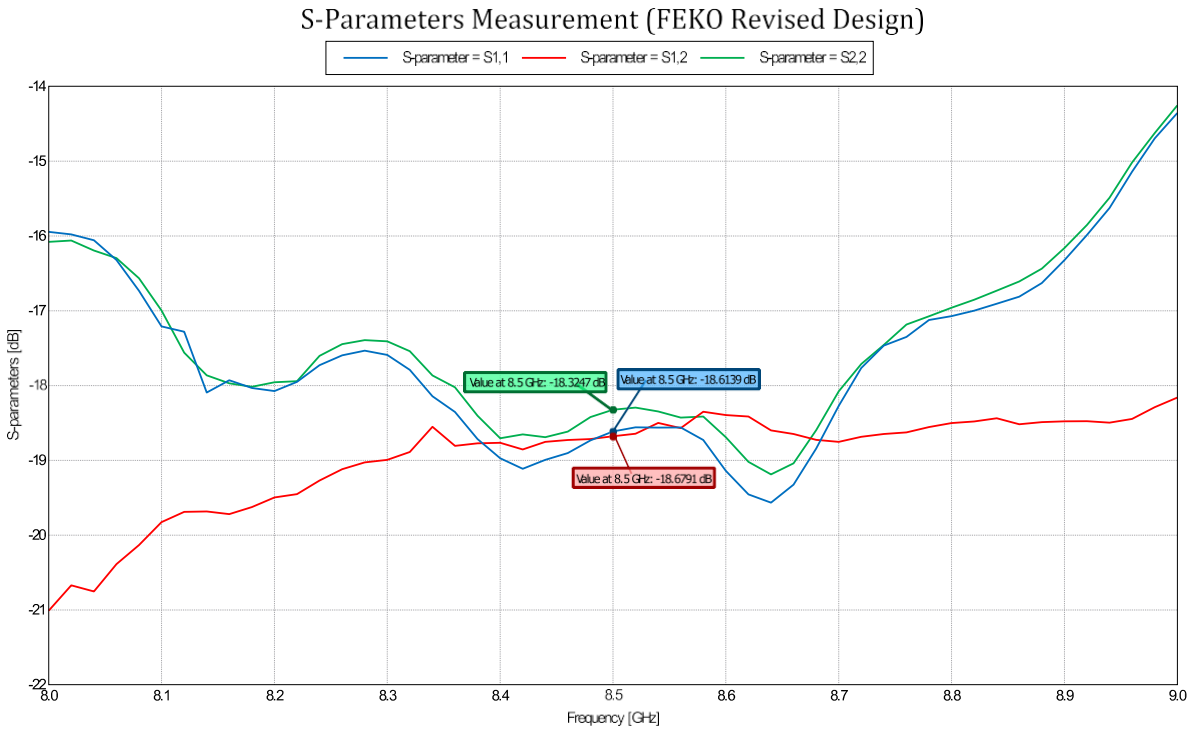

Figure 4-4: Revised FEKO design S-parameters graph between 8 GHz and 9 GHz.

The revised FEKO design provided the best set of S-parameters measurements. The reflection coefficients for S_{11} and S_{22} are -18.61 dB and -18.32 dB respectively. The transmission coefficient S_{12} is -18.68 dB.

4.1.4 Discussion

Table 4-1 summarises the important traces obtained from the prototype and both FEKO S-parameters results.

Table 4-1: Two-port S-parameters results comparison between prototype and FEKO (modified and revised version) dual polarised horn antenna.

		Centre Frequency	**Instantaneous Bandwidth**	
	S-Parameter	**8.5 GHz**	**8.475 GHz**	**8.525 GHz**
Network Analyser	S_{11}	−18.65 dB	−16.63 dB	−16.09 dB
	S_{12}	−17.31 dB	−18.83 dB	−18.64 dB
	S_{22}	−16.33 dB	−17.09 dB	−17.27 dB
FEKO Modified Design	S_{11}	−14.12 dB	−14.46 dB	−13.73 dB
	S_{12}	−18.23 dB	−18.30 dB	−18.17 dB
	S_{22}	−14.35 dB	−14.72 dB	−13.89 dB
FEKO Revised Design	S_{11}	−18.61 dB	−18.78 dB	−18.56 dB
	S_{12}	−18.68 dB	−18.72 dB	−18.61 dB
	S_{22}	−18.32 dB	−18.47 dB	−18.31 dB

Observing the reflection coefficients S_{11} and S_{22} in Table 4-1, the responses are nearly identical for the modified and revised designs because both ports have been simulated with the same dimensions. The prototype's reflection coefficients showed a 1 dB difference between them. The fabrication process introduces the possibility of human errors such as different lengths of the probe and the backshort, soldering of the probes onto the SMA launcher, and the straightness of the probes. Even slight length differences can have an effect on the responses.

In Figure 4-1, the responses worsen for frequencies higher than 8.5 GHz where the reflection coefficients of both ports and transmission coefficient between the ports increase simultaneously. On the other hand, between 6.7 GHz and 8.9 GHz, all the responses are below −10 dB, which implies that both the reflection coefficients and transmission coefficient are less than 10%. Therefore, the prototype operates efficiently in a wide band.

Since the modified design has been simulated according to the dimensions of the prototype, comparisons have been made between them. The prototype surpasses the simulation, showing a reflection coefficient of less than −16 dB for both ports. The simulation has an improved isolation of approximately −1 dB. Overall, the prototype performs better than the modified FEKO design in terms of efficiency. The antenna operates efficiently within the

50 MHz bandwidth.

Both the modified and revised measurements showed efficient responses. The revised version, however, showed superior reflection coefficients. Additionally, the S_{11} and S_{22} plots provide an excellent response from 8.3 GHz through 8.7 GHz. The revised design has not been fabricated, thus the experimental results have not been obtained. Analysis of the prototype and modified FEKO design shows a high possibility that fabricating the revised design would provide similar or better results than the FEKO version.

4.2 Radiation Pattern Results

Following the design and testing procedures outlined in Section 3.4, radiation patterns in V- and H-polarisation have been generated. HPBWs and SLLs have been measured in the elevation and azimuth plane. The results obtained from the field test have been represented on Cartesian plots.

4.2.1 UCT Sports Centre Radiation Pattern

UCT Sports Centre has been selected due to the spacious area, and to avoid the windy weather in Cape Town. Figure 4-5 shows the radiation pattern results obtained from the Sports Centre. The HPBW and SLL measurements is shown in the top left corner of each graph.

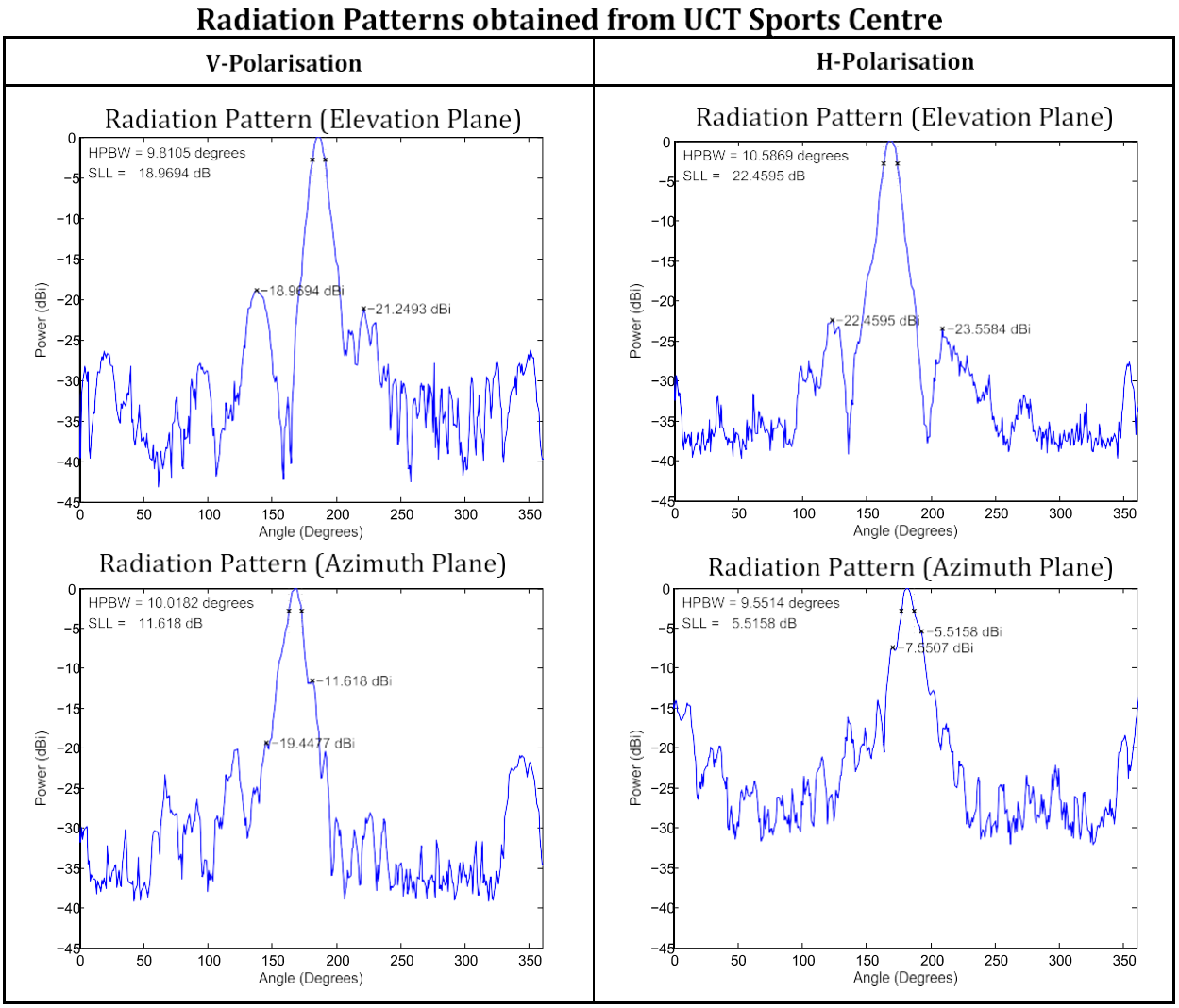

Figure 4-5: Radiation pattern results from UCT Sports Centre including both polarisations, both planes, and HPBW and SLL measurements.

Without a standard gain antenna, the gain of the prototype has not been tested. The gain of the prototype has been calculated using (A-9) and (A-12) by inserting the measured elevation and azimuth HPBWs and assuming $\eta = 0.5$ [17]. Using the V-polarisation's HPBWs, $\theta_{el} = 9.81^{\circ}$ and $\theta_{el} = 10.02^{\circ}$ from Figure 4-5, the gain is calculated to be:

$$
\begin{aligned}
G &= \eta Dir \\
&= \eta \times \frac{41253}{\theta_{\text{el}}\theta_{\text{az}}} \\
&= 0.5 \times 9\frac{41253}{.81^\circ \times 10.02^\circ} \\
&= 209.84 \\
&\approx 23.22 \text{ dBi}
\end{aligned}
$$

In Figure 4-5, the HPBW measurements from the four graphs are close to the required 10°. The SLLs for both elevation planes are below -18 dB, but are not acceptable for both azimuth planes (-11.62 dB and -5.52 dB for V- and H-polarisations respectively). In all four graphs, asymmetry, irregular high peaks, and main lobe distortion are present. It can therefore be assumed that the antenna is detecting multipath and interference. This led to the understanding that another iteration of the test should be carried out at a more appropriate location. The Menzies Building rooftop has been the next best available location.

4.2.2 Menzies Building Rooftop Radiation Pattern

Figure 4-6 shows the radiation pattern results obtained from Menzies rooftop. The HPBW and SLL measurements is shown in the top left corner of each graph.

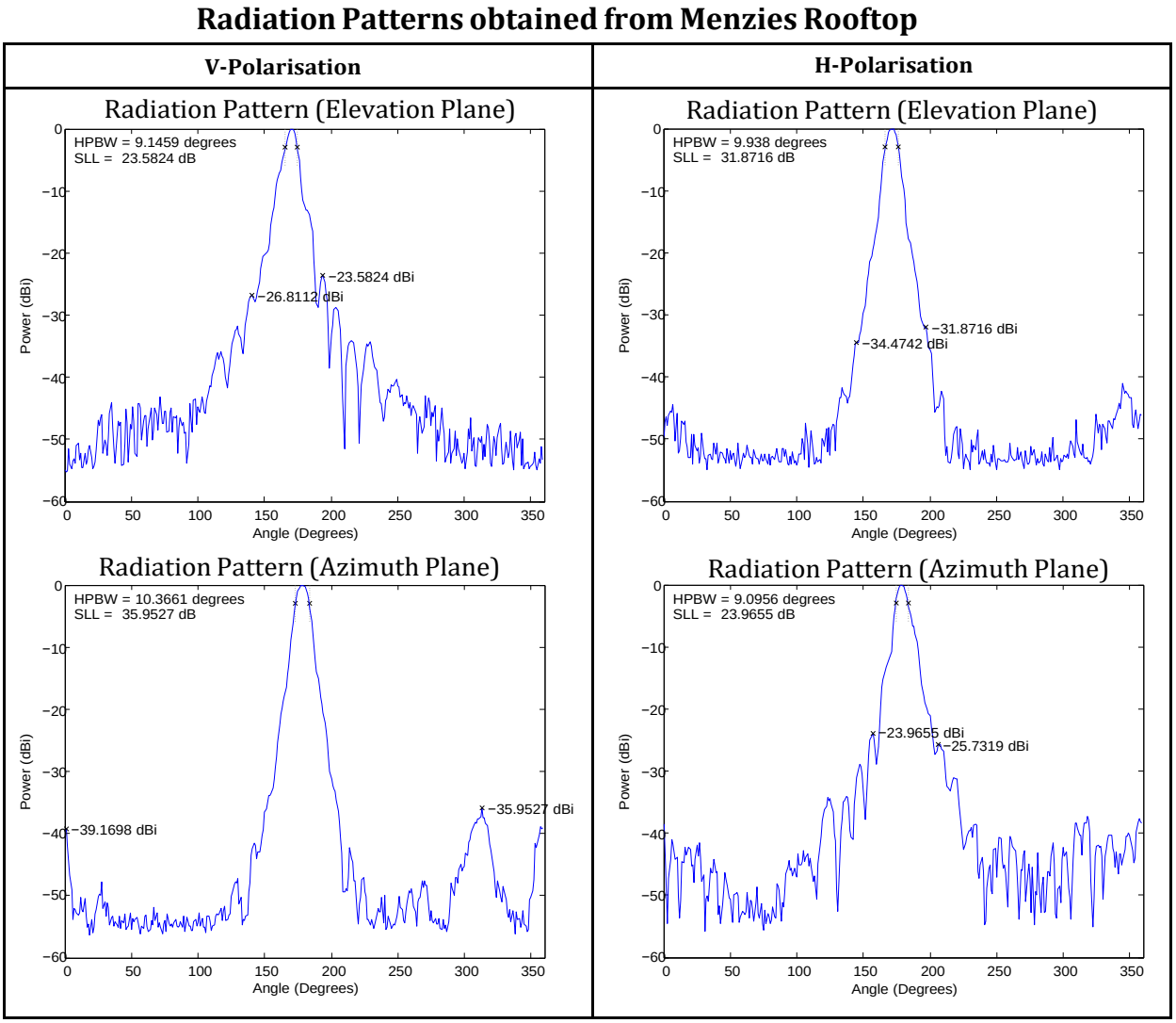

Figure 4-6: Radiation pattern results from Menzies rooftop including both polarisations, both planes, and HPBW and SLL measurements.

In Figure 4-6, the results show low SLLs in comparison to the measurements in the Sports Centre. This proves the assumption that the Sports Centre introduces unwanted interference. A pole has been present behind the prototype while recording in the V-polarised azimuth plane which resulted in a peak on the right side of the main lobe in the following plot. The pole has been removed to avoid interference for the other data. Using the V-polarisation's

HPBWs, $\theta_{el} = 9.14^{\circ}$ and $\theta_{az} = 10.37^{\circ}$ from Figure 4-5, the gain was calculated to be:

$$\begin{aligned} G &= 0.5 \times \frac{41253}{9.14^{\circ} \times 10.37^{\circ}} \\ &= 217.83 \\ &\approx 23.38 \text{ dBi} \end{aligned}$$

The gain value is similar to the one obtained from the Sports Centre's measurement.

4.2.3 Modified FEKO Design Radiation Pattern

The modified FEKO design of the antenna in Figure 4-7 shows the polar and Cartesian plots of the radiation pattern in V- and H-polarisations. The HPBW and SLL measurements is shown on the plots.

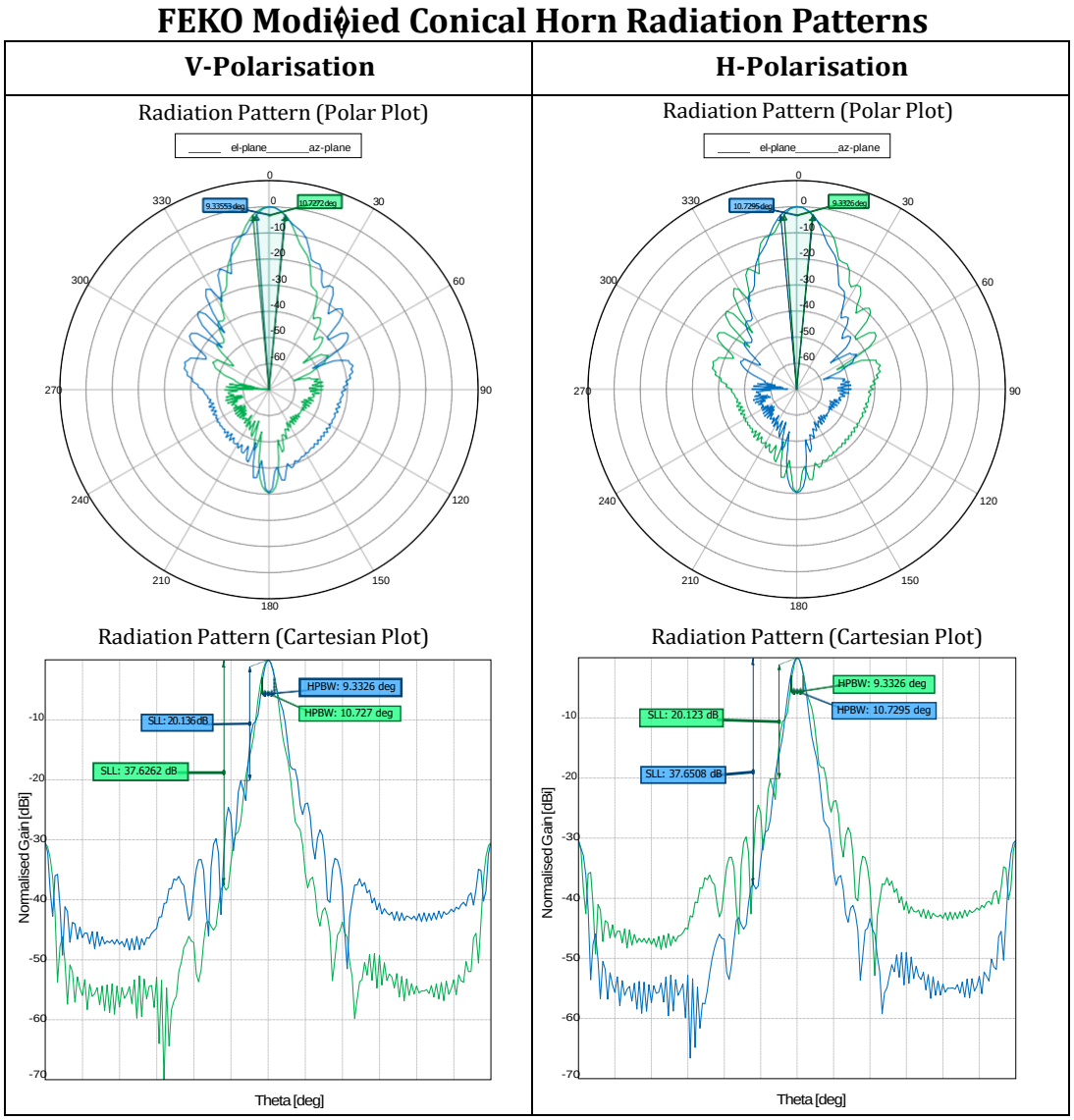

Figure 4-7: Modified FEKO design of the polar and Cartesian plots including both polarisations, both planes, and HPBW and SLL measurements.

The azimuth HPBWs in both polarisations are $\theta_{az(V\text{-}pol)} = 10.73^{\circ}$ and $\theta_{az(H\text{-}pol)} = 9.33^{\circ}$, which are closely aligned to the NeXtRAD required azimuth HPBW of 10°. The SLLs in the azimuth plane are -37.63 dB and -20.12 dB in V- and H-polarisations respectively. The gain has been predicted to be 23.97 dBi in FEKO.

4.2.4 FEKO Revised Design Radiation Pattern

The revised FEKO version of the antenna in Figure 4-8 shows the polar and Cartesian plots of the radiation pattern in V- and H-polarisations. The HPBW and SLL measurements is shown on the plots.

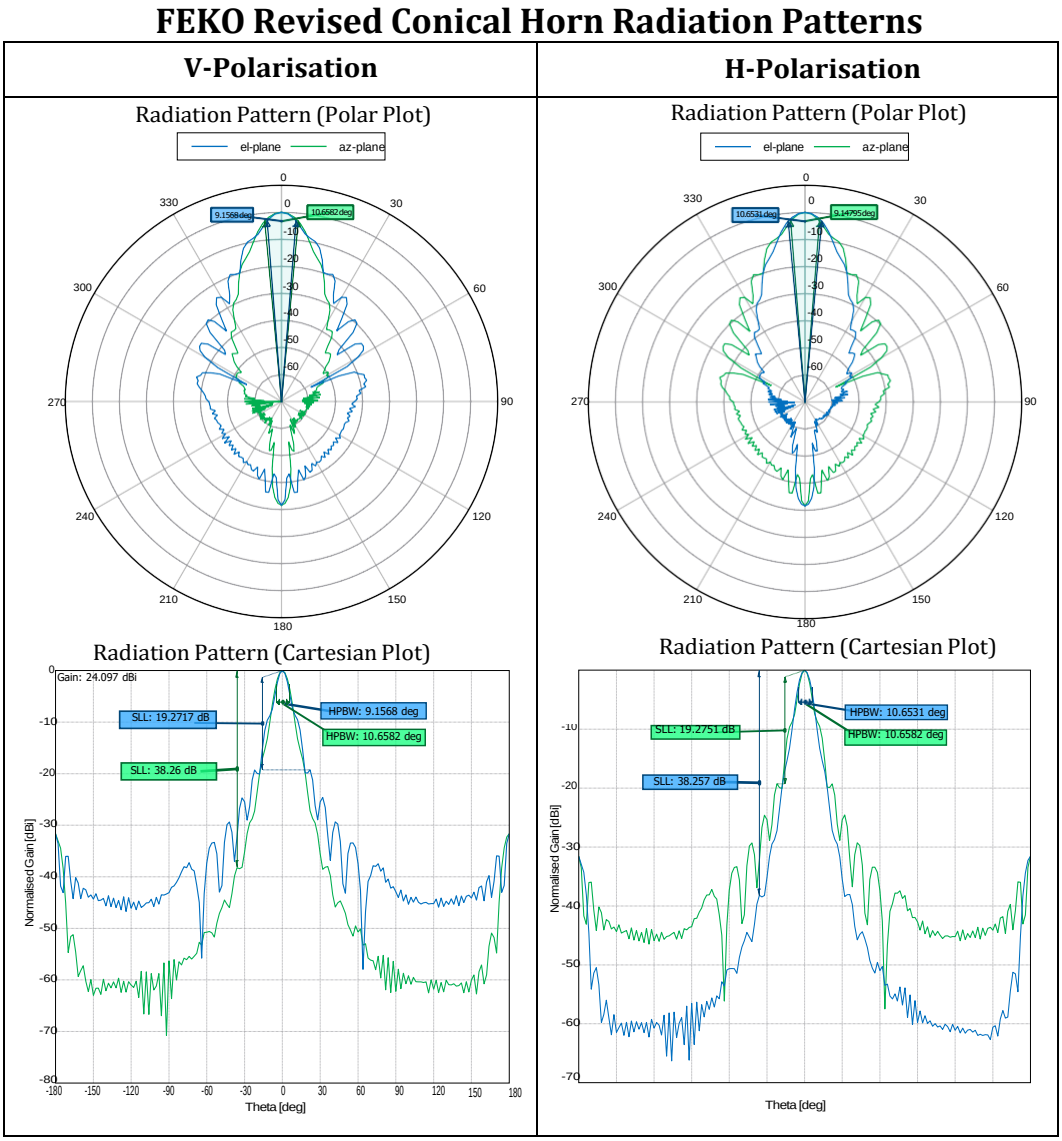

Figure 4-8: Revised FEKO design of the polar and Cartesian plots including both polarisations, both planes, and HPBW and SLL measurements.

The revised and modified versions of the plots show that the measurements are similar. Additionally, the HPBWs and SLLs are also similar with reduced SLLs. The azimuth HPBWs in both polarisations are $\theta_{\text{az(V-pol)}} = 10.66^{\circ}$ and $\theta_{\text{az(H-pol)}} = 9.15^{\circ}$, which are closely aligned

to the required azimuth HPBW of 10°. The SLLs in the azimuth plane are −31.64 dB and −19.28 dB in V- and H-polarisations respectively. The gain has been predicted to be 24.11 dBi in FEKO.

4.2.5 Discussion

The results of this chapter have been summarised in Table 4-2 which includes V- and H-polarisations in the elevation and azimuth plane.

Table 4-2: Radiation pattern results comparison between UCT Sports Centre, Menzies rooftop, modified and revised FEKO design. The measurements include HPBW, SLL, and gain.

		V-Polarisation		H-Polarisation		
		HPBW	**SLL**	**HPBW**	**SLL**	**Gain**
UCT Sports Centre	**El-plane**	9.81°	−18.97 dB	10.59°	−22.46 dB	23.22 dBi
	Az-plane	10.02°	−11.62 dB	9.55°	−5.52 dB	
Menzies rooftop	**El-plane**	9.15°	−23.58 dB	9.94°	−31.87 dB	23.37 dBi
	Az-plane	10.37°	−35.95 dB	9.10°	−23.97 dB	
FEKO Modified Design	**El-plane**	9.34°	−20.14 dB	10.73°	−37.65 dB	23.97 dBi
	Az-plane	10.73°	−37.63 dB	9.33°	−20.12 dB	
FEKO Revised Design	**El-plane**	9.16°	−19.27 dB	10.65°	−38.26 dB	24.11 dBi
	Az-plane	10.66°	−38.26 dB	9.15°	−19.28 dB	

All of the HPBW measurements are close to the required 10°. The Sports Centre's SLL values are not the actual sidelobes of the antenna, but a measurement of the interference. Radiated power has been reflected off small objects and obstructions inside the Sports Centre, despite the large spacious area.

The rooftop location shows a large decrease in interference. This confirms that the rooftop has minimal multipath interference. The SLLs are below −20 dB for both polarisations in both planes. Analysing the azimuth HPBW of both polarisations, the antenna achieved azimuth HPBWs of $\theta_{\text{az(V-pol)}} = 10.37°$ and $\theta_{\text{az(H-pol)}} = 9.10°$. The gain of the prototype and FEKO design are similar, even when using the radiation efficiency assumption of 0.5. The antenna therefore has a high gain of 23.97 dBi.

The best comparison is to compare outside measurements with anechoic chamber measurements. However, without anechoic chamber measurements, the only comparison that can be done is with simulation results. The simulation achieved azimuth HPBW of 10.73° and 9.33°

when V- and H-polarised respectively. In comparison to the azimuth HPBW of the prototype when V- and H-polarised respectively, there is approximately 0.23° to 0.36° difference, thus an accuracy of up to one decimal place.

Comparing the graphs of the prototype and the modified FEKO antenna (Figure 4-6 and 4-7 respectively), the radiation patterns are aligned well. Figure 4-9 shows the polar plot comparisons of V- and H-polarisations in the azimuth plane between Menzies rooftop, the FEKO modified and revised designs.

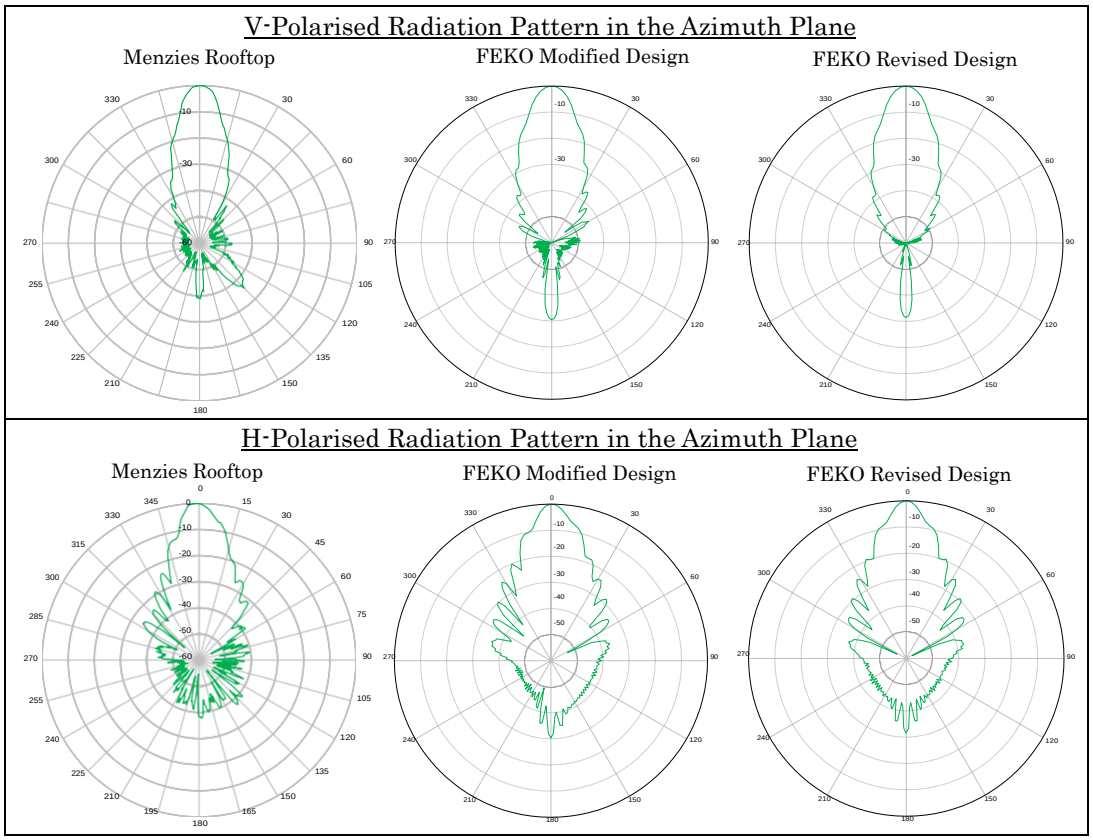

Figure 4-9: Polar plot comparisons of V- and H-polarisations in the azimuth plane between the prototype, modified and revised designs.

In Figure 4-9, comparing the Menzies rooftop and modified FEKO polar plots, the V-polarised main lobes are fairly smooth with low sidelobes. However, for the H-polarised plots, the body of the main lobe is slightly distorted. Therefore, the modified FEKO simulation matches the radiation pattern of the prototype. Furthermore, the method of manually designing the probes and coaxial launchers in FEKO has been successful and is reliable for simulating antennas with a dual polarised waveguide. As discussed in the design procedure, due to the availability of limited resources a 28 mm diameter waveguide has been fabricated.

The next higher-order TM_{01} mode has been excited, which, as a consequence caused a slight distortion in the main lobe. Even though operating at 300 MHz above the cutoff frequency of TM_{01} mode, the efficiency of the dual polarised antenna has not been compromised. The FEKO revised design only allowed the fundamental mode to propagate using a 24 mm diameter waveguide. The FEKO revised polar plot shows no distortions, while maintaining similar HPBW and SLL measurements as the modified FEKO design.

Chapter 5

Conclusions and Recommendations

5.1 Conclusions

The main objectives of this dissertation have been to design, simulate, and implement a dual polarised X-band antenna for the NeXtRAD project. The antenna specifications include operation in 8.5 GHz at X-band and produce an azimuth HPBW of 10° in both polarisations. The antenna will operate in outdoor conditions, therefore it must be portable and able to withstand strong winds. These objectives have been met and conclusions have been drawn based on the implementation and simulation results.

Dual Polarisation

The S-parameters measurement shows that the dual polarised antenna has reflection coefficients of -18.65 dB and -16.33 dB for Port 1 and Port 2 respectively. Furthermore, a transmission coefficient of -17.31 dB between the two ports has been measured. The reflection coefficients are dependent on the quality of soldering between the probe and the SMA launcher, as well as the length of the probe and backshort. With the current configuration, the antenna performs efficiently when dual polarised. Achieving high isolation between the ports has not been a part of the NeXtRAD requirements, however placing the two ports orthogonally has achieved high isolation. From the results it can be concluded that the equations used are reliable and dual polarised circular waveguides can be implemented on hardware.

Conical Horn Antenna

Originally, the conical horn FEKO simulation in Section 2.5.2 does not show any distortions due to the use of the 'waveguide port' function that only allows the fundamental mode to propagate. This configuration ignores any higher-order modes and it has later been discovered that simulating the coaxial launchers along with the probes provides results that correspond well with the experimental results. The 28 mm diameter waveguide introduces the next higher-order TM_{01} mode which creates a distortion in the radiation pattern. From the results of the revised FEKO design, the distortion has been avoided by choosing a 24 mm diameter waveguide. This results in a symmetrical radiation pattern without distortions while still meeting the required azimuth HPBW with below -20 dB SLL. Additionally, the simulation also showed improvements in the measurement of the S-parameters. Due to fabrication limitations, the 28 mm diameter water pipe has been the only feasible choice. The conical horns simulated in FEKO confirm that an X-band antenna is more sensitive to the diameter of the waveguide, whereas minor differences in the dimensions of the conical horn have negligible changes in the results.

The antenna has been simulated successfully in FEKO and the results achieved are close to the antenna specifications. Subsequently, the first antenna prototype has been sent for fabrication. In the absence of a standard gain antenna it was not possible to measure the experimental antenna gain. Nevertheless, according to the gain predicted from the simulations and the estimated gain equation, the antenna achieved a high gain with more than 23 dBi.

Experimental errors may have occurred while capturing the data due to the manual rotation of the rotatable tripod on which the antenna was mounted. Overall, the prototype and the modified FEKO results correspond well in terms of the HPBWs and S-parameters. Realistically, achieving azimuth HPBW of 10° in both polarisations is not possible. However, the prototype achieved an azimuth HPBW of $10^\circ \pm 1^\circ$ in both V- and H-polarisations. When V- and H-polarised respectively, the prototype achieved SLLs in the azimuth plane of -35.95 dB and -23.97 dB.

In comparison to the conical horn antenna and the square horn antenna from the simulations, prototype and the past project, it is concluded that the conical horn produces low sidelobes, and achieves close to 10° HPBWs in both polarisations in both planes. The square horn has not achieved close to 10° HPBWs in both polarisations and has larger sidelobes compared to the conical horn. Therefore, this dissertation concludes that the conical horn with the

circular waveguide is better suited for NeXtRAD.

Fabrication Limitations

Physical constraints in the fabrication process implied that the antenna could not be rolled into a smooth conical shape as desired. The presence of welding residue inside the antenna created bumps. The back wall of the waveguide also left some residue. Even though these bumps and residues affected the radiation pattern, it has been negligible. A comparison of the simulated and prototype radiation patterns confirmed that there is a low possibility that the performance of the antenna will be affected by the residue. The limitations in the fabrication process include the risk of human error, since part of the processes have been performed manually. However, this design is merely the first prototype and it performed well, especially the SLL and reflection coefficients. The material used for the antenna is aluminium, which makes it durable, fairly lightweight and able to withstand wind without shape distortion. As long as the antenna is mounted properly onto the tripod, it can operate effectively in the presence of wind. This conical horn antenna is the first of its kind which operates in the desired manner.

The S-parameters of the dual polarised circular waveguide determines the efficiency of the antenna radiation, which includes:

- Smoothness of the inner and back walls
- SMA launchers
- Identical lengths of the two probes
- Straightness of the probes
- Positioning of the launchers from the back wall
- How orthogonal the two probes are inserted

The probes are manually soldered on the SMA launchers, but are not screwed onto the waveguide. On the other hand, the antenna is able to achieve high reflection coefficients and isolation from the two ports despite the fabrication limitations.

Location

The rooftop test yields better results compared to the Sports Centre which in turn confirms that multipath interference can be detected even in a spacious enclosed area. The only enclosed area suitable for antenna testing is the anechoic chamber, because the reflections are suppressed by the strategically positioned absorbers. Even in the absence of an anechoic chamber, open area antenna testing (i.e., rooftop of Menzies Building) shows acceptable results with low interference.

FEKO

FEKO is a powerful EM simulation software that provides accuracy and precision, but software in general are based on algorithms that generate results which could have caused mismatch or the mismatch could be caused by the experimental errors. However, FEKO is a helpful tool for simulating dual polarised antennas as well as coaxial to waveguide transitions by simulating the launchers and probes manually. It allows the user to analyse the performance of a design and tune the dimensions to achieve better results. Without the use of software, designing antenna will purely rely on calculations, trial and error, and is time consuming.

5.2 Recommendations

It is recommended that the revised FEKO version of the circular waveguide and conical horn antenna be developed further to only allow the fundamental mode to propagate. Additionally, it is also recommended to simulate the coaxial launcher and the probe instead of using the waveguide port function that only allows one mode to propagate. It is recommended to procure standard gain antennas that can operate in X-band to perform antenna gain measurements instead of using equations and radiation efficiency estimations.

The parabolic dish antenna is an alternative design which can be considered. Currently, off-the-shelf dish antennas will not provide the required HPBW, thus the dish needs to be customised. The advantages of dish antennas over horn antennas are that they decrease the overall size and provide more resistance to wind. The same dual polarised waveguide design can be used as the antenna's feed. A revised version of the dish antenna is shown in Appendix F.3.

Computer numerical control (CNC) units provide high precision machining which can be used to fabricate the waveguide. This can also ensure the holes for the SMA launchers are mutually orthogonal. Additionally, threads can be drilled into thicker waveguides for the SMA launchers to be screwed in, which eliminates nuts and bolts protruding in the inner surface of the waveguide. This also provides stability and flexibility when adjusting the probes if needed. Wires for the probes can be designed mechanically with the exact length eliminating manual errors. The two probes can be positioned orthogonal to each other and half a waveguide wavelength apart to improve isolation and avoid fringing fields between the probes.

It is recommended to perform antenna testing in an anechoic chamber that provides accurate results and minimises multipath interferences. Inside an anechoic chamber the antennas are controlled automatically which performs all the rotations and records the data in the elevation and azimuth plane, and the 3D pattern. Without the availability of an anechoic chamber, to provide more accurate results it is recommended to use automated rotatable tripods. This provides better radiation pattern accuracy and avoids manual operation that introduces human error. Additionally, it is also recommended to conduct testing in a variety of locations to compare which location provides the least interferences.

Bibliography

[1] M. Inggs *et al.*, "Multistatic radar: System requirements and experimental validation," in *Radar Conference (Radar), 2014 International*, Oct 2014, pp. 1–6.

[2] W. L. Stutzman and G. A. Thiele, *Antenna Theory and Design*, 3rd ed. New York: John Wiley & Sons, Inc., 2013.

[3] J. R. Hallas, "Antenna Polarization- What does it mean and when is it important?" *QST*, vol. 94, no. 7, pp. 55–56, July 2010, accessed: Sept. 10, 2015.

[4] M. Zennaro and C. Fonda, "Radio Laboratory Handbook," 2004, accessed: Nov. 19, 2015. [Online]. Available: http://wireless.ictp.it/handbook/Handbook.pdf

[5] Natural Resources Canada, "Introduction to polarization," accessed: Nov. 20, 2015. [Online]. Available: http://www.nrcan.gc.ca/earth-sciences/geomatics/satellite-imagery-air-photos/satellite-imagery-products/educational-resources/9275

[6] W.-M. Boerner *et al.*, "Polarimetry in remote sensing: basic and applied concepts," in *Geoscience and Remote Sensing, 1997. IGARSS '97. Remote Sensing - A Scientific Vision for Sustainable Development., 1997 IEEE International*, vol. 3, Aug 1997, pp. 1401–1403.

[7] D. Dogan and O. Civi, "A Novel Edge Wall Waveguide Slot Antenna," in *Phased Array Systems and Technology (ARRAY), 2010 IEEE International Symposium on*, Oct 2010, pp. 453–456.

[8] R. Vilaltella *et al.*, "High-efficiency dual-polarized patch antenna array with common waveguide feed," in *Microwave Conference (GeMIC), 2014 German*, March 2014, pp. 1–3.

[9] S. Ononchimeg *et al.*, "A new dual-polarized horn antenna excited by a gap-fed square patch," *Progress In Electromagnetics Research Letters*, vol. 21, pp. 129–137, 2011.

[10] C. A. Balanis, *Antenna Theory: Analysis and Design*, 3rd ed. New York: John Wiley & Sons, Inc., 2011.

[11] S. B. Gambahaya, "Design and Implementation of the Pillbox Antenna for SASARII," Master's thesis, University of Cape Town, 2005.

[12] C. A. Balanis, "Circular waveguides," in *Encyclopedia of RF and Microwave Engineering*, E. Holzman, Ed. John Wiley & Sons, Inc., 2005, pp. 643–653.

[13] F. L. Teixeira *et al.*, "High-frequency transmission lines," in *Encyclopedia of RF and Microwave Engineering*. John Wiley & Sons, Inc., 2005, pp. 1989–2005.

[14] B. Downing, "Microwave Components and Antennas," EEE5121Z lecture notes, Department of Electrical Engineering, University of Cape Town, South Africa, 2014.

[15] P. Wade, "Rectangular Waveguide to Coax Transition Design," 2006, accessed: Nov. 27, 2015. [Online]. Available: http://www.w1ghz.org/QEX/Rectangular_Waveguide_to_Coax_Transition_Design.pdf

[16] ——, "Understanding Circular Waveguide - Experimentally," 2001, accessed: Nov. 27, 2015. [Online]. Available: http://www.w1ghz.org/QEX/circular_wg.pdf

[17] O. Daniyan *et al.*, "Horn Antenna Design: The Concepts and Considerations," *IJETAE*, vol. 4, no. 5, pp. 706–708, July May 2014, accessed: Nov. 25, 2015. [Online]. Available: http://www.ijetae.com/files/Volume4Issue5/IJETAE_0514_107.pdf

[18] L. Rawoot, "Design of a Dual Polarized X-Band Radar Antenna with a 10° Beamwidth," University of Cape Town, South Africa, 2014.

[19] Rohde&Schwarz, *R&S SMF100A Microwave Signal Generator*, 2015, accessed: Dec. 1, 2015. [Online]. Available: https://www.rohde-schwarz.com/product/smf100a-productstartpage_63493-8447.html

[20] Avalon Test Equipment, *ThinkRF WSA5000-220 Wireless Signal and Spectrum Analysis Platform*, 2015, accessed: Dec. 1, 2015. [Online]. Available: https://avalontest.com/thinkrf-wsa5000-220-wireless-signal-and-spectrum-analysis-platform-100khz-20ghz-100-mhz-ibw/

[21] Keysight Technology, *N5247A PNA-X Microwave Network Analyzer, 67 GHz*, 2015, accessed: Dec. 1, 2015. [Online]. Available: http://www.keysight.com/en/ pdx-x201825-pn-N5247A/pna-x-microwave-network-analyzer-67-ghz

[22] Antenna Theory, "S-parameters," accessed: June. 20, 2015. [Online]. Available: http://www.antenna-theory.com/definitions/sparameters.php

[23] Home of RF and Wireless Vendors and Resources, "S parameters or scattering parameters," accessed: June. 20, 2015. [Online]. Available: http://www.rfwireless-world.com/Terminology/S-Parameters-Scattering-parameter.html

[24] D. M. Polar, *Microwave Engineering*, 4th ed. John Wiley & Sons, Inc., 1949.

[25] PI Manufacturing, "Everything you need to know about antennas," accessed: Nov. 13, 2015. [Online]. Available: http://www.pimfg.com/ifaq/faq_antenna.htm

[26] N. C. Karmakar and S. K. Padhi, "Coaxial lines and waveguides," in *Encyclopedia of RF and Microwave Engineering*. John Wiley & Sons, Inc., 2005, pp. 658–674.

[27] Optical Device and Communications, "Microwave transmission lines (coaxial cable)," accessed: Nov. 25, 2015. [Online]. Available: http://komunikasioptik.com/2013/06/04/coaxial-cable/

[28] T. R. Kuphaldt, "Lessons In Electric Circuits," 2007, accessed: Nov. 25, 2014. [Online]. Available: http://www.ibiblio.org/kuphaldt/electricCircuits/AC/AC.pdf

[29] U. Navy, *Navy Electricity and Electronics Training Series: Module 11 - Microwave Principles*. CreateSpace Independent Publishing Platform, 1998, accessed: Nov. 10, 2015. [Online]. Available: http://www.maritime.org/doc/neets/mod11.pdf

[30] S. Silver, *Microwave Antenna Theory and Design*. New York: McGraw-Hill Book Company, 1949.

[31] Mamaqua Electrical, "Ellies-Caravan Satellite Dish Kit-DCP2," accessed: July. 13, 2015. [Online]. Available: http://namaquaelectrical.co.za/product_info.php?products_id=1969

Appendix A

Relevant Theory

This appendix provides the relevant theory that involves the study of antennas. The basic electromagnetic theory for antennas has been established including the radiation pattern and polarisation. Different field regions have been defined which shows the far field region provides the complete radiation pattern form. Important lobes from the radiation pattern such as the main lobe and sidelobes determine the efficiency of an antenna by measuring the HPBW and SLL.

A.1 Introduction to Antennas

Electrical or radio frequency (RF) signals are very crucial in communications to send and receive information. Signals can be carried between locations in one of two methods: through transmission lines or through air using antennas. The transmitting antenna radiates the electrical signals that covers a large area or distance which is detectable to receiving antennas. RF transmission lines require a guiding structure (i.e., coaxial launchers, hollow tube waveguides) to guide the electrical signal to the antenna where the antenna converts the guided wave into a freespace EM wave for a transmitter or vice versa for a receiver.

EM waves travel at the speed of light ($c = 3 \times 10^8$ m/s) in a vacuum and travels at a similar speed in air. The EM spectrum has several operating frequencies ($f_\circ$) and wavelengths ($\lambda_\circ$)

in different applications. Frequency and wavelength are related by the following equation:

$$\lambda_{\circ} = \frac{c}{f_{\circ}} \tag{A-1}$$

$$= \frac{3 \times 10^8 \text{ m/s}}{f_{\circ}} \quad [\text{m}] \tag{A-2}$$

Microwave frequencies generally operate between 0.3 GHz to 300 GHz, so its relative $\lambda_{\circ}$ is between 0.1 m to 1 mm respectively [24].

Antennas have reciprocity, meaning that an antenna has the same characteristics regardless if it is transmitting or receiving. The size of the antenna is dependent on the operating frequency. It must have an appreciable fraction of a wavelength at the operating frequency to operate efficiently. For example, if the dimension of the antenna is smaller than the fraction of a wavelength the signal will not radiate. The aperture of the antenna affects factors of the radiation pattern such as beam forming, reducing of HPBW, and gain [2].

A.2 Radiation Pattern

A radiation pattern, antenna pattern or far-field pattern is a graphical representation of the radiation properties of the antenna either in the E- or H-field's magnitude as a function of angular space. The structure of an antenna determines the shape of the radiation pattern, and is either a directional antenna or an omnidirectional antenna.

A.2.1 Radiation Pattern Characteristics

The properties of a radiation pattern can be seen in Figure A-1 which includes the radiation intensity, radiation pattern F (θ, φ), directivity D, and power densities (S and S_i) of the isotropic and real antenna [2].

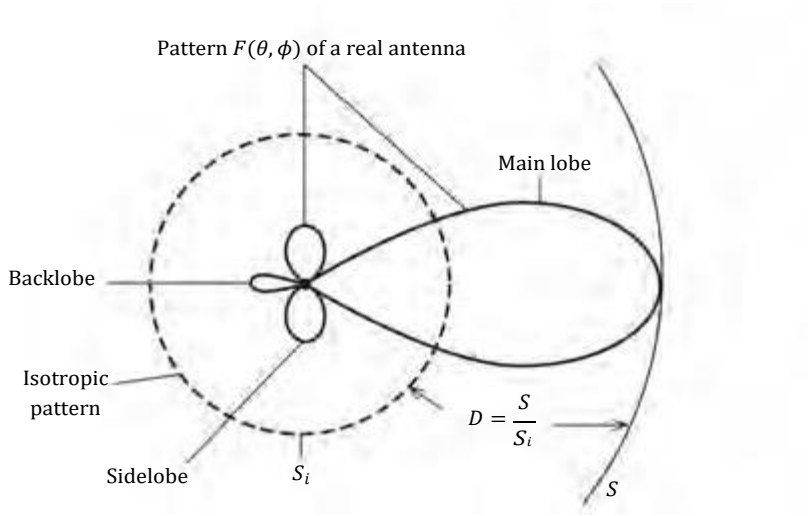

Figure A-1: Demonstration of the radiation pattern of the isotropic and real antenna [2].

It can be determined that the radiation pattern in Figure A-1 is of a directional antenna because the radiated power is in the main lobe. The isotropic pattern shows lower power that radiates in all directions. This implies that directional antennas have higher gain due to the power density in one direction. Not all power will be radiating in the intended direction. Power that radiates in different directions other than in the direction of the main lobe is known as the sidelobes and backlobe.

The radiation pattern is measured in the far field region with respect to the function of directional coordinates, usually normalised with respect to their maximum value and plotted in the logarithmic scale in decibels. The reason for doing so is to emphasise parts of the pattern that have very low values such as the sidelobes [10]. Figure A-2 shows the comparison of the radiation pattern in linear and logarithmic scale.

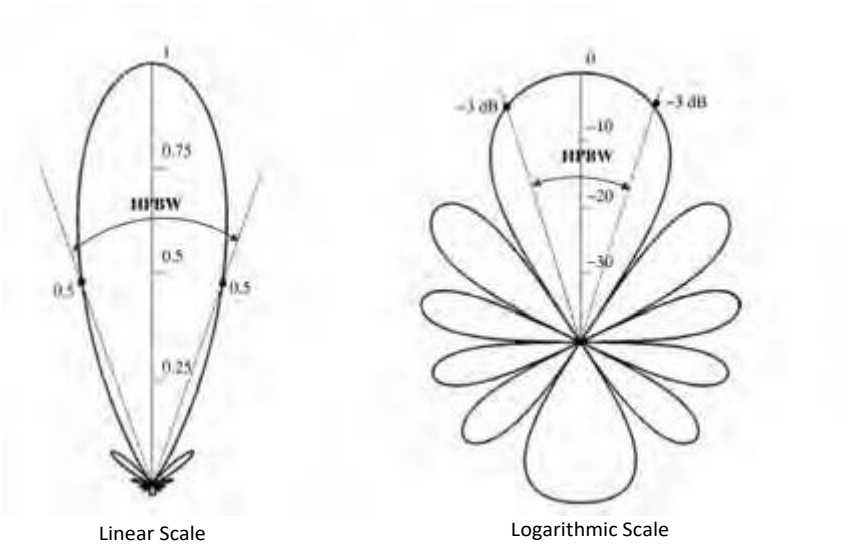

Figure A-2: Normalised radiation pattern in linear and logarithmic scale [10]

In Figure A-2, the main lobe as well as the angle for the HPBW are clear in both patterns. The sidelobes and backlobes are small in the linear scale, but they can be observed clearly in the logarithmic scale. Studies can be done to determine the efficiency of the antenna, the direction and density of maximum power radiation, and the SLL.

A.2.2 Field Regions

The space around the antenna is subdivided into three regions: reactive near field, radiating near field, and far field region as shown in Figure A-3. There are differences in the field structure between the three regions and various principles have been established to identify the regions [2][10]. Figure A-3 shows the three regions and their respective field distributions. The shape of the field changes from the reactive near field to the far field in both magnitude and phase.

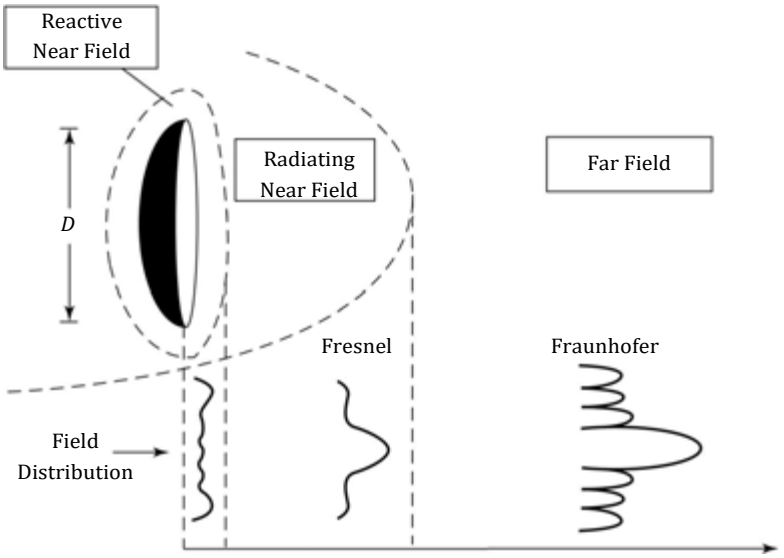

Figure A-3: Changes in the amplitude of the radiation pattern in different field regions [10].

The reactive near field region is the space instantly surrounding the antenna. The boundary of this region is at a distance d from the antenna:

$$d = 0.62 \sqrt{\frac{D^3}{\lambda_\circ}} \tag{A-3}$$

The far field or Fraunhofer region is the space where the angular field distribution is independent of the distance from the antenna. For an antenna that has an overall dimension D larger than $\lambda_\circ$ ($D > \lambda_\circ$), the distance of the far field region from the antenna is given as:

$$d > \frac{2D^2}{\lambda_\circ} \tag{A-4}$$

The term Fraunhofer region is often referred to when the antenna is focused at infinity where the field components are transverse and the angular distribution is independent of the radial distance. The minimum boundary of the far field distance is $d = 2D^2/\lambda_\circ$ to infinity.

A.2.3 Types of Radiation Patterns

Figure A-4 shows the two common types of radiation patterns: broadside and endfire.

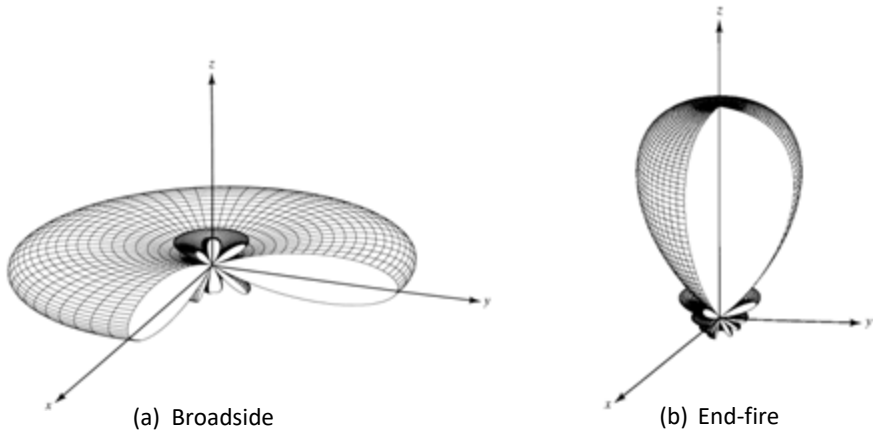

Figure A-4: Three dimensional polar plot of the broadside (a) and endfire (b) radiation pattern [10].

Figure A-4(a) displays the broadside radiation pattern where the power radiates away from the antenna and the main lobe is maximum in the direction normal to the plane containing the antenna. Figure A-4(b) is the endfire radiation pattern where the power is maximum in the same plane containing the antenna and its power is focused in one direction.

A.2.4 Radiation Lobes

A typical cross-sectional normalised polar plot of an endfire radiation pattern in the logarithmic scale is shown in Figure A-5.

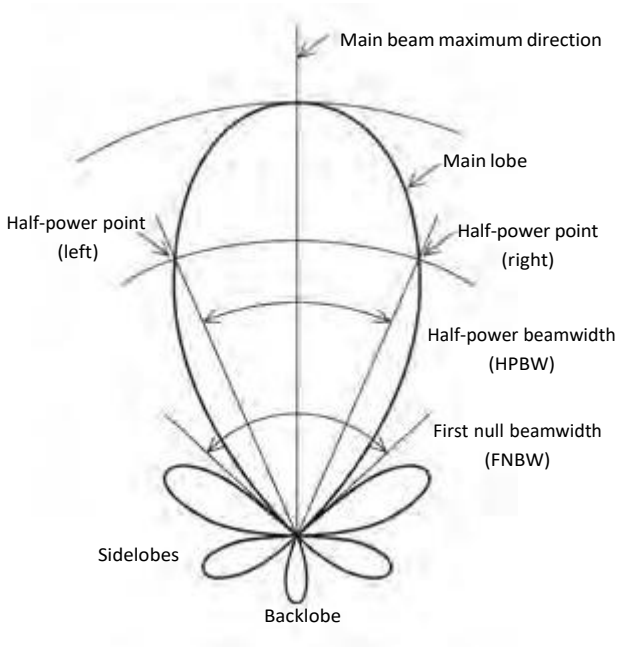

Figure A-5: Polar plot of a endfire radiation pattern [2].

From Figure A-5, a radiation pattern consists of the following:

- **Main lobe** - is a radiation lobe that contains most of the radiation in a direction (pointing in the 0° direction)
- **Sidelobes** - are any small radiation lobes that are not intended to radiate (can be in any direction)
- **Backlobe** - is a radiation lobe that is in the opposite direction to the main lobe (pointing in the 180° direction with respect to the main lobe)

A.2.5 Beamwidth

The beamwidth measures the area over which the antenna transmits or receives the signal. It specifies the strongest direction of an antenna when the angular width is between the points where the gain is less than the peak of the main lobe by a specific value. Generally a high gain antenna has a smaller beamwidth that covers a small area at a long distance, whereas a low gain antenna has a large beamwidth that covers a large area but at a shorter distance [25]. There are a number of beamwidths associated in an antenna pattern. Two of the most commonly measured beamwidths as shown in Figure A-5 are [2]:

- **Half-power beamwidth (HPBW)** - specifies the angular width of the radiation pattern at which the antenna is most sensitive, the angle between the half-power points (left and right) of the main lobe is measured -3 dB down from the peak radiated power and the power will be 50% of the radiated power
- **First null beamwidth (FNBW)** - specifies the angular width of the main lobe measuring between the first nulls of the pattern

Beamwidth can be measured in the vertical (or elevation) and horizontal (or azimuth) plane, associated with the term elevation HPBW (θ_{el}) and azimuth HPBW (θ_{az}) respectively. The elevation plane is described as the plane perpendicular to the ground, whereas the azimuth plane is parallel to ground.

For a uniformly illuminated aperture, the HPBW of a horn antenna in a given plane is [14]:

$$\theta = \frac{60\lambda_\circ}{D} \tag{A-5}$$

where D is the aperture's width.

For a cosinusoidal aperture field distribution, the HPBW is:

$$\theta = \frac{80\lambda_\circ}{D} \tag{A-6}$$

From (A-5) and (A-6), the width of the antenna affects the size of the HPBW. The larger the width, the narrower the HPBW.

A.2.6 Sidelobe Level

The concentration of the power in the main lobe can be determined by calculating the ratio of the pattern value of the first sidelobe peak to the pattern value of the main lobe peak. This is known as the sidelobe level (SLL) and is measured in decibels. Figure A-6 shows the radiation pattern and where the SLL is measured on a Cartesian plane.

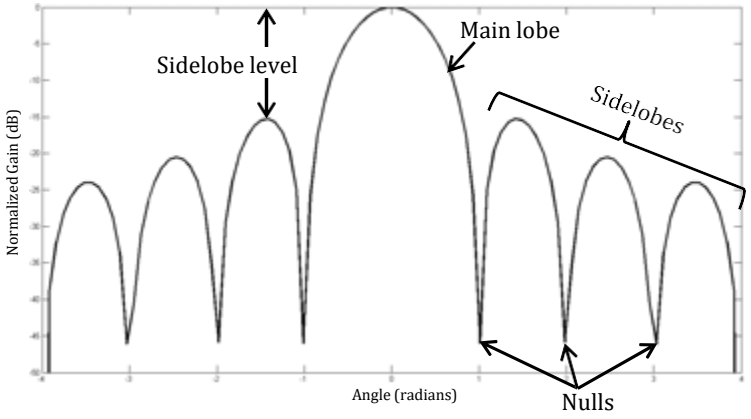

Figure A-6: Radiation pattern on a Cartesian plane displaying the SLL.

For a given radiation pattern in decibels, the SLL can be obtained by measuring from the peak of the main lobe to the peak of the first sidelobe. Under normal circumstances, the power density in the sidelobes are much less than the main lobe, otherwise the antenna is said to be inefficient. There are techniques to suppress sidelobes, however it is beyond the scope of this dissertation.

A.3 Directivity and Gain

The important characteristics of an antenna is the concentration of energy in one direction relative to radiation in other directions. This is known as the antenna directivity and is equal to its gain if the antenna is 100% efficient. Gain can be expressed relative to an isotropic radiator. Antenna gain can be defined as directive gain and power gain. Directive gain is referred to as the directivity (*Dir*), and power gain is referred to as gain (G_p) [2].

A.3.1 Directivity

Directivity is defined as the ratio of the radiation intensity in a certain direction to the average radiation intensity over all directions. Directivity represents a lossless antenna radiating in

a specific direction and can be expressed as [10]:

$$Dir = \frac{4\pi}{\Omega_A} \tag{A-7}$$

where Ω_A is the half-power beam solid angle. Therefore, directivity is entirely determined by the pattern shape. Even though the equations expressed to compute directivity are approximations, it is still very convenient for design purposes.

The directivity in (A-7) can be further simplified and Figure A-7 demonstrates how it can be achieved by approximating the relationship between directivity and the antenna HPBW.

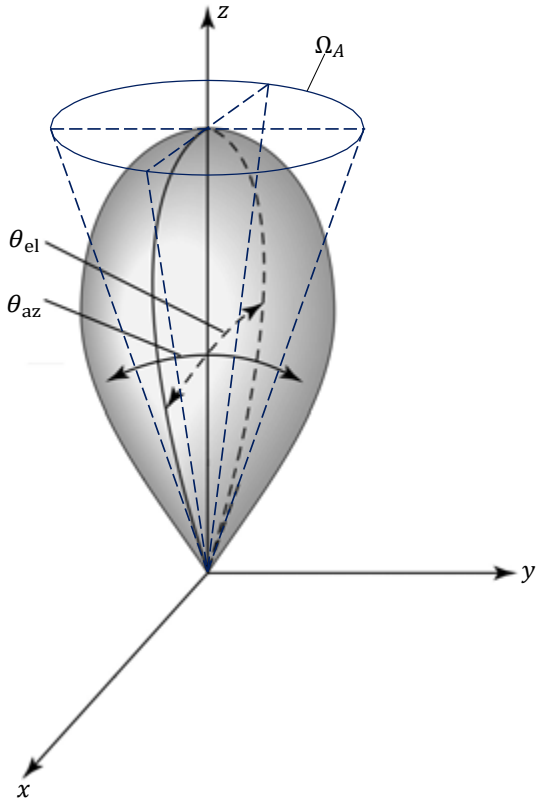

Figure A-7: Radiation intensity pattern [10]

Figure A-7 demonstrates a radiation intensity pattern pointing in the positive z-axis direction. The beam solid angle Ω_A is approximately equal to the product of the HPBW in two perpendicular planes, $\theta_{el(rad)}$ and $\theta_{az(rad)}$ in radians, or $\theta_{el(deg)}$ and $\theta_{az(deg)}$ in degrees.

Therefore, directivity can be estimated as [10]:

$$Dir = \frac{4\pi}{\Omega_A} \approx \frac{4\pi}{\theta_{\text{el(rad)}}\,\theta_{\text{az(rad)}}} \tag{A-8}$$

or

$$Dir = \frac{4\pi(360^{\circ}/2\pi)^2}{\theta_{\text{el(deg)}}\theta_{\text{az(deg)}}} \approx \frac{41253}{\theta_{\text{el(deg)}}\theta_{\text{az(deg)}}} \tag{A-9}$$

where $\theta_{\text{el(rad)}}$ and $\theta_{\text{el(deg)}}$ is the HPBW in the elevation plane, and $\theta_{\text{az(rad)}}$ and $\theta_{\text{az(rad)}}$ is the HPBW in the azimuth plane. Equations (A-8) and (A-9) are based on a pattern that has one major main lobe and if any sidelobes are present, they should have very low intensity.

A.3.2 Gain

Since the gain of the antenna is related to the directivity, it takes the efficiency of the antenna and its directional capabilities into account. The gain of an antenna in a given direction can be defined as the ratio of the radiation intensity (U_m) to the total input power (P_{in}) accepted by the antenna that radiates isotropically [2]. This ratio is multiplied by 4π to quantify how efficient the antenna transforms available power into radiated power and directive properties. Thus, gain can be expressed as [10]:

$$G_p = 4\pi\frac{U_m}{P_{\text{in}}} \tag{A-10}$$

Gain and directivity will be equal if all the radiated power appears at the input, however, real antennas do not behave this way and some of the input power is lost on the antenna or absorbed by other structures. The definition of radiation efficiency η can therefore be defined as the ratio between radiated power and the input power:

$$\eta = \frac{P_{\text{rad}}}{P_{\text{in}}} \tag{A-11}$$

where η is between 0 and 1. Therefore gain can be rewritten as:

$$G = \eta Dir \tag{A-12}$$

Thus, the gain of an antenna is equal to the product of directivity and radiation efficiency. Units for directivity and gain are both dimensionless. In practice, the terms gain and directivity usually refer to the maximum gain and is given in terms of decibels. To convert gain

or directivity into decibels, the following equations can be used [2]:

$$Dir_{(\mathrm{dB})} = 10\log(Dir) \tag{A-13}$$

and

$$G_{(\mathrm{dB})} = 10\log(G) \tag{A-14}$$

A.4 Effective Aperture

The maximum effective aperture is directly proportional to the directivity of an ideal dipole is expressed as [2]:

$$Dir = \frac{4\pi}{\lambda_\circ^2} A_{\mathrm{em}} \tag{A-15}$$

where A_{em} is the maximum effective aperture of a lossless antenna. For antenna with losses, the received power is reduced by η. The effective aperture can be expressed as [2]:

$$A_e = \eta A_{\mathrm{em}} \tag{A-16}$$

Looking back at directivity in (A-15), multiplying both sides by η, the left side of the term becomes ηD which is equal to the gain shown in (A-12), therefore (A-15) becomes:

$$\eta Dir = G = \frac{4\pi}{\lambda_\circ^2} \eta A_{\mathrm{em}} \tag{A-17}$$

Replacing ηA_{em} with A_e from (A-16), the gain equation finally becomes:

$$G = \frac{4\pi}{\lambda_\circ^2} A_e \tag{A-18}$$

Appendix B

Fundamental Theory

In this chapter, various aspects of the antenna is investigated. The basic transmission line theory establishes the different types of propagation modes and the existence of these modes in coaxial lines and waveguides. The waveguide theory provides the understanding of the boundary conditions within a waveguide, and detailed theory on superposition that creates a resultant wave with a period known as the waveguide wavelength. The rectangular and circular shaped waveguide sections discussed different fundamental modes and their cutoff frequencies.

B.1 Transmission Lines

There are several different types of transmission lines and they are used in different applications, such as power transmission lines that operate in low frequencies (LF). In telecommunications and radar systems, high-frequency (HF) transmission lines are used since they optimise the frequency bandwidth and minimize the signal attenuation. Waveguides may be considered as a means of channelling EM waves through space. All transmission lines act as channels for EM waves, but because waveguides are single-conductor elements, the way electrical energy travels through them is different to the way electrical energy travels through a two-conductor transmission line [13].

Several factors are considered when choosing transmission lines, including:

- Operating frequency range and bandwidth
- Attenuation
- Power handling capability
- Fabrication process

No single transmission line can work for all applications. A cross-sectional view of different types of transmission lines can be seen in Figure B-1, and Table B-1 shows the advantages and disadvantages of each type of transmission line.

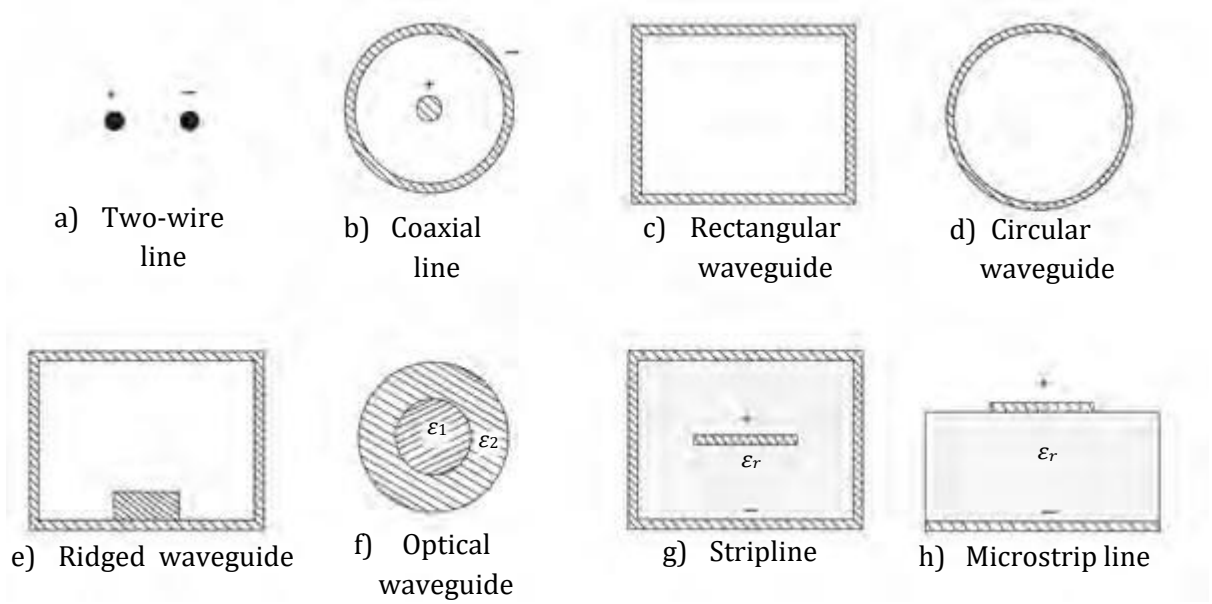

Figure B-1: Cross-sectional view of different types of transmission lines [13].

Table B-1: Advantages and disadvantages of different transmission lines [13].

Type	Advantages	Disadvantages
Two-wire	High power, cheap	LF range, lossy
Coaxial line	Wide bandwidth, small size	Low power, high attenuation
Hollow waveguide	High power, low attenuation	Limited bandwidth, large size
Microstrip line	Wide bandwidth, easily fabricated	Low power, high attenuation

Power transmission lines operating at LF use simple wires to connect two points, but starts to radiate energy as frequency increases. For microwave transmission lines, coaxial lines or coaxial cables consist of a wire inside a outer cylindrical conductor that acts as a shield to minimise radiation losses as shown in Figure B-1b). Coaxial cables have a wide bandwidth,

but suffer from high attenuation and cannot handle high power. However, hollow waveguides such as rectangular, circular, and ridged waveguides have low attenuation and can handle high power, but have small bandwidth [13]. Hollow waveguide structures are conductive hollow tubes that are suitable for transmitting microwave signals at frequencies between 0.3 GHz and 30 GHz. Coaxial lines and hollow waveguides are important in antenna design, thus will be expanded upon in Appendix B.3 and B.4.

B.2 Propagation Modes

Transmission lines can be classified according to the polarisation properties of the EM waves. If the EM wave is propagating in the z-direction, then the modes can be characterized into [26]:

- Transverse Electromagnetic (TEM) mode — both E- and H-fields are transverse to the direction of propagation ($E_z = 0, H_z = 0$)
- Transverse Electric (TE) mode — only the E-field is transverse to the direction of propagation ($E_z = 0, H_z \neq 0$)
- Transverse Magnetic (TM) mode — only the H-field is transverse to the direction of propagation ($E_z \neq 0, H_z = 0$)
- Hybrid mode — contains all six components (E_x, E_y, E_z, H_x, H_y, and $H_z \neq 0$)

Figure B-2 shows the different types of transmission lines and their respective propagation modes.

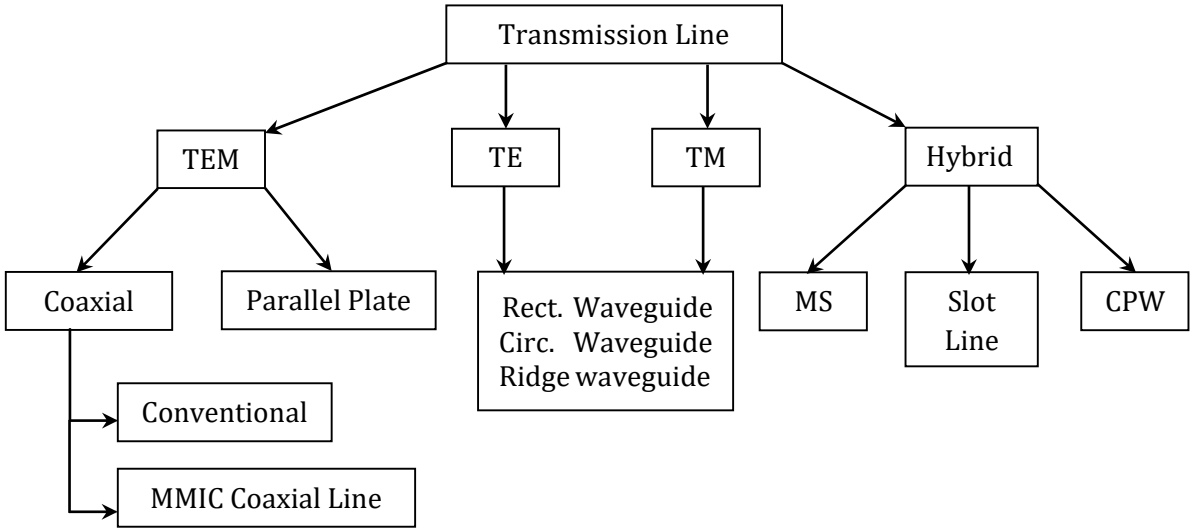

Figure B-2: Various forms of transmission lines in their respective categories of TEM, TE, TM, and hybrid modes [26].

In Figure B-2, TEM mode is the fundamental or dominant mode in coaxial lines and parallel plates where two conductors exist. The TE and TM modes are found in hollow waveguides that have a single conductor. Hybrid modes are known to contain all six components of E- and H-fields, but these modes are not relevant in this dissertation and is not discussed further.

B.3 Coaxial line

TEM mode only exists where there are two conductors such as the coaxial line. Figure B-3 displays the E- and H-field inside the coaxial line.

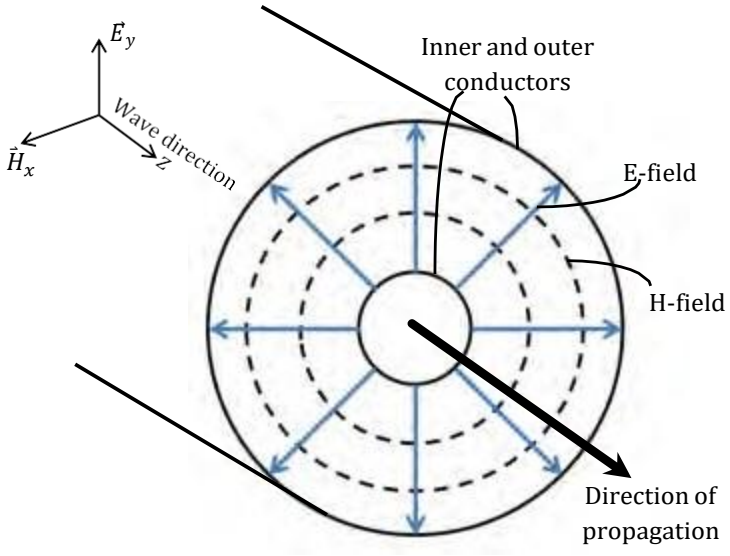

Figure B-3: Cross-sectional view of the coaxial line where both E- and H-field are perpendicular to the direction of propagation [27].

Both the E-field (represented as E_y) and H-field (represented as H_x) are perpendicular to each other, as well as to the direction of propagation. As discussed earlier, TEM mode is the fundamental mode in coaxial lines and parallel plates, however, it does not exist in hollow waveguides due to the single conductor. The TEM mode is dominant where the cross-sectional dimensions of the transmission line are small compared to the wavelength of the signal [28].

B.4 Hollow Waveguides

Hollow waveguides are commonly used to transmit microwave signals. Waveguides do not have a centre conductor and cannot support TEM mode. However, waves propagate by reflecting off the inner conducting walls, thus TE and TM modes can only exist in a single enclosed conductor such as hollow waveguides.

B.4.1 Boundary Conditions within a Waveguide

EM waves travel differently inside a waveguide than in freespace. The difference is due to a waveguide's physical size limitations. For EM waves to travel down a waveguide, two boundary conditions must be satisfied [29]:

1. The E-field can only exist when it is perpendicular to the surface of the conductor. Any E-field parallel to the conductor will dissipate.
2. The H-field can only exist where it can form closed loops in parallel with the conductors.

Both fields will exist at the same time in a waveguide. Under normal circumstances, if one of the conditions is met, the other condition will be satisfied because the two fields are always perpendicular to each other.

B.4.2 Wavefronts within a Waveguide

A quarter freespace wavelength probe acts as a quarter-wave monopole antenna that supplies a signal to the waveguide. From the top view, the wavefronts radiate through the waveguide as shown in Figure B-4.

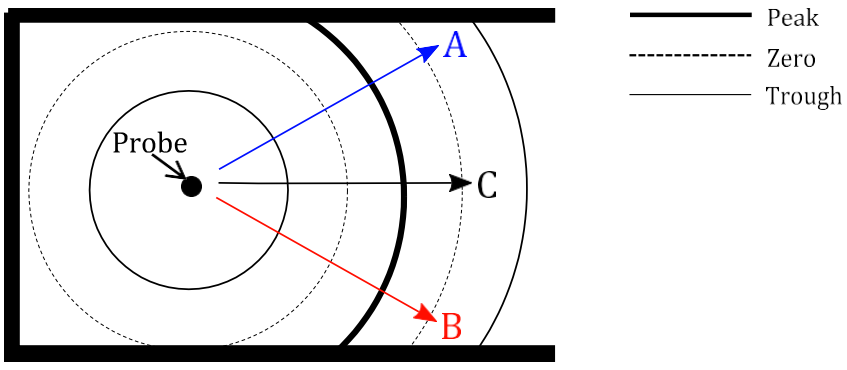

Figure B-4: Top view of the wavefront propagating through the waveguide [29].

If the wavefront propagating down a waveguide is divided into portions A, B, and C, any wave in the direction of C will attenuate rapidly because it does not satisfy either of the

boundary conditions. Comparatively, wavefronts A and B will reflect off the conducting walls, forming reverse-phase wavefronts, and propagate down the centre of the waveguide in a zigzag pattern [29].

As wavefronts A and B propagate through the waveguide and reflect off the conducting walls, the travelling waves constructively interfere with each other creating an interference pattern as shown in Figure B-5, where the fields are superimposed.

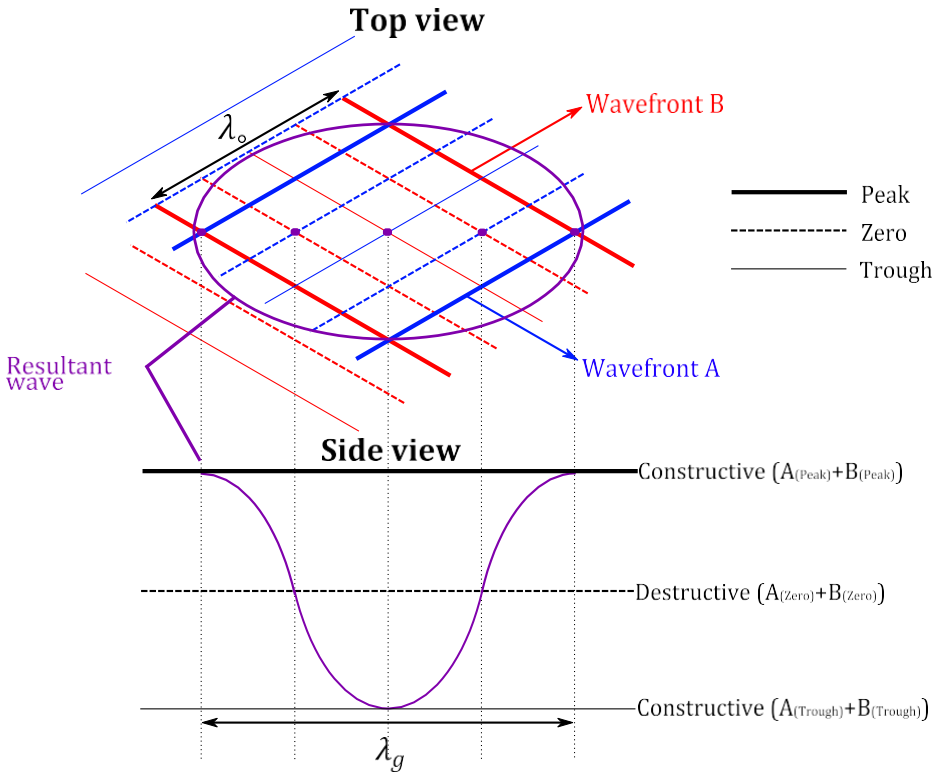

Figure B-5: Superposition of two wavefronts creating a resultant wave with period known as waveguide wavelength [14].

These points of constructive and destructive interference result in a field propagation travelling straight down the centre of the waveguide. This superposition determines the resultant wave propagation which has a larger amplitude and longer wavelength (known as the waveguide wavelength λ_g) than the original wavefront freespace wavelength $\lambda_\circ$ [14].

B.4.3 Rectangular Waveguide

Figure B-6 shows the TE and TM modes propagating through a rectangular waveguide.

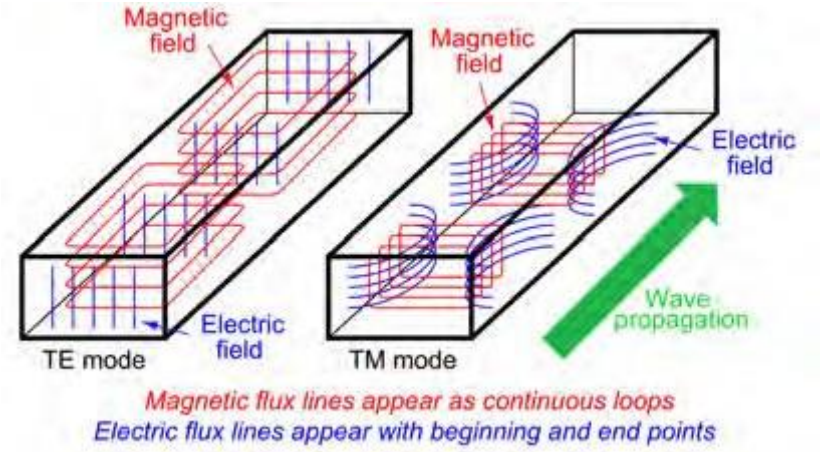

Figure B-6: Rectangular waveguide in TE- and TM-modes [28].

When an EM wave propagates through a rectangular waveguide, only the E- or H-field will be transverse to the wave's direction of travel. The one field is perpendicular to the other field, but it will 'loop' longitudinally to the direction of travel. The field that remains perpendicular to the direction of travel determines the mode in which the wave propagates: TE mode or TM mode [28].

Due to the principle of superposition as discussed in Appendix B.4.2, the longer period is known as the waveguide wavelength and can be calculated using the following equation [14]:

$$\lambda_g = \frac{\lambda_\circ}{\sqrt{1 - \left(\frac{\lambda_\circ}{2a}\right)^2}} \tag{B-1}$$

From (B-1), the denominator '2*a*' represents the cutoff wavelength where '*a*' represents the largest width of the waveguide:

$$\lambda_c = 2a \tag{B-2}$$

Thus, (B-1) is rewritten as:

$$\lambda_g = \frac{\lambda_\circ}{\sqrt{1 - \left(\frac{\lambda_\circ}{\lambda_c}\right)^2}} \tag{B-3}$$

The following conditions are noted:

- if $\lambda_\circ < \lambda_c$, λ_g is real and positive
- if $\lambda_\circ = \lambda_c$, λ_g is infinite and $\lambda_\circ$ will equal to the cutoff wavelength (λ_c)
- if $\lambda_\circ > \lambda_c$, λ_g is imaginary due to a negative value in the square root

Therefore, from the conditions above, EM waves will propagate through the waveguide when $\lambda_\circ < \lambda_c$. The lowest frequency of propagation through a waveguide is the cutoff frequency (f_c), where:

$$f_c = \frac{c}{\lambda_c} \tag{B-4}$$

Equation (B-3) can then be rewritten in terms of $f_\circ$ and f_c:

$$\lambda_g = \frac{c}{f_\circ \sqrt{1 - \left(\frac{f_c}{f_\circ}\right)^2}} \tag{B-5}$$

Equations (B-3) and (B-5) show that the boundary conditions exist. As the operating frequency approaches the cutoff frequency, the waveguide wavelength becomes longer and eventually attenuates rapidly. Thus, it is not recommended to operate at frequencies close to the cutoff frequency.

B.4.4 Circular Waveguide

Circular waveguides are used as an alternative to rectangular waveguides. A circular waveguide has more benefits than a rectangular waveguide because it has less attenuation from the wall losses due to the circular shape. It also allows linear polarisation, circular polarisation, and polarimetry. Thus, circular waveguides are preferable over rectangular waveguides. Circular waveguides support TE and TM modes, but have cutoff frequencies that will attenuate the signal and possibly introduce other modes [13]. The fundamental mode is TE_{11} mode.

The cutoff frequency f_c is calculated by designing the circular waveguide with an inner diameter (l_g) that is large enough to support the fundamental mode across the desired

frequency, and avoid higher-order modes. From Appendix C, with a given diameter of the circular waveguide, the cutoff wavelength for the fundamental TE_{11} mode is:

$$\lambda_{c(TE11)} = 1.706 \times l_g \tag{B-6}$$

for the next higher-order TM_{01} mode is:

$$\lambda_{c(TM01)} = 1.306 \times l_g \tag{B-7}$$

and for the second higher-order TE_{21} mode is:

$$\lambda_{c(TE21)} = 1.029 \times l_g \tag{B-8}$$

With the calculated λ_c, the cutoff frequency is found using (B-4). Operating at frequencies below the cutoff frequency will not propagate any signals through the circular waveguide. The equation to find λ_g that propagates inside a circular waveguide is given as:

$$\lambda_g = \frac{\lambda_\circ}{\sqrt{1 - \left(\frac{\lambda_\circ}{1.706 \times l_g}\right)^2}} \tag{B-9}$$

or

$$\lambda_g = \frac{\lambda_\circ}{\sqrt{1 - \left(\frac{\lambda_\circ}{\lambda_c}\right)^2}} \tag{B-10}$$

The calculation for λ_g in (B-3) and (B-10) are the same for rectangular and circular waveguides respectively. Only the calculation for finding λ_c is different.

Appendix C

Launching Methods

The propagation modes are dependant on the method of launching the EM waves. The two modes that exist in a waveguide are the TE and TM modes. Figure C-1 displays the top view of positioning a probe to launch TE or TM mode within a waveguide. Only the H-field will be observed.

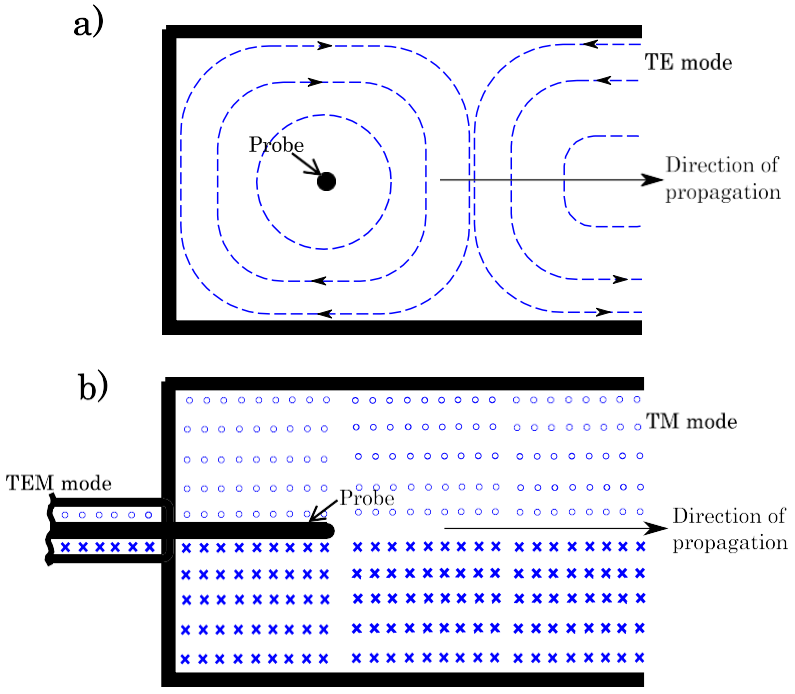

Figure C-1: Launching methods for TE and TM modes within a waveguide. The method of launching depends which mode the waveguide excites.

In Figure C-1a), TE modes are launched by placing the probe in parallel to the back wall with some distance apart (backshort length). The H-field loops around the probe and this creates vectors perpendicular and parallel to the direction of propagation. In Figure C-1b), for launching TM mode, the probe is placed perpendicular to the back wall. The H-field also loops around the probe, however the vectors are always perpendicular to the direction of propagation, hence the term 'transverse magnetic field'.

The existence of other higher-order TE or TM modes depends on whether the TE or TM mode is launched, and whether the mode's cutoff frequency is exceeded. When launching the fundamental TE_{11} mode, the next higher-order mode, TM_{01} mode, has a low possibility of propagating due to the launching method. Only the other higher-order TE modes will exist when the operating frequency is above these mode's cutoff frequencies [12]. Figure C-2 shows the cross-sections of the first three modes in a circular waveguide.

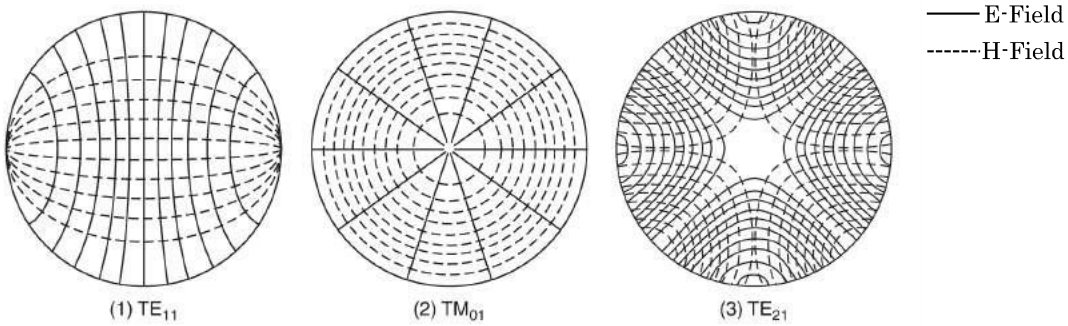

Figure C-2: The cross-sections of TE_{11}, TM_{01}, and TE_{21} modes in a circular waveguide.

The equation for finding the cutoff wavelength for a circular waveguide is [12]:

$$\lambda_c = \frac{l_g \pi}{X_{mn}} \tag{C-1}$$

where l_g is the diameter of the waveguide, X_{mn} is the factor of the propagation mode and is found in [12].

The fundamental mode is TE_{11} mode with $X_{11} = 1.8412$, so the cutoff wavelength is:

$$\begin{aligned} \lambda_{c(\mathrm{TE11})} &= \frac{l_g \pi}{1.8412} \\ &= 1.706 \times l_g \end{aligned} \tag{C-2}$$

The next higher-order mode is TM_{01} mode with $X_{01} = 2.4049$, and its cutoff wavelength is:

$$\lambda_{c(TM01)} = 1.306 \times l_g \tag{C-3}$$

The second higher-order mode is TE_{21} mode with $X_{21} = 3.0542$, and its cutoff wavelength is:

$$\lambda_{c(TE21)} = 1.029 \times l_g \tag{C-4}$$

Thus, operating above any of the cutoff frequencies and the launching method will excite the higher-order modes.

Appendix D

Square Horn Antenna Past Project

In partnership with Luqmaan Rawoot[1], the X-band horn antenna has been designed and completed in 2014. However, the length of the antenna is long. $f_\circ$ is equal to 8.5 GHz, and $\lambda_\circ$ is 35.29 mm. The length l of the horn has been calculated to be 1.25 m long. For a uniformly illuminated aperture, the HPBW of a horn antenna in a given plane is:

$$\theta = \frac{60\lambda_\circ}{D} \tag{D-1}$$

where D is the aperture width. Substituting the required HPBW of $\theta = 10^\circ$ into (D-1) and rearranging the equation to solve for D:

$$\begin{aligned} D &= \frac{60\lambda_\circ}{\theta} \\ &= \frac{60 \times (35.29 \text{ mm})}{10^\circ} \\ &= 210.74 \text{ mm} \end{aligned}$$

[1]Luqmaan Rawoot submitted his undergraduate thesis on the design and implementation of dual polarised X-band antenna. Luqmaan Rawoot focused on the hardware design, and I focused on the simulations, whereas the calculations were done individually and compared. Experimental testing and data capturing has been completed together.

Thus, the aperture length of the antenna is found to be 21 cm in both width and length for dual polarisation. A summary of the dimensions is shown in Table D-1.

Table D-1: Dimensions and lengths of the square horn antenna

Dimensions	Length (mm)
$\lambda_\circ$	35.29
Horn length *l*	1249.65
Aperture *D*	210.74
Waveguide length	22.86

D.1 Simulation

To ensure that the dimensions calculated earlier will achieve the required specifications, the design was simulated in FEKO. Figure D-1 displays the radiation pattern of the horn antenna. With some tuning, the length of the antenna has been reduced to 86.4 cm and still produce similar results.

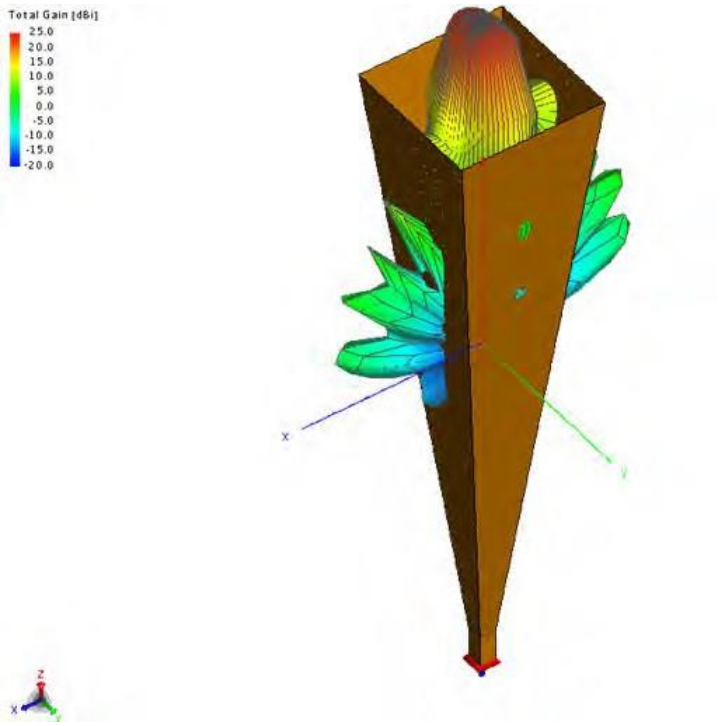

Figure D-1: Horn antenna design simulated in FEKO.

D.2 Hardware Design

Aluminium plates has been cut into the required size and welded at UCT's Mechanical Workshop. Aluminium is a fairly good conductor, making it suitable for waves to propagate. It is also lightweight and reasonably priced in comparison with other viable materials. An aluminium thickness of 2 mm (754-H111) has been chosen for fabrication so that it maintains its shape during welding and its prolonged exposure to heat extremes. Figure D-2 is a photo of the horn antenna and the configuration on the rooftop for testing.

Figure D-2: Horn antenna configuration on the rooftop of Menzies Building.

For the testing procedure:

- The transmitting antenna will be V-polarised and stationary with a transmission power of 13.3 dBm.
- The receiving antenna will also be V-polarised and measurements will be recorded for a range of 30° on each side.
- Both antennas will then be H-polarised and the same process repeated.

D.3 Results

After collecting all the measurements, the data in the azimuth plane can be analysed in Excel to plot the far field radiation pattern. The results of the rooftop measurements and FEKO are compared with their respective azimuth HPBW which is shown in Figure D-3.

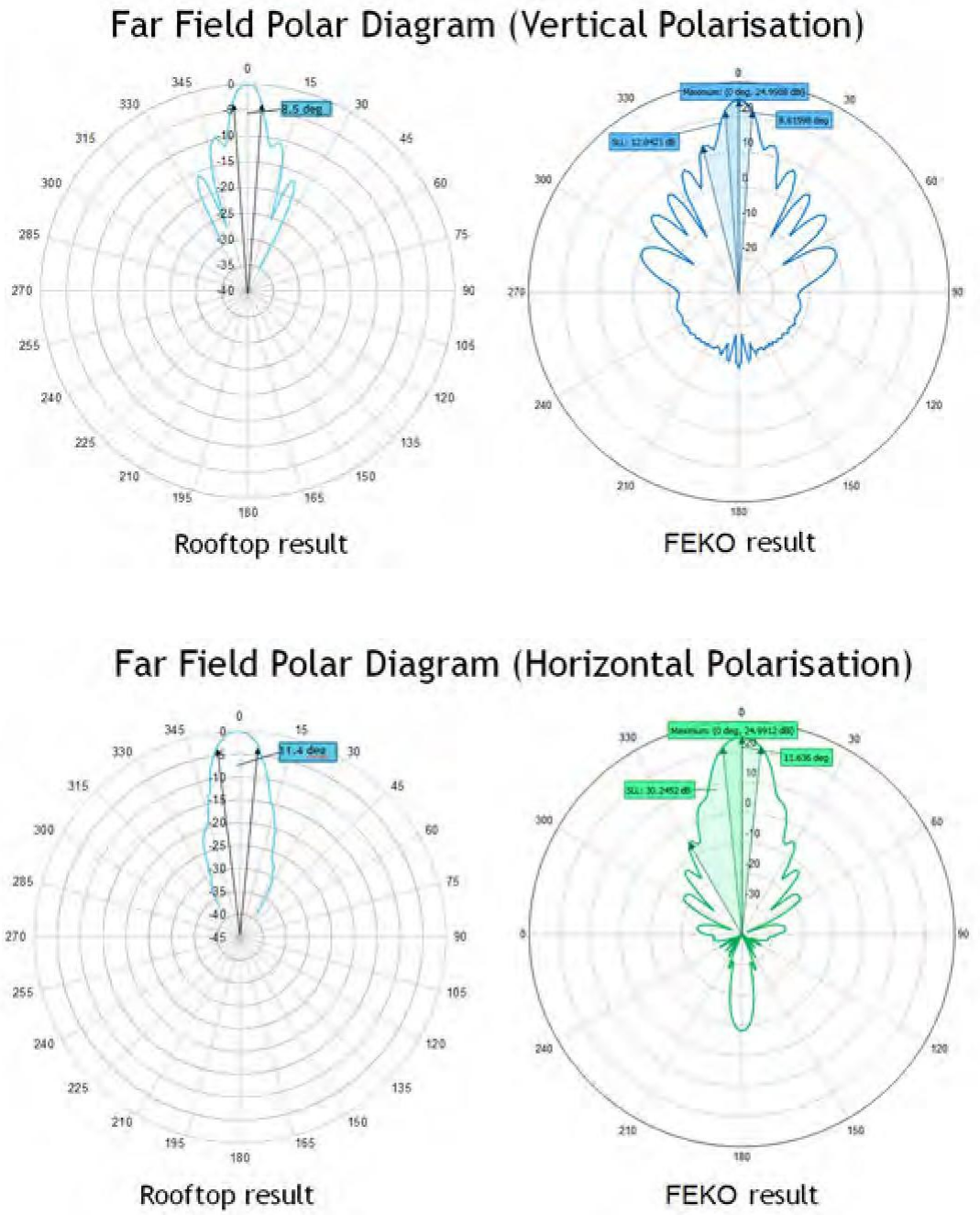

Figure D-3: Rooftop and FEKO's far-field polar diagram for V- and H-polarisation in azimuth plane.

D.4 Discussion

Table D-2 can be drawn from the results obtained in FEKO and the field testing.

Table D-2: Summary and comparison of the square horn results in FEKO and the fabricated antenna.

	V-Polarisation		**H-Polarisation**	
	$\boldsymbol{\theta}_{\text{az}}$	**SLL**	$\boldsymbol{\theta}_{\text{az}}$	**SLL**
FEKO	8.62°	−12.04 dB	11.64°	−30.25 dB
Fabricated Antenna	8.5°	−9.8 dB	11.4°	−27 dB

For V-polarisation, the rooftop testing shows an azimuth HPBW of 8.5°, whereas the FEKO testing shows 8.62°. For H-polarisation, the rooftop testing shows an azimuth HPBW of 11.4°, whereas the FEKO testing shows 11.64°.

Although the testing that has been executed is not 100% perfect, the results and simulations are aligned well with adequate performance. The azimuth HPBW results are approximately 10° and does achieve the NeXtRAD project requirements. However, the SLL in V-polarisation is poor, and the size of the antenna is large.

Appendix E

Conical Horn Simulation

The aperture in (2-5) has been used from [2]. The aperture is calculated to be:

$$\begin{aligned} D &= \frac{58.4\lambda_\circ}{\theta} \\ &= \frac{58.4 \times 35.29 \text{ mm}}{10^\circ} \\ &= 206.09 \text{ mm} \end{aligned}$$

Using the same methods and equations in Section 2.4.3, the length of the horn is found where:

$$l_h = 335.04 \text{ mm}$$

The conical horn antenna is then designed in FEKO to observe the performance.

E.1 FEKO Results

Figures E-1 and E-2 shows the 3D radiation pattern, azimuth HPBW, and SLL for V- and H-polarisation.

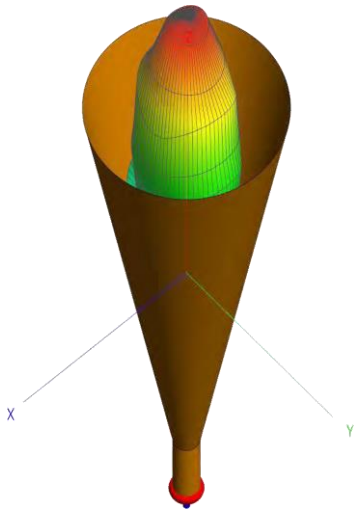

Figure E-1: Conical horn 3D radiation pattern in FEKO.

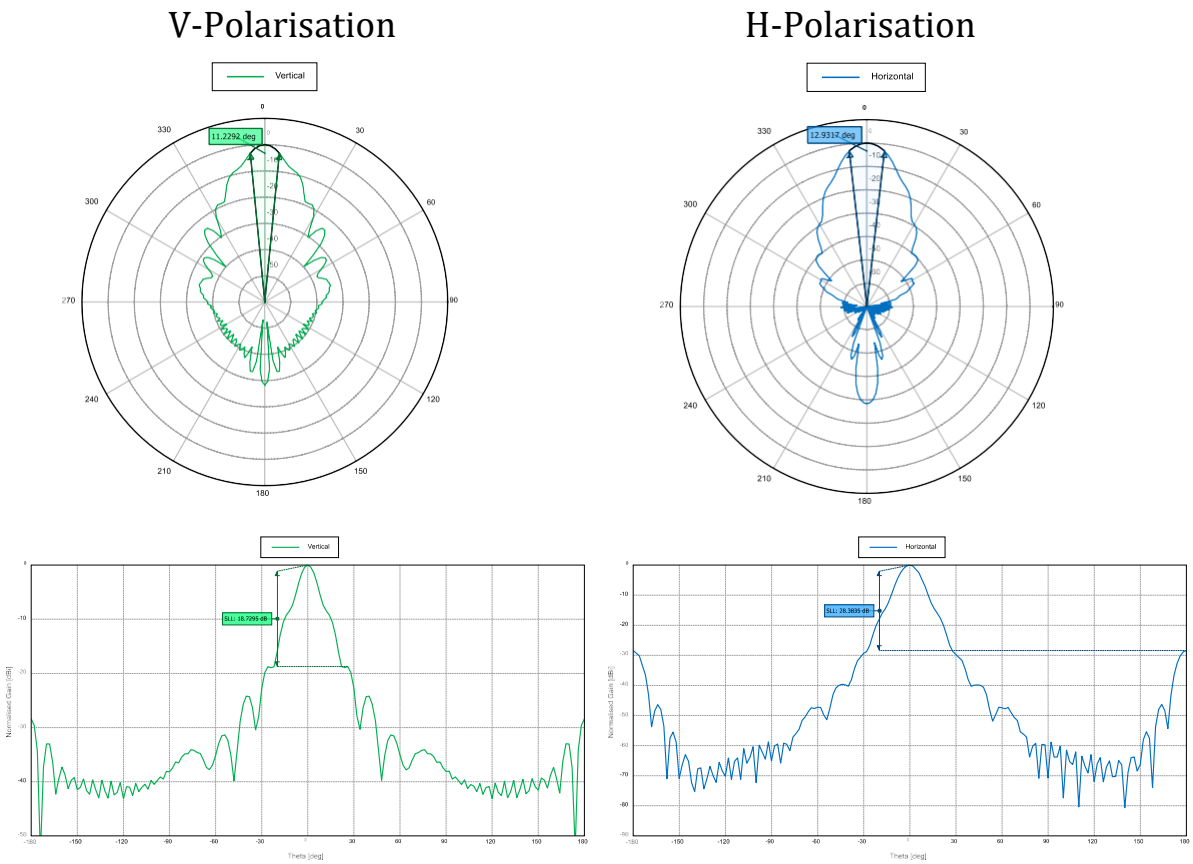

Figure E-2: Polar plots in the horizontal plane showing azimuth HPBW and SLL for V- and H-polarisation.

E.2 Discussion

The summary in Table E-1 can be drawn from the results obtained in FEKO.

Table E-1: Summary of the conical horn results in FEKO.

V-Polarisation		**H-Polarisation**	
$\boldsymbol{\theta_{az}}$	**SLL**	$\boldsymbol{\theta_{az}}$	**SLL**
11.23°	-18.72 dB	12.93°	-28.38 dB

The conical horn antenna is smaller than the values found in Section 2.4.3 and has low SLLs. However, the azimuth HPBW error for V- and H-polarisation are $+1.23^{\circ}$ and $+2.93^{\circ}$ respectively from the required 10°. Therefore, this design does not meet the azimuth HPBW requirement.

Appendix F

Parabolic Dish Antenna

F.1 Portable Caravan Dish

The commercial portable caravan dish antenna has been around for the past few years and manufactured by Ellies. Fig. F-1 shows the dish antenna or reflector antenna operates using a waveguide feed and a parabolic reflector. The waveguide radiates an EM wave towards the reflector, is reflected by the reflector, and radiates outwards into space. Thus, the feed is responsible for the operating frequency, and the gain and HPBW is dependent on the reflector [30].

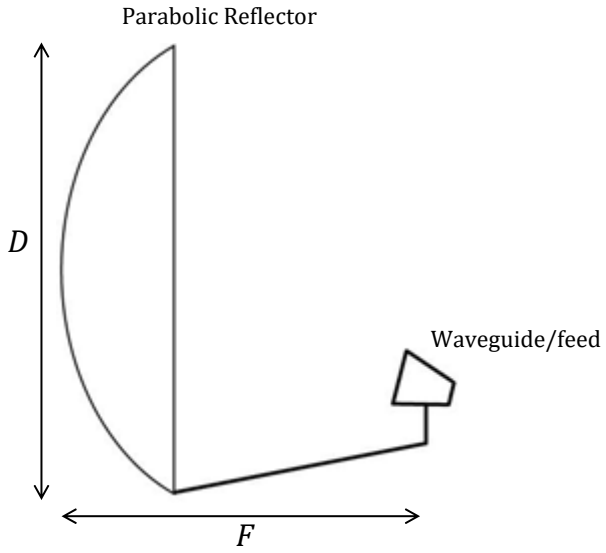

Figure F-1: Parabolic dish antenna.

The specifications of the caravan dish antenna are [31]:

- Diameter of dish: 35 cm × 37 cm
- Focus length (F): 21 cm
- Ku-band gain at 12.5 GHz: 32.08 dBi
- Aperture efficiency: 75%
- F/D ratio: 0.6

The waveguide operating at 12.5 GHz has been replaced with a circular waveguide with a centre frequency of 8.5 GHz circular waveguide. The waveguide has been designed in Section 2.3.5 with a diameter of 24 mm, and the rest of the dimensions are kept the same. The reflector and the circular waveguide have been simulated in FEKO and the performance is analysed. Only the V-polarisation has been simulated due to the symmetry.

F.2 FEKO Caravan Dish Antenna Results

Figure F-2 and Figure F-3 display the 3D radiation pattern, azimuth HPBW, and SLL for V-polarisation. The caravan dish has a oval shape and not a circular dish. FEKO does not have the function to create a oval shaped dish, thus the circular dish was simulated.

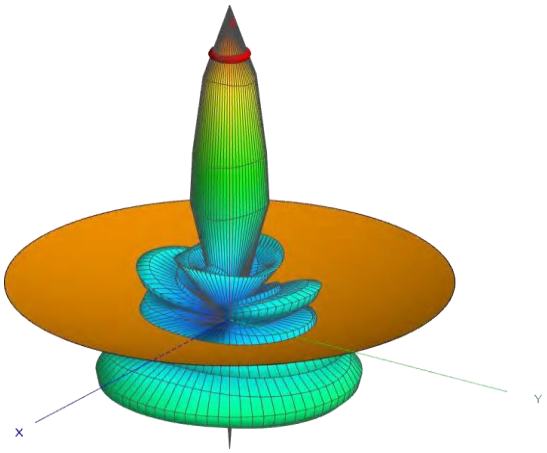

Figure F-2: 3D radiation pattern in FEKO for the dish antenna operating at 8.5 GHz

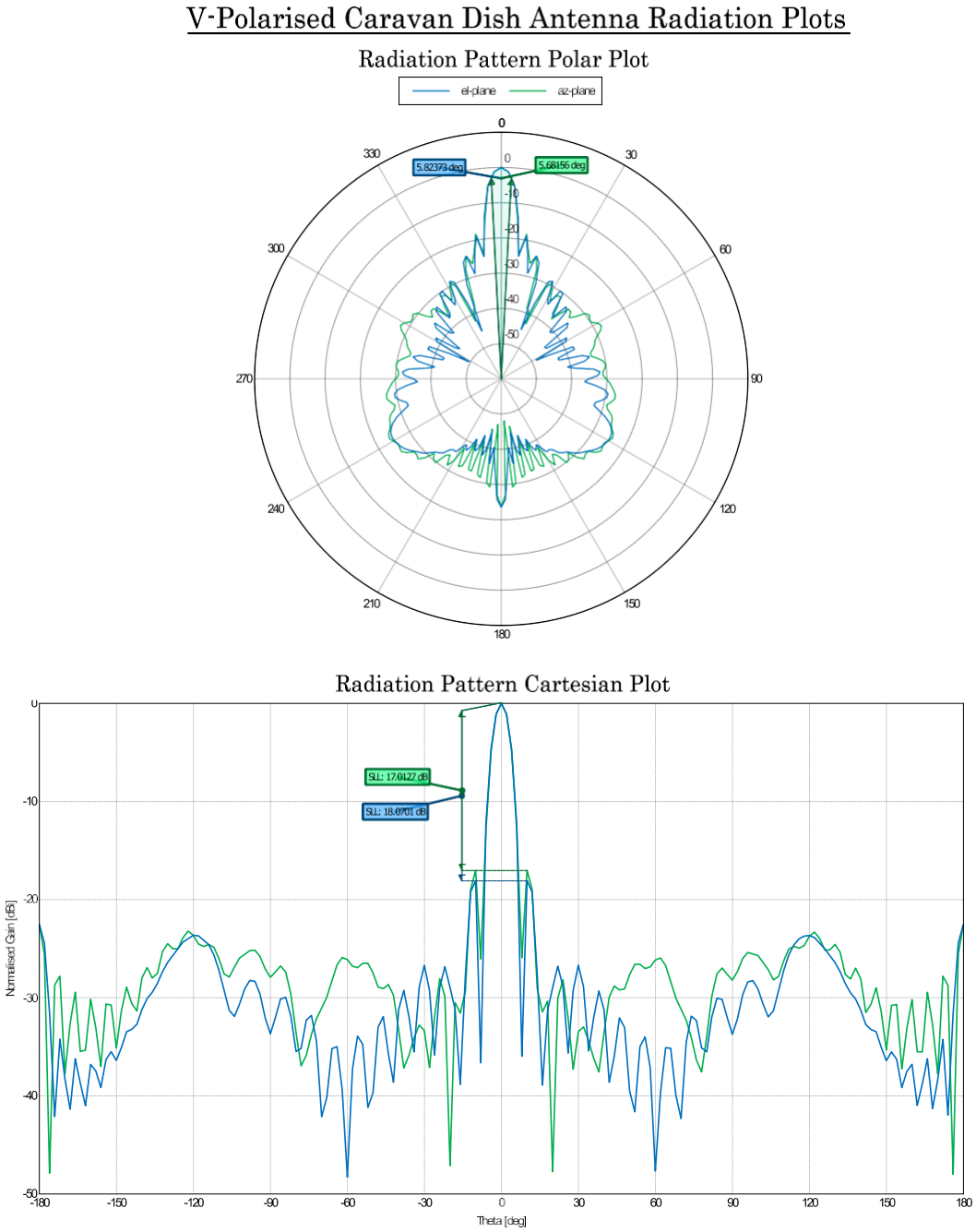

Figure F-3: Caravan dish antenna simulated in FEKO measuring HPBWs and SLLs in both planes of V-polarisation.

The caravan dish antenna achieved 5.68° with SLL in the azimuth plane of −18.07 dB. From FEKO, the gain of the caravan dish antenna has been predicted to be 26.89 dBi.

F.3 Revised FEKO Dish Antenna Results

The diameter of the dish can be calculated using the uniform distribution equation in (A-5):

$$\begin{aligned} D &= \frac{60\lambda_\circ}{\theta} \\ &= \frac{60 \times 35.29 \text{ mm}}{10^\circ} \\ &= 211.62 \text{ mm} \end{aligned}$$

Using the same *F/D* ratio of 0.6 the distance of the focus length *F* is 126.97 mm. Using the same waveguide of diameter 24 mm with centre frequency of 8.5 GHz, the FEKO simulations in Figure F-4 shows the polar and Cartesian plots when V-polarised.

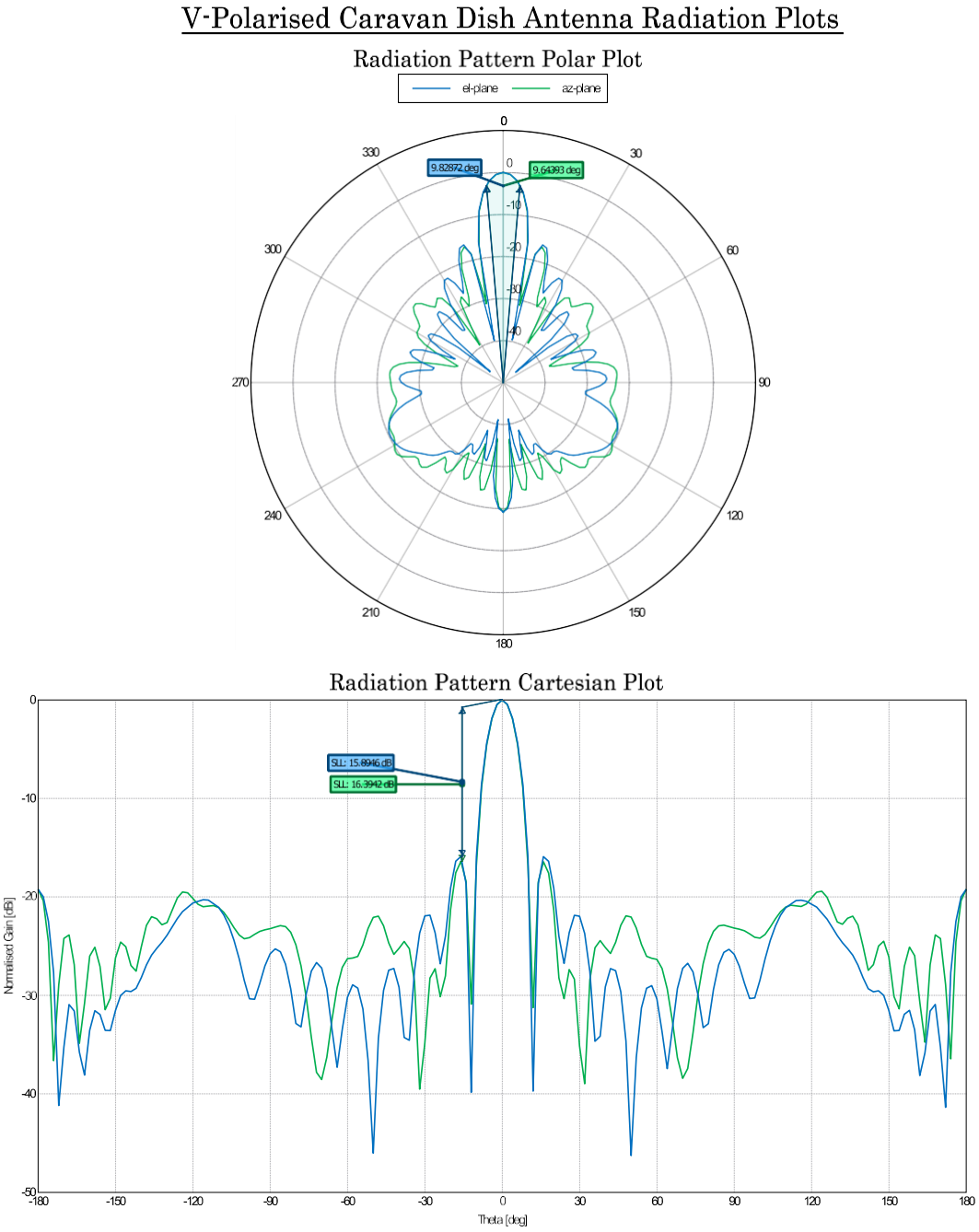

Figure F-4: Revised dish antenna simulated in FEKO measuring HPBWs and SLLs in both planes of V-polarisation.

The revised dish antenna achieved an azimuth HPBW of 9.64° with SLL in the azimuth plane of −16.39 dB. From FEKO, the gain of the revised dish antenna has been predicted to be 22.16 dBi.

F.4 Discussion

A summary in Table F-1 can be drawn from the caravan dish antenna and the revised dish antenna results obtained in FEKO.

Table F-1: Summary of the caravan dish and revised dish results in FEKO.

		V-Polarisation		
	Plane	**HPBW**	**SLL**	**Gain**
Caravan Dish Antenna	**Elevation**	5.82°	−17.01 dB	26.89 dBi
	Azimuth	5.68°	−18.07 dB	
Revised Dish Antenna	**Elevation**	9.83°	−15.89 dB	22.16 dBi
	Azimuth	9.64°	−16.39 dB	

From the caravan dish antenna simulated results, it can be observed that changing the waveguide to operate at 8.5 GHz will still illuminate its power on the dish without leakage. However, one important point is that the azimuth HPBW is too narrow compared to the required 10° due to the oversized parabolic reflector. Since FEKO does not have the function to create oval-shaped dishes, the simulated results have not been accurate. Therefore, this design does not meet the NeXtRAD project azimuth HPBW requirement. In order to widen the HPBW, the parabolic reflector will have to be adjusted.

The revised dish antenna uses the uniform distribution equation to find the correct diameter to achieve a HPBW of 10°. Furthermore, the HPBWs and SLLs in both planes are very similar, as well as the shape of the radiation patterns. Thus, a parabolic dish antenna shows more symmetry between the planes. This design reduces the overall size but simultaneously worsens the SLLs by approximately 2 dBs. Analysing Table F-1, the revised version of the dish has higher SLL in both planes, and lower gain compared to the caravan dish. However, the SLL and gain are in an acceptable range, and the results showed that the antenna achieved slightly below 10° in both planes when V-polarised. With the circular waveguide, dual polarisation is supported. The simulation shows that the dish antenna can achieve the antenna specifications, but requires the whole dish to be rebuilt. Fabricating the dish antenna is difficult and does not provide a feasible solution. Therefore, this design was not studied further.

Appendix G

AutoCAD Drawings

G.1 AutoCAD for Conical Horn

Figure G-1 shows the variables of the conical horn antenna and the unrolled version of the cone.

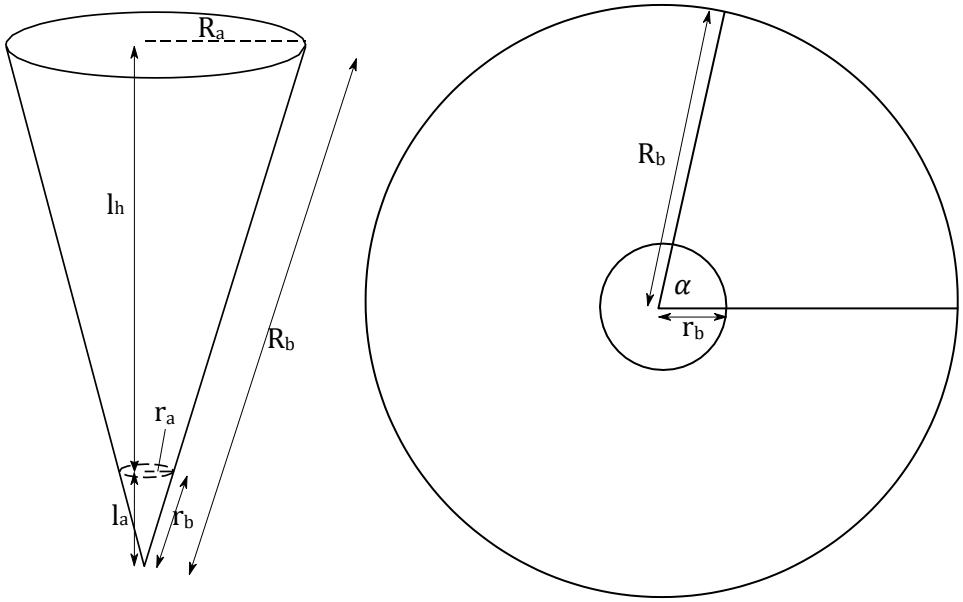

Figure G-1: Flat version of the conical horn for manufacture.

Using the dimensions calculated for the conical horn from Section 2.4.3: $l_h = 511.14$ mm, $l_a = 65.33$ mm, let $r_a = l_g/2 = 14$ mm, and let $R_a = D/2 = 123.53$ mm. To calculate the radii of R_b (outer radius) and r_b (inner radius) of the disc, right angle triangles are shown in Figure G-1 so Pythagoras is used. Thus, for the inner radius of the disc:

$$\begin{aligned} r_b &= \sqrt{l_a^2 + r_a} \\ &= 66.82 \text{ mm} \end{aligned}$$

Using similar triangles, the outer radius of the disc has been found by using ratios:

$$\begin{aligned} \frac{R_b}{R_a} &= \frac{r_b}{r_a} \\ R_b &= \frac{r_b}{r_a} \times R_a \\ &= 589.56 \text{ mm} \end{aligned}$$

Finally, the angle α has been determined:

$$\begin{aligned} \alpha &= \frac{R_a}{R_b} \times 360^\circ \\ &= 75.43^\circ \end{aligned}$$

Using the calculated dimensions, the portion of the disc can be designed in AutoCAD and sent for fabrication. Figure G-2 shows the AutoCAD drawing of the disc portion.

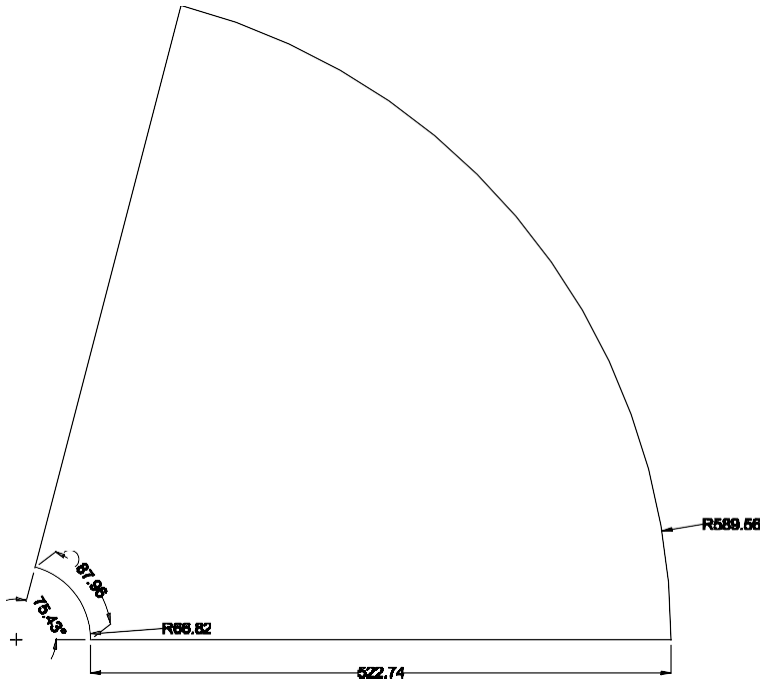

Figure G-2: AutoCAD drawing of the unrolled conical horn disc.

G.2 Other AutoCAD Drawings

Figure G-3 shows the AutoCAD flange design for the opening of the horn and the circular waveguide. Due to the slanted structure of the conical horn, it is difficult to mount the horn on any tripod or stand. So a bracket was designed for an easier tripod mount and the AutoCAD drawing of the bracket is shown in Figure G-4.

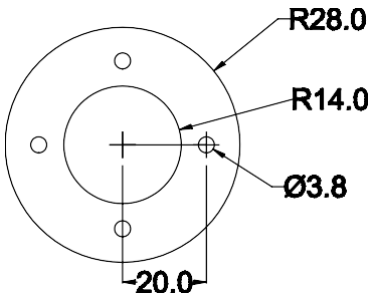

Figure G-3: AutoCAD drawing of the flange design

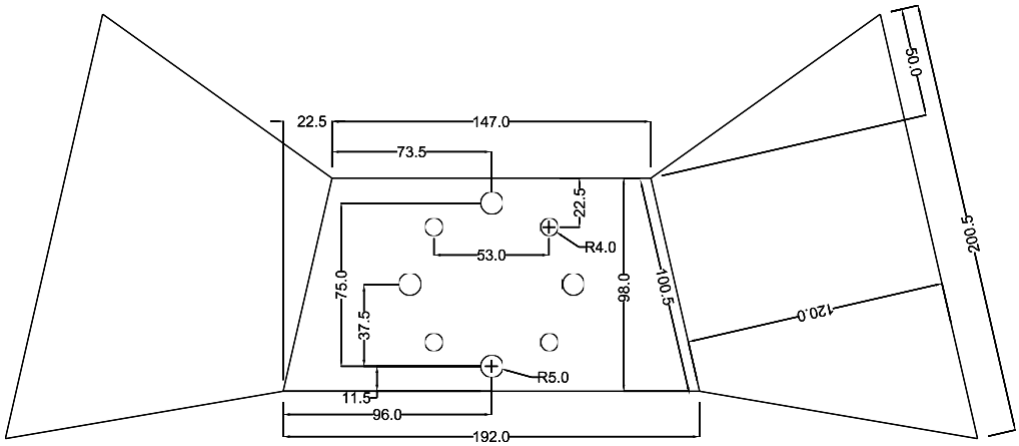

Figure G-4: AutoCAD drawing of the bracket design.

A 3D version in Figure G-5 shows the entire design in AutoCAD, providing an alternative view of the complete structure, which includes the conical horn, flanges, waveguide, and bracket.

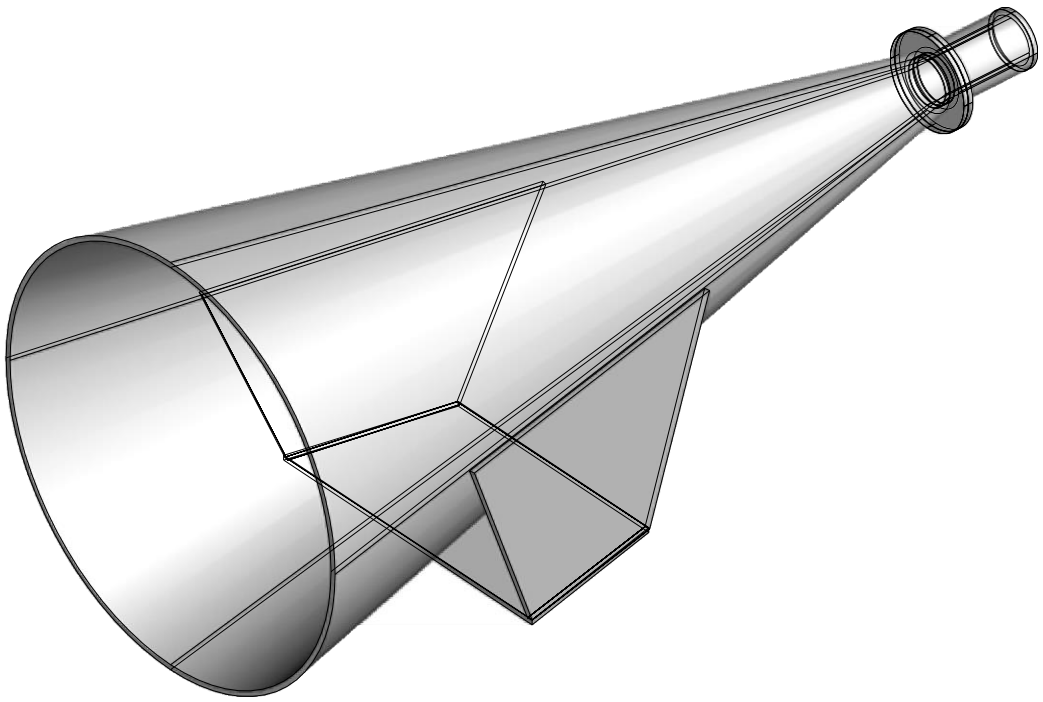

Figure G-5: AutoCAD drawing of the complete design in 3D.

Appendix H

Revised Conical Horn Antenna Calculations

H.1 Waveguide Calculations

The same methods and equations in Section 2.3 have been followed in designing the circular waveguide with diameter l_g = 24 mm. The cutoff wavelengths for the fundamental and next higher-order TM_{01} mode have been found to be:

$$\begin{aligned}\lambda_{c(\mathrm{TE11})} &= 1.706 \times l_g \\ &= 1.706 \times 24 \text{ mm} \\ &= 40.94 \text{ mm}\end{aligned}$$

and

$$\begin{aligned}\lambda_{c(\mathrm{TM01})} &= 1.306 \times l_g \\ &= 1.306 \times 24 \text{ mm} \\ &= 31.35 \text{ mm}\end{aligned}$$

The cutoff frequencies are:

$$\begin{aligned} f_{c(\mathrm{TE11})} &= \frac{c}{\lambda_{c(\mathrm{TE11})}} \\ &= \frac{3 \quad 10^8 \text{ m/s}}{0.04094 \text{ m}} \\ &= 7.33 \text{ GHz} \end{aligned}$$

and

$$\begin{aligned} f_{c(\mathrm{TM01})} &= \frac{c}{\lambda_{c(\mathrm{TM01})}} \\ &= \frac{3 \quad 10^8 \text{ m/s}}{0.03657 \text{ m}} \\ &= 9.57 \text{ GHz} \end{aligned}$$

An operating frequency of 8.5 GHz is above the fundamental mode's cutoff frequency and below the next higher-order mode's cutoff frequency. The diameter of $l_g = 24$ mm only allows the fundamental mode to propagate and avoids the all other higher-order modes.

The centre frequency $f_\circ$ is 8.5 GHz, and $\lambda_\circ$ is 35.29 mm. The waveguide wavelength is:

$$\begin{aligned} \lambda_g &= \frac{\lambda_\circ}{\sqrt{1 - \left(\frac{\lambda_\circ}{\lambda_c}\right)^2}} \\ &= \frac{35.29 \text{ mm}}{\sqrt{1 - \left(\frac{35.29 \text{ mm}}{40.94 \text{ mm}}\right)^2}} \\ &= 69.62 \text{ mm} \end{aligned}$$

The respective lengths of the probe and backshort are:

$$\begin{aligned} L_{\mathrm{probe}} &= \frac{\lambda_\circ}{4} \\ &= \frac{35.29 \text{ mm}}{4} \\ &= 8.82 \text{ mm} \end{aligned}$$

and

$$\begin{aligned} L_{\text{backshort}} &= \frac{\lambda_g}{4} \\ &= \frac{69.62 \text{ mm}}{4} \\ &= 17.40 \text{ mm} \end{aligned}$$

H.2 Conical Horn Calculations

The same methods and equations in Section 2.4.3 have been followed in designing the conical horn. The diameter of the aperture is:

$$\begin{aligned} D &= \frac{70 \times \lambda_\circ}{\theta} \\ &= \frac{70 \times 35.29 \text{ mm}}{10^\circ} \\ &= 247.06 \text{ mm} \end{aligned}$$

The total length of the cone from the apex to the centre aperture of the horn is:

$$\begin{aligned} l_{\text{tot}} &= \frac{D^2}{3\lambda_\circ} \\ &= \frac{(247.06 \text{ mm})^2}{3 \times 35.29 \text{ mm}} \\ &= 576.47 \text{ mm} \end{aligned}$$

The length of the horn l_h is:

$$\begin{aligned} l_h &= l_{\text{tot}} \left(1 - \frac{l_g}{D}\right) \\ &= 576.47 \text{ mm} \left(1 - \frac{24 \text{ mm}}{247.06 \text{ mm}}\right) \\ &= 520.47 \text{ mm} \end{aligned}$$

EBE Faculty: **Assessment of Ethics** In **Research Projects**

Anyperson planning to under1ake research In theFaculty of Engineeringand theBullt Environment at the University of cape Townis required to complete this fonn before collectlng or analysing date. When completed nshouldbe subnvtted to the supervisor (where ap icable) andfrom then, to the Heed of Department If anyof the questions below have been answered YES, and the applicant is NOTa fourth yearsrudent, theHead should foiward this *tom*,forapproval by the Faculty EIR oommlttee: submit to Ms Zakiya Chikte (Zaklya.chlkta@uclac.zal:New EBEBuilding, Ph021 650 5739). Students mustInclude **a**copyof the completed form with the dissertation/thesis when nls submitted for examination.

Name of PrincipalResearcherlStudent:Po-Kai Cheng Department: Electrical Engineering

If a Student: Yes **Degree:** MSc In Electrical Engineering Supervisor: Prof. Michael lnggs

If a Research Contract Indicate source of fundlng(spom,orshlp:

Research Project Title: NeXIRAD Antenna Design - X-Band Dual Polarised Conical Hom Antenna

Overview of ethics Issues In your research project:

Question1: Is there a possibility that your research couldcause harm to **a** third party **(I.e. a** ""rson notInvolved In vour nrolectl?	YES	[O,
Queatlon 2: la your research making use of human subjects as aourcea of data? If vour answeris YES. olaasa comr>lete Addendum 2.	YES	1)
Question 3: **Does** your **research** Involve the partlelpaUon of or provision of aervlees to communitlea? If =ur answerls YES. Dleasa comolete Addendum 3.	YES	NS
QuHtlon **4:** If your **reaaarch Is sponsored, Is** there any potenUal for conflicts of Intarast? If •-ur answeris YES. !>lease comclele Addendum 4.	YES	NO

If you have answered YES to any of the above questions, please append a copy of your research proposal, as well as any interview schedules or questionnaires /Addendum 1) andplease complete further addenda as appropriate.

I hereby undertake to cany out myresearch In such **a way** that

- there Is no apparent legal objection to the nature or the method of research; and
- the research will notcompromise staff or students or the other responsibilities of the University;
- the stated objective will be achieved, and the findings will have a highdegree of validity;
- limitations and alternative Interpretations will beconsidered:
- the findings could be subject to peer review and publicly available; and
- I will comply with the conventions of copyright and avoid any practice thatwould constitute plagiarism.

Signed by: Principal Researcher/Student:	Full name and signature Pokai Cheng Signed	Date 15/02/16
This application is approved by: Supervisor (if applicable):		15/02/16
HOD (or delegated nominee): Finalauthority for all assessments with NO to all uestions and for all unde raduate research.	Signed	15/2/16.
Chair: Faculty EIR Committee For applicants other than undergraduate students who have answered YES toany of the above uestions.		

ADDENDUM 1:
Please append a copy of the research proposal here, as well as any interview schedules or questionnaires:

ADDENDUM 2: To be completed If you answered YES toQuestion 2:

It is assumed that you have read the UCTCode for Research Involving Human Subjects (available at h11p:/lweb.uct.ac.za/depts/educate/download/uctcodeforresearchinvolvinghumansubjects.pdf\in order to **be** able to answer **the** questions in this addendum.

2.1 **Does theresearch** discriminate against participation by Individuals, or differentiate**between** participants, on the grounds of gender, race or ethnic group, age range, religion, Income, handican Illness or anysimilar classiflcetion?	YES	NO
2.2 Does the research require the participation of socially or physicaly vulnerable people (children, aged, disabled,etc) or legally restJ1cted groups?	YES	NO
2.3 Wi l you not beable to secure the Informedconsent of all participants In the research? (In the case of children, will you not beable toobtain the oonsent of their guardians or narents?l	YES	NO
2.4WIiianyconfidential data becollected or WIii iden tifiabie records of Individuals bekept?	YES	NO
2.5 In reporting on this research is there any possibility that you WIii not be able to keep the identities of the individuals involved anonymous?	YES	NO
2.6Are there anyforeseeable risks of physical, psychological or social harm to participants that might oocur in the course of tha research?	YES	NO
2.7Does the research include makingpayments or giving g to any participants?	YES	NO

If you have answered YES to any of these questions, please describe how you plan to address these Issues (append to form):

ADDENDUM 3: To be completed If you answered YES to Question 3:

3.1Is the community expected tomake decisions for, during or based on the research?	YES	NO
3.2 At the end of the research will any economic or social process be terminated or left unsupported, or equipment or facllltles used in the research **be** recovered from the participants or cornmunlhn	YES	NO
3.3 Will any service be provided at a level below the generally accepted standards?	YES	NO

If you have answered YES to any of these questions, please describe how you plan to address these Issues (append to form)

ADDENDUM 4: To be completed If you answered YES to Question 4

4.1 Is there any existing or potenUel conftlclof Interest between a research sponsor, academic supervisor, otherresearchers or participants?	YES	NO
4.2 Will information that reveals the identity of participants be suppiledto a researdl sponsor, other than with thepermission of the individuals?	YES	NO
4.3 Does theproposed researdl potentially conftict with theresearch of any other individual or group within the University?	YES	NO

If you have answered YES to any of these questions, please describe how you plan to address these issues(append to form)